

**ON ELECTROMAGNETIC AND QUANTUM INVISIBILITY**

by

Pattabhiraju Chowdary Mundru, B.Tech., M.S.

A Dissertation Presented in Partial Fulfillment  
of the Requirements for the Degree  
Doctor of Philosophy

COLLEGE OF ENGINEERING AND SCIENCE  
LOUISIANA TECH UNIVERSITY

MAY 2014

Replace this page with the Signature Page.

## ABSTRACT

The principle objective of this dissertation is to investigate the fundamental properties of electromagnetic wave interactions with artificially fabricated materials i.e. metamaterials for application in advanced stealth technology called electromagnetic cloaking. The main goal is to engineer a metamaterial shell around an object that completely eliminates the dipolar scattering thus making the object invisible.

In this context we developed a quasi-effective medium theory that determines the optical properties of multi-layered-composites beyond the quasi-static limit. The proposed theory exactly reproduces the far field scattering/extinction cross sections through an iterative process in which mode-dependent quasi-effective impedances of the composite system are introduced. In the large wavelength limit our theory is consistent with Maxwell-Garnett formulism. Possible applications in determining the hybridization particle resonances of multi-shell structures and electromagnetic cloaking are identified.

In this thesis we proposed a multi-shell generic cloaking system. A transparency condition independent of the objects optical and geometrical properties is proposed in the quasi-static regime of operation. The suppression of dipolar scattering is demonstrated in both cylindrically and spherically symmetric systems. A realistic tunable-low loss shell design is proposed based on composite metal-dielectric shell. The effects due to dissipation and dispersion on the overall scattering cross-section

are thoroughly evaluated. It is shown that a strong reduction of scattering by a factor of up to  $10^3$  can be achieved across the entire optical spectrum. Full wave numerical simulations for complex shape particle are performed validating the analytical theory. The proposed design does not require optical magnetism and is generic in the sense that it is independent of the objects material and geometrical properties.

A generic quantum cloak analogous to the optical cloak is also proposed. The transparency conditions required for the shells to cloak an object with arbitrary potential are derived. A realistic cloaking system with semiconductor material shells is studied.

Replace this page with the approval for scholarly dissemination form.

## **DEDICATION**

Priya,  
Senaka Krishna Kanakamedala,  
Krishna Chaitanya Inturi,  
Veerunna Chowdary and Sarojini Yadagani,  
&  
Satyanarayana Mallireddi.

*To Them I Owe My Life*

## TABLE OF CONTENTS

ABSTRACT .....	iii
DEDICATION .....	vi
LIST OF FIGURES.....	x
ACKNOWLEDGMENTS .....	xv
CHAPTER 1 INTRODUCTION.....	1
1.1 Motivation.....	1
1.2 Previous Work.....	4
1.3 Significance of this Work.....	5
1.4 Organization of the Dissertation.....	6
CHAPTER 2 SCATTERING OF ELECTROMAGNETIC WAVES: A REVIEW	7
2.1 Time Harmonic Plane-Waves .....	7
2.2 Scattering of Electromagnetic Radiation .....	8
2.2.1 Cross Section and Scattering Amplitude .....	9
2.2.2 Integral representations of scattering amplitude .....	12
2.3 Rayleigh Scattering .....	13
2.4 Mie Theory .....	15
2.4.1 Intensity and Polarization of the Scattered Light .....	18
2.4.2 Small-Particle Limit .....	21
2.5 Scattering from a Circular Cylinder.....	22

2.5.1	Normal Incidence.....	22
2.5.2	Small Dielectric Cylinders .....	24
2.5.3	Oblique Incidence .....	25
CHAPTER 3	MANY PARTICULATE SYSTEMS .....	29
3.1	Coated Cylinder .....	29
3.1.1	Small Particle Limit .....	31
3.2	Inhomogeneous Particles .....	32
3.2.1	Effective Medium Models .....	32
3.2.2	Maxwell-Garnett Theory .....	33
3.2.3	Generalized Maxwell-Garnett .....	36
3.2.4	Tuning of the Composite .....	37
3.2.5	Bruggeman Theory.....	38
3.2.6	Extended Effective Medium Theories.....	39
3.3	Multilayer Composites .....	41
3.3.1	Maxwell-Garnett Theory: Multilayer Cylinder.....	41
3.3.2	Multilayer Planar Composites .....	43
3.3.3	Quasi-Effective Medium Theory: Multilayer Cylindrical Composites.....	45
3.3.4	Application: Surface Plasmon (PSP) Hybridization.....	49
CHAPTER 4	INVISIBILITY .....	52
4.1	Theory.....	52
4.2	Cloak Design and Tunability .....	55
4.2.1	Metallic Inner shell.....	55

4.2.2	Cloaking system with Composite Inner shell.....	58
4.3	Full Wave Analysis of the Generic Cylindrical Cloak .....	63
4.3.1	Full Wave Simulation .....	65
4.4	Invisibility by Eliminating Two Arbitrary Monopoles .....	67
CHAPTER 5 QUANTUM INVISIBILITY .....		72
5.1	Analogy to Optical Index of Refraction .....	72
5.2	Partial Wave Analysis: Faxen–Holtsmark’s Theory.....	73
5.2.1	Phase shifts .....	76
5.3	2–Dimensional scatterer .....	76
5.4	Generic quantum cloak .....	79
5.4.1	single shell cloak .....	79
5.4.2	Multi-shell cloaking system .....	82
CHAPTER 6 CONCLUSIONS .....		87
APPENDIX A APPENDICES (IF DESIRED) .....		89
BIBLIOGRAPHY .....		92
VITA .....		97

Note that an “orphan” such as this last table of contents entry for the vita would need to be remedied.

## LIST OF FIGURES

Figure 1.1: (a)Homogeneous optical space, and (b) Curved coordinate system representing the desirable light paths that evolve around an object...	1
Figure 2.1: Scattering from an object of permittivity $\varepsilon_0(\mathbf{r})$ . $\mathbf{E}_i$ , $\mathbf{E}_s$ are the incident and scattered fields in the direction of $\hat{\mathbf{k}}_i$ , $\hat{\mathbf{k}}_s$ respectively.....	9
Figure 2.2: Scattering from an object of permittivity $\varepsilon(\mathbf{r})$ with arbitrary shape and finite size. $R =  \mathbf{r} - \mathbf{r}' $ is the distance between $\mathbf{r}'$ and the observation point $P$ .....	12
Figure 2.3: Dielectric Sphere of permittivity $\varepsilon_0$ in uniform electric field $\mathbf{E}_i$ .....	13
Figure 2.4: Extinction efficiency of a spherical water droplet at $\lambda = 0.55\mu m$ (blue) and $\lambda = 20\mu m$ (red).....	17
Figure 2.5: Scattering intensity as a function scattering angle for a spherical water droplet of refractive index $m = 1.33 + i10^{-8}$ at $\omega = 2.25eV$ in air for particle sizes (a) $0.07\mu m$ , (b) $1.6\mu m$ , (c) $0.26\mu m$ , and (d) $0.9\mu m$ .....	19
Figure 2.6: (a) Scattering intensity functions $i_1$ and $i_2$ and (b) Polarization as function of scattering angle for a spherical water droplet of refractive index $m = 1.33 + i10^{-8}$ in air. ....	20
Figure 2.7: Circular cylinder of permittivity $\varepsilon_0$ illuminated by a plane wave. Magnetic field $\mathbf{H}$ is parallel to the axes of the cylinder. ....	22
Figure 2.8: Comparison of scattering efficiency of a homogenous (a) metallic cylinder and (b) dielectric cylinder calculated using the exact solution (Eq. 2.67) and the Rayleigh scattering theory (Eq. 2.30). Insert shows the applicability of the Rayleigh theory for very small particles. ....	24
Figure 2.9: Cylinder of permittivity $\varepsilon_0$ and $\mu_0$ illuminated by an $E$ -polarized wave at oblique incidence.....	26

Figure 3.1: Coated cylinder with core permittivity $\varepsilon_0$ and coating permittivity $\varepsilon_1$ illuminated by a plane wave. Magnetic field $\mathbf{H}$ is parallel to the axes of the cylinder. ....	30
Figure 3.2: Geometry of the composite with inclusions of permittivity $\varepsilon_i$ embedded in matrix $\varepsilon_h$ . ....	33
Figure 3.3: A comparison of the effective permittivity in case of complementary mixtures as a function of inclusion volume fraction. In the plot we consider spherical inclusions with (I) permittivity $\varepsilon_{eff} = 20\varepsilon_h$ and a glass host with $\varepsilon_h = 2.2$ (blue solid line) and (II) $\varepsilon_{eff} = 20\varepsilon_i$ and $\varepsilon_i = 2.2$ (red dashed line). ....	35
Figure 3.4: Real and imaginary parts of the effective permittivity as a function of frequency for different volume fractions. The host is glass with $\varepsilon_h = 2.2$ and the inclusions are Drude metal particles. Two separate designs are being investigated (I) $f = 0.1$ (blue solid line) (II) $f = 0.05$ (red dashed line). ....	36
Figure 3.5: Real and imaginary parts of the effective permittivity as a function of frequency for different aspect ratios ( $a/b$ ) at $f = 0.05$ . The host is glass with $\varepsilon_h = 2.2$ and the inclusions are Drude metal particles. Two separate designs are being investigated (I) $a/b = 10$ (blue solid line) (II) $a/b = 100$ (red dashed line). ....	37
Figure 3.6: Perpendicular incidence of a plane wave on a multilayered structure with $l$ – layers. ....	43
Figure 3.7: A schematic representing the quasi-effective medium approach for concentric multi-shell objects. (a) The concentric $l$ – shell system with shell radii $r_m$ and impedance $z_m$ is (b) equivalent to a system consisting of $l - m$ shells and a core with effective impedance $\tilde{z}_m$ and radius $r_m$ immersed in a homogeneous background with impedance $z_{l+1}$ ....	45

Figure 3.8: Particle surface plasmon (PSP) hybridization. (a) The effect of the shell geometrical factor $p$ on the resonance frequencies are calculated using Eq. 8 for a system comprising of a metal (silver) shell and a core with permittivity equal to that of the host $\epsilon_0 = \epsilon_3 = 1$ . (b) The core-shell particle scattering cross section normalized by the particle radius is calculated using the quasi-effective medium theory Eq. 2. Due to the small particle size $a = r_0 = 10\text{nm}$ , the dipolar response is dominant while the quadrupole contribution to the far field scattering is only marginal. (c) For a large core-shell particle with radius $a = 200\text{nm}$ , the scattering cross-section reveals both the quasi-static resonances for large $p$ and the branches due to the surface plasmon polariton (SPP) resonances of the shell. ....	49
Figure 4.1: (a) Generic multi-shell cloaking system with shell radii $r_i$ and permittivity $\epsilon_i$ , a two shell (b) cylindrically symmetric cloaking system and (c) spherically symmetric cloaking system.....	53
Figure 4.2: (a) Relative scattering length (RSL) and cross-section (RSCS) versus outer shell permittivity for two-shell (a) cylindrically symmetric cloak and (b) spherically symmetric cloak with inner shell made of bulk silver. Two separate designs are being investigated in case of cylindrical system: (I) $p_2 = 0.67$ and (II) $p_2 = 0.82$ , and spherical system (I) $p_2 = 0.73$ and (II) $p_2 = 0.86$ . The object permittivity is $\epsilon_0 = 10$ and for all cases we use the optimal radii ratio $p_1 = 1/(1 + \sqrt{d})$ . The limiting case as per Eq. (4.8) is presented with dotted (black) lines.....	57
Figure 4.3: (a) Depolarization factor for composite host materials $\epsilon_h = 1$ (solid line) and $\epsilon_h = 2$ (solid line)(dashed line) at different frequencies and $f=0.05$ . Relative scattering length (RSL) and cross-section (RSCS) versus outer shell permittivity of two-shell (b) cylindrically symmetric cloaking system and (c) spherically symmetric cloaking system, respectively. The composite inner shell is designed with two different hosts $\epsilon_h = 1$ (dashed red line) and $\epsilon_h = 2$ (dotted green line) at $\omega = 1.14\text{eV}$ . In the plots we also consider two separate shell designs; cylindrical system (I) $p_2 = 0.67$ and (II) $p_2 = 0.82$ , and spherical system (I) $p_2 = 0.73$ and (II) $p_2 = 0.86$ . The embedded object has permittivity $\epsilon_0 = 10$ and for all cases we use the optimal shell radii ratio $p_1 = 1/(1 + \sqrt{d})$ . The ideal lossless cases are represented with solid (blue) lines. The limiting case (as per Eqs. (4.7) and (4.9)) is presented with horizontal (dotted and dashed) black lines for both the host media.....	59

- Figure 4.4: (a) Relative scattering length (RSL) and (b) relative scattering cross-section (RSCS) calculated as function of outer-shell permittivity ( $\varepsilon_2$ ) and incident light frequency for a dielectric particle( $\varepsilon_0 = 12$ ) with  $\varepsilon_h = 1$  and spheroids volume/surface fraction  $f = 0.05$ . The shells radii ratios are (a) cylindrical system  $(p_1, p_2) = (0.41, 0.67)$ , and (b) spherical system  $(p_1, p_2) = (0.37, 0.73)$ ..... 62
- Figure 4.5: (a) Relative scattering length (RSL) and (b) relative scattering cross-section (RSCS) calculated as function of composite host permittivity ( $\varepsilon_h$ ) and operational frequency  $\omega_{op}$  for a dielectric particle  $\varepsilon_0 = 10$  and spheroids volume/surface fraction  $f = 0.05$ . The shells radii ratios are (a) cylindrical system  $(p_1, p_2) = (0.41, 0.67)$ , and (b) spherical system  $(p_1, p_2) = (0.37, 0.73)$ ..... 64
- Figure 4.6: Full wave calculations of the relative scattering length (RSL) as function of outer shell permittivity ( $\varepsilon_2$ ) and incident light frequency for dielectric particle  $\varepsilon_0 = 10$  enclosed in a cloaking system with radii (a)  $r_2 = 50\text{nm}$  and (b)  $r_2 = 100\text{nm}$ . ..... 66
- Figure 4.7: Quasi-static cloaks. The dipole (a) and quadrupole (b) scattering amplitudes vs. the corresponding scattering amplitudes of the object (core) calculated as function of the core diameter. Dramatic reduction in dipolar scattering is observed in the three shells (red solid line) and two shells designs (dashed black lines). The quadrupole scattering is only reduced in the three shell design as expected. Schematics of the scattering far field profiles are also included as inserts with dashed lines corresponding to elimination of a particular multipole while a solid line correspond to uninterrupted mode radiation. The effects of the second shell permittivity and geometrical factor  $p$  on the total scattering cross section in the case of two shells (c, d) and three shell (e,f) cloaks are calculated for object (core) sizes equal to (c,e)  $d = 20\text{nm}$  and (d, f)  $d = 100\text{nm}$ . The cloak's transparency conditions Eq. 4.4 and Eq. 4.4 are represented with dashed lines. Provided the transparency conditions are satisfied the total cross sections for small particles are reduced by a factor up to  $10^3$ . The effect is persistent for particle's sizes comparable to the wavelength of the incoming radiation  $\lambda = 2c/\tilde{\omega}_p = 306\text{nm}$ . In the calculations, we have used silver to form the internal near-zero permittivity shell. ..... 69

- Figure 4.8: Object independent cloaking. The scattering effects due to the object are tested for a cross shape inclusion (see the schematics on the top of the scale bar) positioned at the core. The size of the inclusion is  $100\text{nm}$  and has permittivity  $\varepsilon = 10$ . (a) The magnetic field profiles under a plain wave illumination with (a) and without (b) the cloak are calculated using finite difference commercial software (COMSOL Multiphysics). The bare object strongly disturbs the incoming wave while the introduction of the three shell cloak (Eq. 4.14) around the object substantially eliminates scattering..... 70
- Figure 5.1: 2D scatterer with radius  $r_0$  and effective mass  $m_0$  located in an environment with effective mass  $m_e$ ..... 77
- Figure 5.2: Matter wave incident on a 2D multilayer scatterer with layer radii  $r_0$ ,  $r_1$  and effective mass  $m_0$ ,  $m_1$ , respectively. Located in an environment with effective mass  $m_e$ ..... 80
- Figure 5.3: Relative scattering length (RSL) versus the radii ratio cylindrically symmetric cloak. The ideal case as per Eq. (5.61) is presented in solid lines. The dotted lines represent RSL with respect to physical materials. The inner and outer shell made of InSb ( $m_3 = 0.013$ ) and AlSb ( $m_2 = 0.102$ ) respectively. The host is GaAs with electron effective mass  $m_e = 0.067$ . Three separate designs are being investigated in case of cylindrical system: (I)  $r_2 = 2$  nm (Red), (II)  $r_2 = 5$  nm (Blue) and  $r_2 = 10$  nm (pink). The object electron effective mass is  $m_0 = 0.083$ ..... 84
- Figure 5.4: Relative scattering length/width (RSL) versus the radii ratio cylindrically symmetric cloak. The ideal case as per Eq. (5.61) is presented. The inner and outer shell made of  $m_1 = 0.0$  and  $m_2 = 0.102$  respectively. The potentials or the band offsets are  $V_0 = 0.48$ ,  $V_1 = 0.60$  and  $V_2 = -0.28$  respectively. The host electron effective mass  $m_e = 0.067$ . The object electron effective mass is  $m_0 = 0.083$ ... 85
- Figure 5.5: Relative scattering length/width (RSL) versus the radii ratio cylindrically symmetric cloak. The ideal case as per Eq. (5.61) is presented. The inner and outer shell made of  $m_1 = 0.013$  and  $m_2 = 0.102$  respectively. The potentials or the band offsets are  $V_0 = 0.48$ ,  $V_1 = 0.60$  and  $V_2 = -0.28$  respectively. The host electron effective mass  $m_e = 0.067$ . The object electron effective mass is  $m_0 = 0.083$ ... 86

## **ACKNOWLEDGMENTS**

I would like to express my sincere gratitude to my advisor, Dr. Dentcho Angelo Genov. His sound advice has been my inspiration throughout my stay at Louisiana Tech. I am grateful for his valuable feedback and suggestions, for they have greatly added to the value of this dissertation. From him, I learnt how to take an idea from its abstract infancy, give it shape and put it down effectively on a paper. I hope to achieve his level of organization and work ethic one day.

I would also like to thank Dr. Neven simicevic for being patient with my numerous questions and comments (from teaching to research). Many thanks to Dr. Lee Sawyer for his encouragement and support throughout my stay at Louisiana Tech will never be forgotten. Many Thanks also go to Dr. Long Que and Dr. John Shaw for agreeing to serve on my committee and reviewing this work. A grant from Louisiana Optical Network Initiative (LONI), obtained through kind assistance of Dr. Genov and Dr. Bety E. Rodriguez-Milla enabled me to utilize the state of art computational facilities at the LONI Institute.

My deepest gratitude goes to Venkatesh K. Pappakrishnan, for driving me to all the important scientific conferences (sometimes across the country) and his constant support and suggestions in writing this dissertation. I am also thankful to my colleagues, Shravan R. Animilli, Mona Asaleh, and Raj Vinnakota for their valuable suggestions. I'm grateful to my friends Gowtham Tummala, Sandeep Guduru, Pattem,

Balakrishna Velgapudi, Sridhar Rekula and Kautilya Buchapudi. I will always cherish the lively discussions we had ranging from politics to religion to cricket. Even if many of these discussions did not come close to the discovery of any global solutions, they provided me with a good break.

Dr. Kiran Balagani was an insightful critic, without his constant pushing, my dissertation would be a new beginning everyday. Dr. Raja Mannam, a big thanks for your wise words, important hints and keen discussions. I know that I still owe you some money, but dont worry, I'll pay you sooner or later. Special thanks to Krishna Karthik Koilada for teaching me a new way of looking at *life*. I would also like to thank Mr. & Mrs. Patel for all their help. Varsha Bhatia, I will not forget what you have done for me, a big thanks!

Finally, I express my sincere gratitude to my Mother and Grandfather. Who made sure that I had the best of opportunities growing up. Their belief in my judgment, gave me the confidence to pursue a doctorate degree.I know they will always be there for me.

# CHAPTER 1

## INTRODUCTION

### 1.1 Motivation

According to the Fermat's principle, in a homogeneous optical space, light travels as straight lines in extremal optical paths. If the refractive index varies due to inhomogeneities, the optical paths are no longer straight lines, but are curved. This curving in optical paths can be used to create optical illusions like concentrating light at one region or the opposite, an area void of light. The question to answer is, How to obtain the optical properties of the materials that could enable us with a possibility of manipulating light at will?

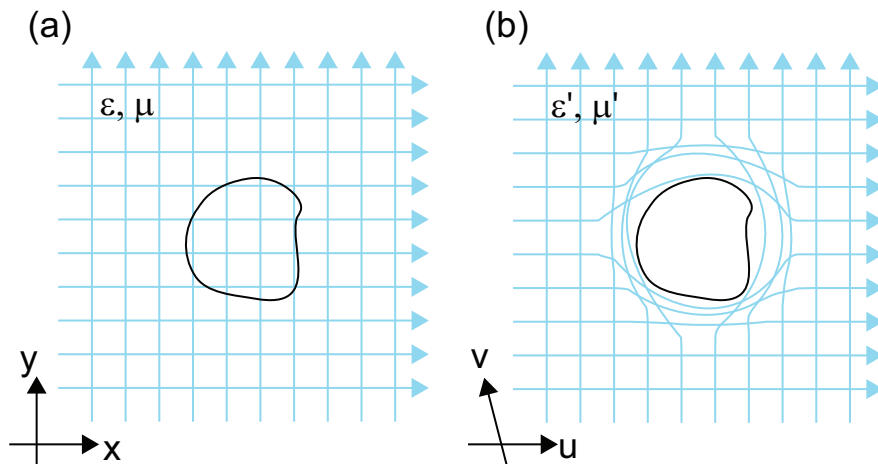


**Figure 1.1:** (a)Homogeneous optical space, and (b) Curved coordinate system representing the desirable light paths that evolve around an object.

The answer lies in the fact that the Maxwell's equations are invariant under co-ordinate transformations. For instance, Flat space when transformed in to a curved space, light rays precisely comply with the transformed space and they bend in accord (see Fig. 1.1). Mathematically, If  $f = f(x, y)$  is a transformation that maps a flat space into a curved space  $f = (u, v)$  then the transformation invariance assures that light rays track curved paths along the coordinate lines in an effective media with refraction index  $n' = \sqrt{\epsilon/\mu}$ . The light behaves in flat space filled with specifically designed effective refractive index precisely as it did in a curved space. This equivalence principle is the fundamental concept that accounts for achieving electromagnetic invisibility. This investigation of transformation of coordinates for obtaining spatial variations in optical parameters evolved in to a new area of study known as "Transformation Optics (TO)".

Now one can ask that are these materials (due to transformation) readily available in nature?. Well, the answer is a not always a *yes*. However, the developing trends in nanotechnology and sub-wavelength optics now opened doors for the development of such artificial materials—*electromagnetic metamaterials* or artificially engineered composite materials which possess wide range of optical properties which are difficult to find nature.

Recently, cloaking or invisibility has received significant attention from the scientific community. Several methods have been proposed to cloak macroscopic and microscopic objects: transformation optics (TO) and elimination of dipolar scattering are widely used. Both of these approaches are based on engineering a specific material shell(s) around an object to render it invisible for external observers.

TO places no limit on the size of the object being cloaked and in principle can provide perfect cloaking (both amplitude and phase of the incident wave being recovered), however this approach demands higher refractive indices and designs of complex materials. Furthermore, associated imperfections due to impedance mismatch and metal-dielectric losses affect substantially the device performance. New optical transformations must be investigated to determine the optimum material properties for achieving near-perfect invisibility.

On the other hand designs that rely on eliminating dipolar scattering are simpler and do not necessitate high refractive indices and magnetism. However, the so far considered in the literature designs are not generic and could cloak only objects whose sizes are less than and sometimes comparable to the wavelength of the impinging electromagnetic waves. Another important drawback in these systems is that each design is object dependent which makes it incapable to cloak objects with diverse optical properties. Therefore, it is important to design cloaking systems that can conceal large range of objects without putting any constraints on the objects geometrical or material properties.

This dissertation studies achieving cloaking by elimination of scattering from an arbitrary object. A set of transparency conditions independent of the object are derived for both cylindrically and spherically symmetric systems. Most importantly, as a material realization of our system, we propose a zero index-lowloss-tunable shell design based on metal-dielectric composite materials. Our results show that the proposed design can achieve cloaking across the entire optical spectral range and can decrease the scattering-cross section by a factor up to  $10^3$ .

## 1.2 Previous Work

Pendry *et al.* [41], using transformational optics (TO) designed an electro-magnetic metamaterial (EMM) shell that can bend light rays around an object. On the other hand, Leonhardt *et al.* [40] based on conformal mapping, designed an isotropic cloaking system with spatially dependent refractive index around an object, achieving invisibility in the ray approximation. Using TO, Lai *et al.* [49] designed a complementary media with an “anti-object” [50] to conceal an object placed at distance outside the cloaking system from electromagnetic radiation. McCall *et al.* [51], by transforming both space and time reported a spacetime cloak (STC) design that can hide events rather than objects. In contrast to spatial transformation cloaks which bend light around a finite region of space, STC works on the variation of the velocity of light before and after the occurrence of the event to be cloaked and its realization demands sophisticated temporal EMM designs.

Alternatively, Kerker [52, 53] was the first to explore the idea of elimination of dipolar scattering to render an object invisible. The approach consisted of a non-absorbing ellipsoidal particles encapsulated within a shell of specific geometrical and optical properties. More recently, Alú *et al.* [18] presented a similar study in the case of spherical and cylindrical geometries using plasmonic shells around an object. Zhou *et al.* [19] furthered this concept by using the idea of neutral inclusion to derive a generalized transparency condition in the quasi-static limit. However, all these studies place explicit geometrical and material constraints upon the shells of the cloaking system as well as the object. These constraints make the cloak crucially dependent on the optical and geometrical properties of the object and arguably limit its applicability.

### 1.3 Significance of this Work

The related literature does not address the problem of achieving a generic cloaking system i.e., a cloaking system that is independent of the object's material or geometric properties. This dissertation provides a design and the material specifications for a cloaking system to successfully make an arbitrary object invisible. The contributions of this dissertation are:

1. Derivation of transparency condition independent of the objects optical and geometrical properties in the quasistatic regime of operation.
2. A Proposal of realistic tunable low-loss shell design based on a composite metal-dielectric shell.
3. Demonstrate optical invisibility without the use of metamaterials and also underlines the role of zero-index materials in the general phenomenon of optical transparency.
4. Derivation of quasi-effective medium theory that determines the optical properties of multi-layered-composites beyond the quasi-static limit.
5. Derivation of transparency condition independent of the objects properties for eliminating arbitrary monopoles from the scattering amplitude.

The work done for this dissertation has contributed to the following publications. Object independent multishell cloaking device is presented in [17]. The quasi-effective medium theory is presented in [54].

#### **1.4 Organization of the Dissertation**

The remainder of the dissertation is organized as follows. Chapter 2 presents an overview of the electromagnetic scattering theory. It also presents the calculations of scattering fields for standard geometries such as a homogeneous cylinder and sphere. Chapter 3 studies many particulate systems and effective medium theories. In addition, an explicit expression for the effective optical properties of multishell cylinder beyond long wavelength limit are derived. Chapter 4 discusses the transparency condition for achieving object independent cloaking system design. Chapter 5 provides an analogous quantum cloaking design that can conceal an arbitrary object from matter waves.

## CHAPTER 2

### SCATTERING OF ELECTROMAGNETIC WAVES: A REVIEW

This chapter reviews the scattering characteristics of the electromagnetic waves in the presence of an obstacle. A formal theory for obtaining scattering cross section of an arbitrarily shaped particle using the integral representation of scattering equations is studied. In addition, scattering parameters of regularly shaped objects such as spheres, and cylinders are calculated, in the electrostatic and full wave regime. This topic is exhaustively covered in number of references [1, 2, 3, 4]. Here, we present only the essential summary.

#### 2.1 Time Harmonic Plane-Waves

Time harmonic plane waves or simply plane waves are an example of time harmonic fields whose time variation assumes sinusoidal form i.e.  $\sin(\omega t)$  or  $\cos(\omega t)$ , where  $\omega = 2\pi f$  is the angular frequency,  $f$  is the frequency and  $t$  is the time. In the exponential form this can written as  $e^{i\omega t}$  or  $e^{-i\omega t}$ , where  $i = \sqrt{-1}$ . In this thesis, we use  $e^{-i\omega t}$  to represent time variance in electromagnetic fields. The Electric field of an uniform plane waves is given by the following form:

$$\mathbf{E} = \mathbf{E}_0 \exp(i\mathbf{k} \cdot \mathbf{x} - i\omega t + \varphi), \quad (2.1)$$

where  $\mathbf{E}_0 = E_0 \hat{\mathbf{u}}_e$  is a constant vector, where  $E_0$  is the magnitude and  $\hat{\mathbf{u}}_e$  is the unit vector along the direction of the electric field.  $\varphi$  is the phase of the electric field.  $\mathbf{k}$  is the wave vector and may be complex with two real vectors  $\mathbf{k}'$  and  $\mathbf{k}''$

$$\mathbf{k} = \mathbf{k}' + i\mathbf{k}'', \quad (2.2)$$

on substituting Eq.(2.2) in Eq. (2.1), we obtain

$$\mathbf{E} = \mathbf{E}_0 \exp(-\mathbf{k}'' \cdot x) \exp(i\mathbf{k}' \cdot \mathbf{x} - i\omega t + \varphi). \quad (2.3)$$

As the magnetic field vector is perpendicular to the electric field vector, the corresponding magnetic field is given by

$$\mathbf{H} = \frac{1}{z_0} \mathbf{k} \times \mathbf{E}, \quad (2.4)$$

where  $z_0 = 377\Omega$  is the intrinsic impedance.

The time-averaged power per unit area is given by the Pointing vector of the plane wave

$$\mathbf{S} = \frac{1}{2} \Re \{ \mathbf{E} \times \mathbf{H}^* \}, \quad (2.5)$$

where  $\mathbf{H}^*$  is the complex conjugate of  $\mathbf{H}$ . The magnitude of  $\mathbf{S}$  is called the irradiance which has dimensions of energy per unit area and time.

## 2.2 Scattering of Electromagnetic Radiation

Figure 2.1 illustrates the general problem of scattering of electromagnetic radiation by an obstacle. An object is illuminated by an incident time varying electric field  $\mathbf{E}_i$ . A part of the incident radiation is absorbed by the object  $\mathbf{E}_0$  and the remaining is re-radiated in to the background as scattered wave  $\mathbf{E}_s$ .

### 2.2.1 Cross Section and Scattering Amplitude

Consider a plane polarized electromagnetic wave traveling in the direction  $\hat{\mathbf{k}}_i$  impinging on a particle with permittivity  $\varepsilon_0(\mathbf{r})$  in a homogeneous space of permittivity  $\varepsilon_e$  and permeability  $\mu_e$  (see Fig. 2.1) The incident electric and magnetic fields are given by

$$\mathbf{E}_i(\mathbf{r}) = \hat{\mathbf{e}}_i \exp(ik_e \hat{\mathbf{k}}_i \cdot \mathbf{r}) \quad (2.6)$$

$$\mathbf{H}_i = \frac{1}{\eta_0} \hat{\mathbf{k}}_i \times \mathbf{E}_i \quad (2.7)$$

where  $\mathbf{r}$  is the position vector,  $k_e = \omega \sqrt{\varepsilon_e \mu_e} = 2\pi/\lambda$  is the wave vector,  $\omega$  is the frequency,  $\lambda$  is the wavelength,  $\eta_0$  is the free space impedance and  $\hat{\mathbf{e}}_i$  is the unit vector along the direction of the electric field. The scattered field behaves as a spherical wave

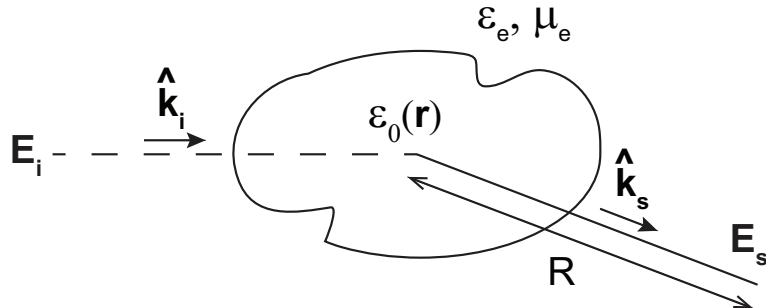


**Figure 2.1:** Scattering from an object of permittivity  $\varepsilon_0(\mathbf{r})$ .  $\mathbf{E}_i$ ,  $\mathbf{E}_s$  are the incident and scattered fields in the direction of  $\hat{\mathbf{k}}_i$ ,  $\hat{\mathbf{k}}_s$  respectively.

in the far-field region i.e.  $R > D^2/\lambda$  (where  $D$  is the physical dimension of the object) and the scattered electric and magnetic fields are given by

$$\mathbf{E}_s = \hat{\mathbf{e}}_s \mathbf{F}(\hat{\mathbf{k}}_i, \hat{\mathbf{k}}_s) \frac{\exp(ik_e R)}{R} \quad (2.8)$$

$$\mathbf{H}_s = \frac{1}{\eta_0} \hat{\mathbf{k}}_s \times \mathbf{E}_s \quad (2.9)$$

where  $\mathbf{F}(\hat{\mathbf{k}}_i, \hat{\mathbf{k}}_s)$  is the scattering amplitude and  $\hat{\mathbf{e}}_s$  is perpendicular to  $\hat{\mathbf{k}}_s$ . In the near field i.e.  $R < D^2/\lambda$  the scattered field assumes complex amplitude and phase forms due to the interference of radiation from the different regions of the object.

The incident and scattered power flux per unit area are given by

$$\mathbf{S}_i = \frac{1}{2}(\mathbf{E}_i \times \mathbf{H}_i^*) = \frac{|E_i|^2}{2\eta_0} \hat{\mathbf{k}}_i \quad (2.10)$$

$$\mathbf{S}_s = \frac{1}{2}(\mathbf{E}_s \times \mathbf{H}_s^*) = \frac{|E_s|^2}{2\eta_0} \hat{\mathbf{k}}_s \quad (2.11)$$

substituting Eq. (2.8) in to Eq. (2.11) yields

$$\mathbf{S}_s = \frac{|E_s|^2}{2\eta_0} \hat{\mathbf{k}}_s = \frac{|\mathbf{F}(\hat{\mathbf{k}}_i, \hat{\mathbf{k}}_s)|^2}{2\eta_0 R^2} \hat{\mathbf{k}}_s \quad (2.12)$$

The differential scattered power ( $dP_s$ ) through the differential area  $dA$  subtended by the differential solid angle  $d\Omega$  in spherical coordinates is:

$$dP_s = |\mathbf{S}_s| dA = |\mathbf{S}_s| R^2 d\Omega. \quad (2.13)$$

substituting Eq. (2.12) in to Eq. (2.13) yields

$$dP_s = \frac{|\mathbf{F}(\hat{\mathbf{k}}_i, \hat{\mathbf{k}}_s)|^2}{2\eta_0} d\Omega, \quad (2.14)$$

Using the definition of incident power in Eq. (2.10), Eq. (2.14) can be rewritten as

$$\frac{dP_s}{|\mathbf{S}_i|} = |\mathbf{F}(\hat{\mathbf{k}}_i, \hat{\mathbf{k}}_s)|^2 d\Omega, \quad (2.15)$$

The dimensions of the above equation is area. We define the differential scattering cross-section as

$$\sigma_d = \lim_{R \rightarrow \infty} \frac{R^2 S_s}{S_i} = |\mathbf{F}(\hat{\mathbf{k}}_i, \hat{\mathbf{k}}_s)|^2, \quad (2.16)$$

integrating Eq. (2.16) over all angles surrounding the object yields scattering cross section  $\sigma_s$  which is the amount of scattering produced by the cross-section of an object

$$\sigma_s = \int d\Omega \sigma_d = \int_v d\Omega |\mathbf{F}(\hat{\mathbf{k}}_i, \hat{\mathbf{k}}_s)|^2. \quad (2.17)$$

Alternatively, one can define scattering cross-section as

$$\sigma_s = \frac{\int_{S_0} \frac{1}{2} \Re \{ \mathbf{E}_s \times \mathbf{H}_s^* \} \cdot d\mathbf{a}}{|S_i|}, \quad (2.18)$$

where  $S_0$  is an the arbitrary surface enclosing the object and  $d\mathbf{a}$  is the differential surface are directed outward from the surface. Similarly, the total power absorbed by the object or the absorption cross section can be defined as:

$$\sigma_a = -\frac{\int_{S_0} \frac{1}{2} \Re \{ \mathbf{E} \times \mathbf{H}^* \} \cdot d\mathbf{a}}{|S_i|}. \quad (2.19)$$

The total cross-section or the extinction cross section  $\sigma_e$  is defined as the sum of both scattering and absorption cross sections

$$\sigma_e = \sigma_s + \sigma_a. \quad (2.20)$$

The *albedo* of an object is defined is given by

$$\varpi = \frac{\sigma_s}{\sigma_e} = \frac{1}{\sigma_e} \int d\Omega |\mathbf{F}(\hat{\mathbf{k}}_i, \hat{\mathbf{k}}_s)|^2 = \frac{1}{4\pi} \int d\Omega p(\hat{\mathbf{k}}_i, \hat{\mathbf{k}}_s), \quad (2.21)$$

where  $p(\hat{\mathbf{k}}_i, \hat{\mathbf{k}}_s)$  is called the phase function. The absorption, scattering and the total cross sections can be normalized by the geometrical cross section of the object  $\sigma_g$  are called the *efficiencies*:

$$Q_a = \frac{\sigma_a}{\sigma_g}, \quad Q_s = \frac{\sigma_s}{\sigma_g}, \quad Q_e = \frac{\sigma_e}{\sigma_g}, \quad (2.22)$$

where  $Q_a$ ,  $Q_s$  and  $Q_t$  are absorption, scattering and total efficiencies, respectively. The total or extinction cross section of the scatterer is related to the forward scattering

amplitude by the *Optical theorem* or the *Forward scattering theorem*

$$\sigma_e = \frac{4\pi}{k} \Im \left\{ \mathbf{F}(\hat{\mathbf{k}}_{ei}, \hat{\mathbf{k}}_s) \right\} \cdot \hat{\mathbf{e}}_i, \quad (2.23)$$

where  $\hat{\mathbf{e}}_i$  is the incident wave polarization.

### 2.2.2 Integral representations of scattering amplitude

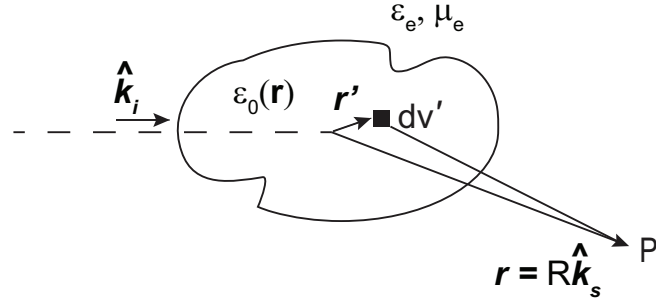


**Figure 2.2:** Scattering from an object of permittivity  $\varepsilon(\mathbf{r})$  with arbitrary shape and finite size.  $R = |\mathbf{r} - \mathbf{r}'|$  is the distance between  $\mathbf{r}'$  and the observation point  $P$ .

Let us consider a dielectric object with permittivity  $\varepsilon_0(\mathbf{r})$  of volume  $V$  present in a medium of permittivity  $\varepsilon_e$ . The scattered far-field from the object is given by (see appendix for derivation):

$$\mathbf{E}_s = -\frac{k_e^2 \exp(ik_e R)}{4\pi\varepsilon_e R} V(\varepsilon_0 - \varepsilon_e) \hat{\mathbf{k}}_s \times (\hat{\mathbf{k}}_s \times \mathbf{E}), \quad (2.24)$$

where  $R = |\mathbf{r} - \mathbf{r}'|$  is the distance between  $\mathbf{r}'$  and the observation point  $P$ . For an arbitrary particle as shown in Fig 2.2, the scattered field due to a volume element  $dv'$  is given by [4]

$$d\mathbf{E}_s = -\frac{k_e^2 \exp(ik_e R)}{4\pi\varepsilon_e R} dv' (\varepsilon_0(\mathbf{r}) - \varepsilon_e) \hat{\mathbf{k}}_s \times (\hat{\mathbf{k}}_s \times \mathbf{E}), \quad (2.25)$$

If the distance between the object and the observer is substantial then  $|\mathbf{r} - \mathbf{r}'| \simeq R - \mathbf{r}' \cdot \hat{\mathbf{k}}_s$  and  $\exp(ik_e |\mathbf{r} - \mathbf{r}'|) = \exp(ik_e R - ik_e \mathbf{r}' \cdot \hat{\mathbf{k}}_s)$  and now integrating Eq. (2.25) over the

volume gives

$$\mathbf{E}_s = \mathbf{F}(\hat{\mathbf{k}}_i, \hat{\mathbf{k}}_s) \frac{\exp(ik_e R)}{R} \quad (2.26)$$

$$= -\frac{k_e^2 \exp(ik_e R)}{4\pi\varepsilon_e R} \hat{\mathbf{k}}_s \times \left( \hat{\mathbf{k}}_s \times \int_v dv' (\varepsilon_0(\mathbf{r}') - \varepsilon_e) \mathbf{E} \exp(-ik\mathbf{r}' \cdot \hat{\mathbf{k}}_s) \right). \quad (2.27)$$

Equation (2.27) is the exact solution of the scattering amplitude of an arbitrarily shape particle with inhomogeneous permittivity. However, the internal electric field  $\mathbf{E}$  is unknown and can be obtained by solving Maxwell's Equations. However, for simpler geometries (such as spheres, cylinders, and ellipsoids) and small particles i.e. particles whose dimensions are smaller than the impinging wavelength one can use Rayleigh scattering theory.

### 2.3 Rayleigh Scattering

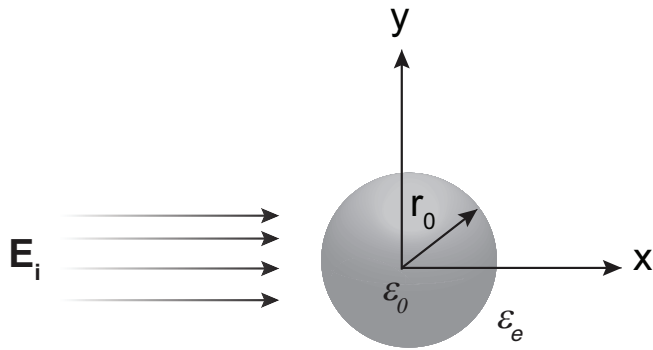


**Figure 2.3:** Dielectric Sphere of permittivity  $\varepsilon_0$  in uniform electric field  $\mathbf{E}_i$ .

Consider a dielectric sphere of permittivity  $\varepsilon_0$  illuminated by an electric field  $\mathbf{E}_i$  as shown in Fig. 2.3. As the size of the sphere is much smaller than the incident wavelength the field inside the sphere can be treated as a static field. In such a case, the electric potentials inside and outside the sphere are solutions of the Laplace

equation and can be written as [5]:

$$\varphi = \sum_{n=1}^{\infty} (A_n r^n + S_n r^{-n}) P_n(\cos \theta), \quad (2.28)$$

where  $A_n$ ,  $S_n$  are the amplitude coefficients and  $P_n(\cos \theta)$  are the associated Legendre polynomials. On applying appropriate boundary conditions, the electric field inside the sphere is given by

$$\mathbf{E} = \frac{3\epsilon_e}{\epsilon_0 + 2\epsilon_e} \mathbf{E}_i, \quad (2.29)$$

substituting Eq. (2.29) in Eq. (2.27) and simplifying yields the scattering amplitude:

$$\mathbf{F}(\hat{\mathbf{k}}_i, \hat{\mathbf{k}}_s) = \frac{3}{4\pi} k_e^2 \frac{\epsilon_0 - \epsilon_e}{\epsilon_0 + 2\epsilon_e} V \sin(\chi) \quad (2.30)$$

where  $\chi$  is the angle between  $\hat{\mathbf{k}}_i$  and  $\hat{\mathbf{k}}_s$ . The polarizability i.e., the ability of the sphere to be polarized is given by  $\alpha = 3V\epsilon_e(\epsilon_0 - \epsilon_e)/(\epsilon_0 + 2\epsilon_e)$ . By substituting Eq. (2.30) in Eq. (2.16) one can obtain differential scattering cross section:

$$\sigma_d = |\mathbf{F}(\hat{\mathbf{k}}_i, \hat{\mathbf{k}}_s)|^2 = \left( \frac{3}{4\pi} \right)^2 k_e^4 \left| \frac{\epsilon_0 - \epsilon_e}{\epsilon_0 + 2\epsilon_e} \right|^2 V^2 \sin^2(\chi), \quad (2.31)$$

Using Eq. (2.17) the scattering cross section of the sphere is given by

$$\sigma_s = \int d\Omega \sigma_d = \int_v d\Omega \left( \frac{3}{4\pi} \right)^2 k_e^4 \left| \frac{\epsilon_0 - \epsilon_e}{\epsilon_0 + 2\epsilon_e} \right|^2 V^2 \sin^2(\chi) \quad (2.32)$$

$$= \frac{8\pi}{3} k_e^4 r_0^6 \left| \frac{\epsilon_0 - \epsilon_e}{\epsilon_0 + 2\epsilon_e} \right|^2, \quad (2.33)$$

If we compare the scattering cross section in Eq. (2.33) with geometric cross section

$\sigma_g = \pi r_0^2$  we obtain the Rayleigh equation:

$$\sigma_s = \frac{8\pi}{3} (k_e r_0)^4 \left| \frac{\epsilon_0 - \epsilon_e}{\epsilon_0 + 2\epsilon_e} \right|^2, \quad (2.34)$$

A similar solution can be obtained for a homogeneous infinite cylinder

$$\sigma_s = \frac{\pi^2}{4} (k_e r_0)^3 \left| \frac{\varepsilon_0 - \varepsilon_e}{\varepsilon_0 + \varepsilon_e} \right|^2, \quad (2.35)$$

## 2.4 Mie Theory

In 1908, Mie *et al.*[8] reported an exact solution for the scattering of a plane electromagnetic wave by an isotropic, homogeneous sphere.

Consider a sphere of permittivity  $\varepsilon_0$  located at the origin of the spherical coordinate system and is illuminated by a plane wave propagating in  $+z$  direction and polarized in the  $x-$  direction (see Fig. 2.3):

$$\mathbf{E}_i = \exp(ik_e z) \hat{\mathbf{x}} \quad (2.36)$$

Instead of directly dealing with the vector equations [6, 5, 2] in spherical co-ordinates one can explicitly define electromagnetic fields in terms of two scalar functions  $\Pi_1$  and  $\Pi_2$  called the Debye potentials which are radial components of the electric and magnetic hertz vectors given by [1, 6, 7]

$$\Pi_e = \Pi_1 \hat{\mathbf{r}} \quad (2.37)$$

$$\Pi_m = \Pi_2 \hat{\mathbf{r}} \quad (2.38)$$

In terms of the Debye potentials the electric and magnetic fields are given by

$$\mathbf{E} = \nabla \times \nabla \times (r \Pi_1 \hat{\mathbf{r}}) + i\omega \mu_e \nabla \times (r \Pi_2 \hat{\mathbf{r}}) \quad (2.39)$$

$$\mathbf{H} = \nabla \times \nabla \times (r \Pi_2 \hat{\mathbf{r}}) - i\omega \varepsilon_e \nabla \times (r \Pi_1 \hat{\mathbf{r}}) \quad (2.40)$$

The incident field in Eq. (2.36) can be derived from two scalar functions and is given by

$$r\Pi_1^i = \frac{1}{k_e^2} \sum_{n=1}^{\infty} i^{n-1} \frac{(2n+1)}{n(n+1)} \psi_n(k_e r) P_n^1(\cos\theta) \cos\varphi \quad (2.41)$$

$$r\Pi_2^i = \frac{1}{\eta_0 k_e^2} \sum_{n=1}^{\infty} i^{n-1} \frac{(2n+1)}{n(n+1)} \psi_n(k_e r) P_n^1(\cos\theta) \cos\varphi \quad (2.42)$$

where  $\psi_n(kr)$  are Riccati-Bessel functions. Similarly, the expression for the scattered fields  $r > r_0$  are given by

$$r\Pi_1^s = \frac{1}{k_e^2} \sum_{n=1}^{\infty} i^{n-1} \frac{(2n+1)}{n(n+1)} a_n \zeta_n(k_e r) P_n^1(\cos\theta) \cos\varphi \quad (2.43)$$

$$r\Pi_2^s = \frac{1}{\eta_0 k_e^2} \sum_{n=1}^{\infty} i^{n-1} \frac{(2n+1)}{n(n+1)} b_n \zeta_n(k_e r) P_n^1(\cos\theta) \cos\varphi \quad (2.44)$$

where  $\zeta_n(k_e r)$  are the Riccati-Henkels functions. The fields inside the sphere ( $r < r_0$ ) are

$$r\Pi_1^{in} = \frac{1}{k_0^2} \sum_{n=1}^{\infty} i^{n-1} \frac{(2n+1)}{n(n+1)} c_n \psi_n(k_0 r) P_n^1(\cos\theta) \cos\varphi \quad (2.45)$$

$$r\Pi_2^{in} = \frac{1}{\eta k_0^2} \sum_{n=1}^{\infty} i^{n-1} \frac{(2n+1)}{n(n+1)} d_n \psi_n(k_0 r) P_n^1(\cos\theta) \cos\varphi \quad (2.46)$$

The boundary conditions are that the tangential components of electric and magnetic field be continuous across the boundary  $r = r_0$ . In terms of the Debye potentials we get, continuity of  $m^2\Pi_1$ ,  $(\partial/\partial r)(r\Pi_1)$ ,  $\Pi_2$  and  $(\partial/\partial r)(r\Pi_1)$ . Applying these boundary conditions, we get

$$a_n = \frac{\psi_n(\alpha) \psi'_n(\beta) - m\psi_n(\beta) \psi'_n(\alpha)}{\zeta_n(\alpha) \psi'_n(\beta) - m\psi_n(\beta) \zeta'_n(\alpha)} \quad (2.47)$$

$$b_n = \frac{m\psi_n(\alpha) \psi'_n(\beta) - \psi_n(\beta) \psi'_n(\alpha)}{m\zeta_n(\alpha) \psi'_n(\beta) - \psi_n(\beta) \zeta'_n(\alpha)} \quad (2.48)$$

where  $\alpha = k_e r_0$ ,  $\beta = m k_e r_0$  and  $m$  is the relative refractive index. The scattering cross section is given by

$$Q_s = \frac{\sigma_s}{\pi r_0^2} = \frac{2}{\alpha^2} \sum_{n=1}^{\infty} (2n+1) (|a_n|^2 + |b_n|^2), \quad (2.49)$$

Using the optical theorem the total cross section is

$$Q_e = \frac{\sigma_e}{\pi r_0^2} = \frac{2}{\alpha^2} \sum_{n=1}^{\infty} (2n+1) \Re \{a_n + b_n\}. \quad (2.50)$$

Figure 2.4 depicts the extinction efficiency of the water droplets as a function of size

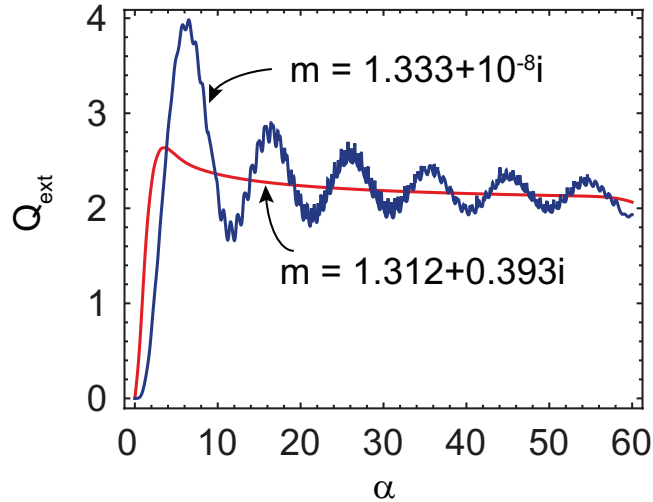


**Figure 2.4:** Extinction efficiency of a spherical water droplet at  $\lambda = 0.55\mu m$  (blue) and  $\lambda = 20\mu m$  (red).

parameter  $\alpha$ . As can be seen, as the size of the water droplets increases the extinction efficiency approaches the limiting value 2. This is twice as large as predicted by the geometrical optics, and is known as the *extinction paradox* [1, 2, 9]. The most cited explanation of the paradox is due to Ref. [1] which uses a combination of geometrical optics and diffraction theory.

The amount of energy removed from the beam due to reflection, refraction and absorbtion of the rays on a spherical particle contribute an extinction cross section equal to the geometrical cross section of the object *i.e.*  $\sigma_e = \sigma_g$ . In addition, the rays in the near vicinity of the particle undergo diffraction at the sphere boundary, rays that, according to geometrical optics have passed unperturbed, remove an amount of energy equal to an opaque disk with same size and shape as  $\sigma_g$ . An alternative explanation of destructive interference in the shadow region of the scatterer is reported by Brillouin *et. al.* [9].

#### 2.4.1 Intensity and Polarization of the Scattered Light

In the far-field *i.e.*  $\alpha = k_e r \gg n$  where  $n$  is the order of the Riccati-Bessel function, the radial component of the electric  $E_r$  and magnetic field  $H_r$  decay with  $\lambda/r^2$  and can be neglected. The transverse components of the field vectors are given by

$$E_\phi = -\frac{i \exp(-ik_e r)}{k_e r} \sin \phi S_1, \quad (2.51)$$

$$E_\theta = \frac{i \exp(-ik_e r)}{k_e r} \cos \phi S_2, \quad (2.52)$$

where  $E_\theta$  and  $E_\phi$  are complex and elliptically polarized. The corresponding magnetic fields can be obtained using maxwell's equations. The amplitudes  $S_1$  and  $S_2$  are given by

$$S_1 = \sum_{n=1}^{\infty} \frac{2n+1}{n(n+1)} a_n \pi_n(\cos \theta) + b_n \tau_n(\cos \theta), \quad (2.53)$$

$$S_2 = \sum_{n=1}^{\infty} \frac{2n+1}{n(n+1)} a_n \tau_n(\cos \theta) + b_n \pi_n(\cos \theta), \quad (2.54)$$

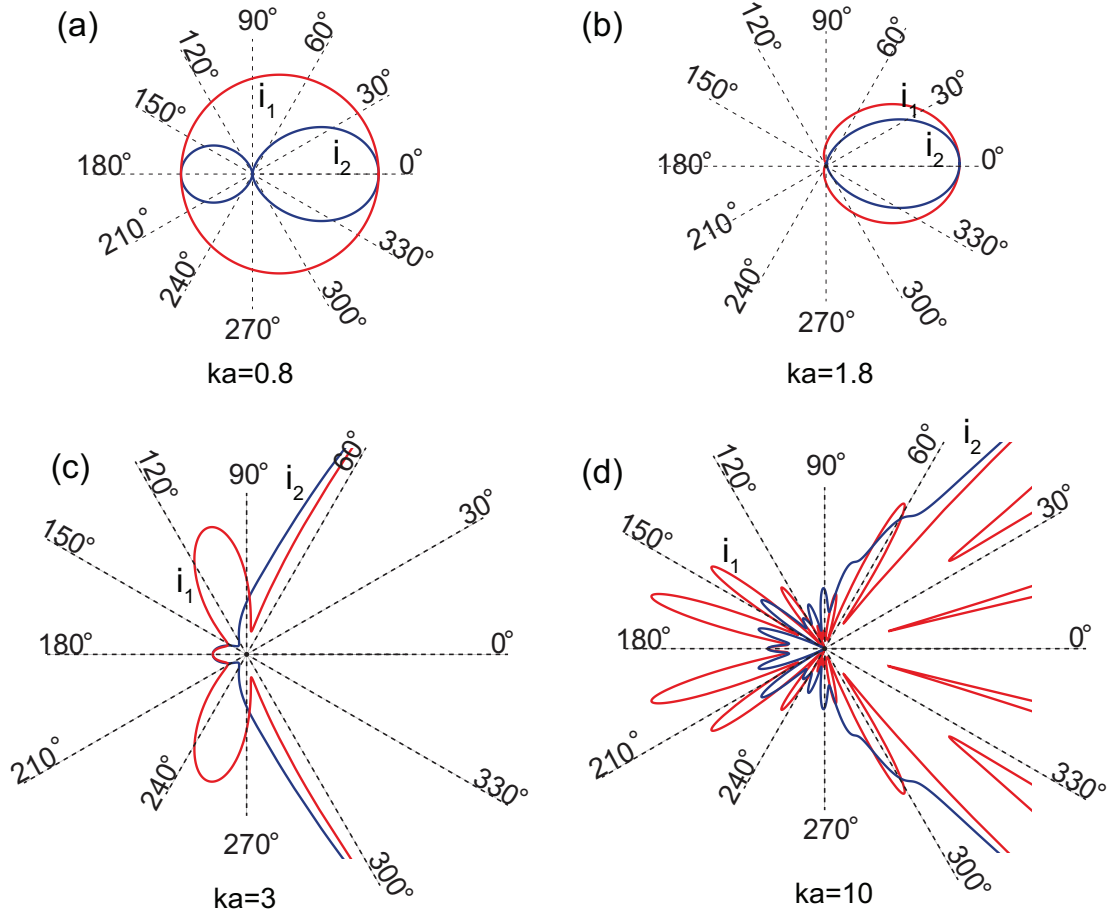


**Figure 2.5:** Scattering intensity as a function scattering angle for a spherical water droplet of refractive index  $m = 1.33 + i10^{-8}$  at  $\omega = 2.25\text{eV}$  in air for particle sizes (a)  $0.07\mu\text{m}$ , (b)  $1.6\mu\text{m}$ , (c)  $0.26\mu\text{m}$ , and (d)  $0.9\mu\text{m}$

where  $\pi_n(\cos \theta) = P_n^{(1)}(\cos \theta)/\sin \theta$  and  $\tau_n = (\partial/\partial\theta)P_n^{(1)}(\cos \theta)$ . Now, the intensity of scattered waves polarized along  $\theta$  and  $\phi$  is given by

$$I_\phi = \frac{\lambda^2}{4\pi^2 r^2} |S_1|^2 \sin^2 \phi = \frac{\lambda^2}{4\pi^2 r^2} i_1 \sin^2 \phi, \quad (2.55)$$

$$I_\theta = \frac{\lambda^2}{4\pi^2 r^2} |S_2|^2 \cos^2 \phi = \frac{\lambda^2}{4\pi^2 r^2} i_2 \cos^2 \phi, \quad (2.56)$$

where  $i_1$  and  $i_2$  are called polarization intensity functions which are parallel and perpendicular to the scattering plane, respectively. The state of polarization of electromagnetic radiation is conveniently described by a set of values called the stokes

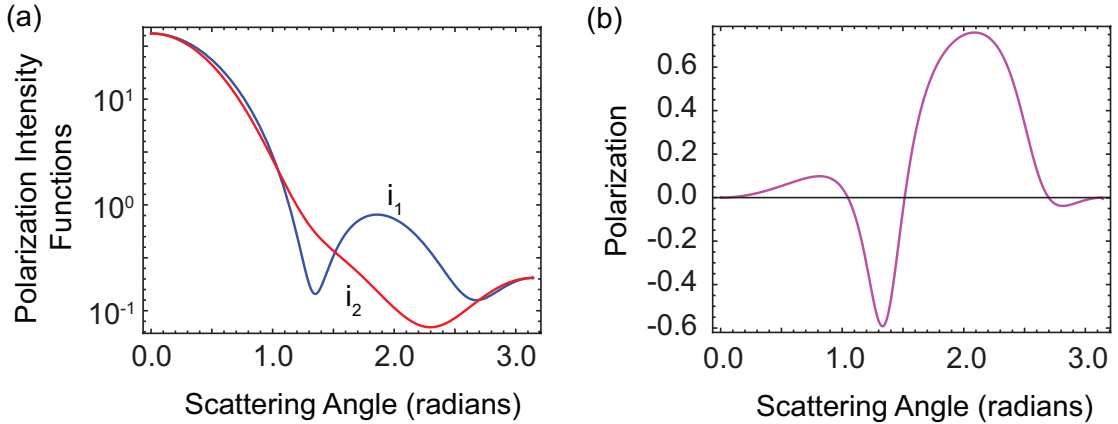


**Figure 2.6:** (a) Scattering intensity functions  $i_1$  and  $i_2$  and (b) Polarization as function of scattering angle for a spherical water droplet of refractive index  $m = 1.33 + i10^{-8}$  in air.

parameters [10]. The relationship between the incident and the scattered stokes parameters is given by

$$\begin{pmatrix} I_s \\ Q_s \\ U_s \\ V_s \end{pmatrix} = \frac{1}{k^2 r^2} \begin{pmatrix} S_{11} & S_{12} & 0 & 0 \\ S_{12} & S_{11} & 0 & 0 \\ 0 & 0 & S_{33} & S_{34} \\ 0 & 0 & -S_{34} & S_{33} \end{pmatrix} \begin{pmatrix} I_i \\ Q_i \\ U_i \\ V_i \end{pmatrix} \quad (2.57)$$

where

$$S_{11} = \frac{1}{2}(|S_2|^2 + |S_1|^2), \quad (2.58)$$

$$S_{12} = \frac{1}{2}(|S_2|^2 - |S_1|^2), \quad (2.59)$$

$$S_{33} = \frac{1}{2}(S_2^* S_1 + S_2 S_1^*), \quad (2.60)$$

$$S_{34} = \frac{i}{2}(S_1 S_2^* - S_2 S_1^*), \quad (2.61)$$

and  $S_{11} = S_{12}^2 + S_{33}^2 + S_{34}^2$ . For unpolarized incident light, the Stokes parameters of the scattered light are

$$I_s = S_{11}I_i, \quad Q_s = S_{12}I_i, \quad U_s = V_s = 0, \quad (2.62)$$

and the polarization is

$$P = -\frac{S_{12}}{S_{11}} = \frac{i_1 - i_2}{i_1 + i_2}, \quad (2.63)$$

$P$  is positive or negative depending on the scattered light is partially polarized perpendicular or parallel to the scattering plane respectively. The degree of polarization is given by  $|P| \leq 1$ .

Figures 2.5 and 2.6 (a) shows polar and normal plots of the scattering intensity functions versus scattering angle, respectively. As can be seen from Fig. 2.5, the forward scattering is dominant even in case of very small spherical water droplets (as small as  $0.26\mu m$ ). However, as the particle size increase (see Fig. 2.5 (d)) forward scattering becomes substantial. We have magnified the polar plots for comparing the magnitude of the backward scattering and forward scattering lobes.

#### 2.4.2 Small-Particle Limit

If the size of the sphere is much smaller than the incident wave length i.e.,  $k_e r_0 \ll 1$  the Riccati-Bessel functions in Eq. (2.47) and Eq. (2.48) can be expanded as a power series in the argument that converges very rapidly. The scattering coefficients  $a_n$  and  $b_n$  are approximately

$$a_n = i \frac{n+1}{n(2n+1)} \frac{\alpha^{2n+1}}{1 \cdot 3^2 \dots (2n-1)^2} u_n \frac{m^2 - v_n}{m^2 + [(n+1)/n]w_n} \quad (2.64)$$

$$b_n = -i \frac{n+1}{n(2n+1)} \frac{\alpha^{2n+1}}{1 \cdot 3^2 \dots (2n-1)^2} u_n \frac{1 - v_n}{1 + [(n+1)/n]w_n} \quad (2.65)$$

where  $u_n$ ,  $v_n$  and  $w_n$  are series in terms  $\alpha^2$  and  $\beta^2$ .

For  $n = 1$  the Eq. (2.64) and Eq. (2.65) are reduced to

$$a_1 = i \frac{2}{3} \left( \frac{m^2 - 1}{m^2 + 2} \right) \alpha^3 \quad (2.66)$$

$$b_1 = i \frac{1}{45} (m^2 - 1) \alpha^5 \quad (2.67)$$

The remaining coefficients are proportional to still higher powers of  $\alpha$ . For small  $\alpha$  and  $m$  the dominant term is the dipolar term or  $a_1$ .

## 2.5 Scattering from a Circular Cylinder

### 2.5.1 Normal Incidence

Consider an plane transfer magnetic (TM) wave traveling in  $x$ -direction impinging on an infinite cylinder of permittivity  $\epsilon_0$  with its axes along  $z$ -axis. The incident field is given by

$$H_z^i = \exp(ikx) \quad (2.68)$$

Jacobi-Anger expansion allows us to expand exponential trigonometric functions in

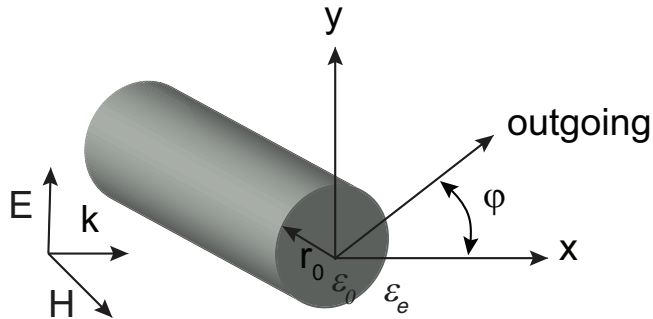


**Figure 2.7:** Circular cylinder of permittivity  $\epsilon_0$  illuminated by a plane wave. Magnetic field  $\mathbf{H}$  is parallel to the axes of the cylinder.

basis of their harmonics. Thus, equation (2.50) can be written as

$$\exp(ikr \cos \varphi) = \sum_{n=-\infty}^{\infty} i^n J_n(k_e r) \exp(in\varphi) \quad (2.69)$$

where  $J_n$  is the Bessel function of the first kind, and  $k_e = \omega \sqrt{\varepsilon_e \mu_e}$  is wave vector in the host medium. The outgoing wave from the cylinder is a typical cylindrical wave which varies as  $\exp(ikr/\sqrt{r})$  in the far-field. The appropriate function that satisfies such condition is  $H_n^{(1)}(k_e r) = J_n(k_e r) + iN_n(k_e r)$  which is called the Hankel function of first kind. Thus the scattered wave is of the form:

$$H_z^s = \sum_{n=-\infty}^{\infty} i^n S_n J_n(k_e r) \exp(in\varphi) \quad (2.70)$$

The wave inside the cylinder is represented by the Bessel function of the kind  $J_n(kr)$  to avoid the singularity the origin

$$H_z^0 = \sum_{n=-\infty}^{\infty} i^n A_n J_n(k_e r) \exp(in\varphi) \quad (2.71)$$

$A_n$  and  $S_n$  are arbitrary constants determined by the boundary conditions that the normal and tangential components i.e.,  $E_r = -i\omega\mu/k^2 r \partial/\partial\varphi$  and  $E_\varphi = i\omega\mu/k^2 \partial/\partial r$  be continuous at  $r = a$ . Thus the scattering coefficient is given by

$$S_n^m = \frac{J_n(\alpha) J'_n(m\alpha) - m J_n(m\alpha) J'_n(\alpha)}{H_n^{(1)}(\alpha) J'_n(m\alpha) - m J_n(m\alpha) H_n^{(1)'}(\alpha)} \quad (2.72)$$

Using equation (2.13) the scattering cross section is:

$$\sigma_s = \frac{4}{k} \sum_{m=-\infty}^{\infty} |S_n|^2 \quad (2.73)$$

Similar arguments apply for the transverse electric (TE) waves i.e. when electric field vector is parallel to the axis of the cylinder. The scattering coefficient in this case is

given by

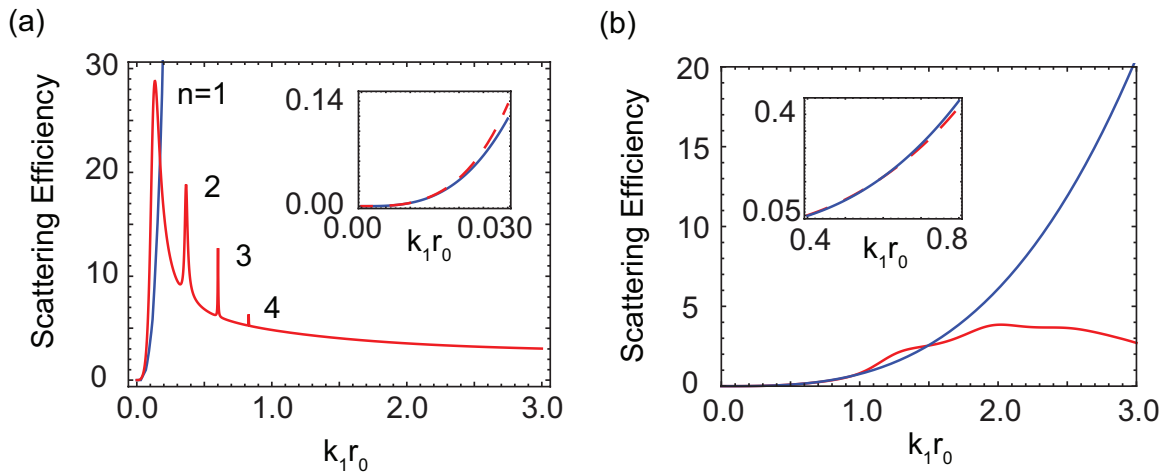
$$S_n^e = -\frac{J_n(\alpha)J'_n(m\alpha) - mJ_n(m\alpha)J'_n(\alpha)}{H_n^{(1)}(\alpha)J'_n(m\alpha) - mJ_n(m\alpha)H_n^{(1)'}(\alpha)} \quad (2.74)$$

### 2.5.2 Small Dielectric Cylinders

If the diameter of the cylinder is much smaller than the incident wave length i.e.,  $ka \ll 1$  the Bessel functions in equation (2.42) and equation (2.43) can be expanded as a power series in the argument that converges very rapidly. The scattering coefficient  $S_n$  is approximately given by

$$S_0 = \frac{\pi\alpha^4}{32}(m^2 - 1) \quad (2.75)$$

$$S_1 = \frac{\pi\alpha^2}{4} \left( \frac{m^2 - 1}{m^2 + 1} \right) \quad (2.76)$$



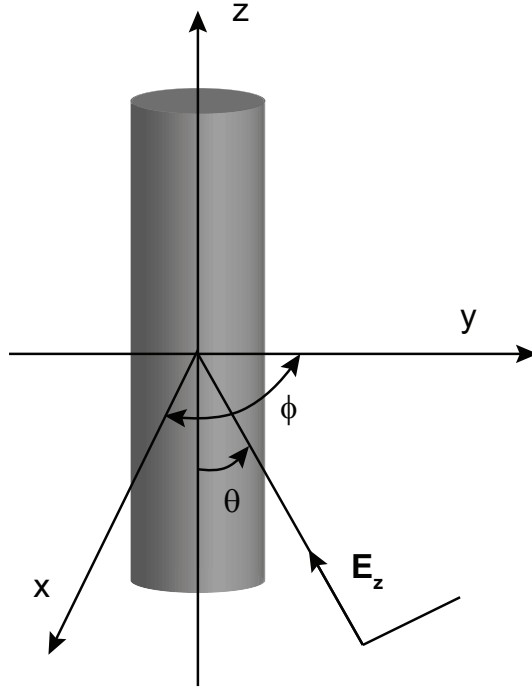
**Figure 2.8:** Comparison of scattering efficiency of a homogenous (a) metallic cylinder and (b) dielectric cylinder calculated using the exact solution (Eq. 2.67) and the Rayleigh scattering theory (Eq. 2.30). Insert shows the applicability of the Rayleigh theory for very small particles.

Figure. 2.8 illustrates the scattering efficiency of a metallic and a dielectric cylinder as a function of the size parameter. The permittivity of the metallic cylinder in Fig. 2.8(a) is given by the Drude formula (see appendix for details) with out dissipation. As can be seen in the Fig. 2.8(a), the dipolar resonance ( $n = 1$ ) dominates when the size of the particles is very small. However, as the size of the cylinder increases, one can observe the contribution of higher order multipoles ( $n = 2, 3, 4$ ) to the scattering efficiency. Similarly, for a dielectric particle the scattering efficiency increases with size factor and reaches the limiting value of 2 as in the case of a dielectric sphere. Scattering efficiency due to rayleigh scattering is also shown in the Fig. 2.8 for the sake of comparison. One can notice a drastic difference in the scattering efficiency predicted by Eq. (2.35) at large particle sizes. Insert in Fig. 2.8 shows the validity of the Rayleigh scattering theory is very small particle size factors, for instance  $k_e r_0 \approx 0.03$  in case of a metallic cylinder (see insert in Fig. 2.8(a)).

### 2.5.3 Oblique Incidence

Light scattering by a circular cylinder at oblique incidence was first discussed by Wait [11, 12]. Farone *et al* obtained computationally convenient solution and also extended their work to radially inhomogeneous cylinders [13]. An extensive computational study on infinite cylinders at oblique incidence was reported by Kerker *et al* [14].

Consider a cylinder with permittivity  $\epsilon_0$  and permeability  $\mu_0$  and radius  $r_0$  with its axis along the  $z$ -axis (see figure 1) in medium with permittivity  $\epsilon_e$  and permeability  $\mu_e$ . The cylinder is illuminated by a  $E$ - polarized (electric field vector is



**Figure 2.9:** Cylinder of permittivity  $\varepsilon_0$  and  $\mu_0$  illuminated by an  $E$ -polarized wave at oblique incidence.

parallel to the  $\phi = 0$ ) incident wave with an angle of incidence  $\theta$  with negative  $z$ -axis.

The  $z$ -component of the electric field is given by

$$E_z^i = E_0 \sin \theta \exp(ik_e r \sin \theta \cos \phi) \exp(-ik_e z \cos \theta) \exp(-i\omega t), \quad (2.77)$$

$$= E_0 \sin \sum_{n=-\infty}^{\infty} i^n J_n(\tilde{k}_e r) F_n \quad (2.78)$$

where  $F_n = e^{-ik_e z \cos \theta} e^{-i\omega t} e^{-in\phi}$ ,  $k_e = \omega \sqrt{\mu_0 \varepsilon_0}$ ,  $\tilde{k}_e = k_e \sin \theta = (k_e^2 - h^2)^{1/2}$  and  $h = k_e \cos \theta$ . The polarization is chosen such that the incident magnetic field  $z$ -component  $H_z = 0$ . However, the other components of the magnetic field are not zero as in the case of perpendicular incidence or a perfectly conducting cylinder. One can see that by applying the boundary conditions the general case of oblique incidence is not complete without the  $z$ -component of the scattered magnetic field. Thus, for an  $E$ -

polarized case the scattering terms also contain the H- polarized terms and vice- versa (Kerker[6] refers to them as cross polarization terms). The scattered and transmitted electric fields are given by:

$$E_z^0 = \sum_{n=-\infty}^{\infty} a_n^e J_n(\tilde{k}_0 r) F_n, \quad (2.79)$$

$$E_z^s = \sum_{n=-\infty}^{\infty} S_n^e H_n(\tilde{k}_e r) F_n, \quad (2.80)$$

where  $\tilde{k}_0 = (k_0^2 - h^2)^{1/2}$ ,  $h = k_e \cos \theta$  and  $k_0 = \omega \sqrt{\epsilon_0 \mu_0}$ . The magnetic field components

inside and scattered are:

$$H_z^0 = \sum_{n=-\infty}^{\infty} a_n^m J_n(\tilde{k}_0 r) F_n, \quad (2.81)$$

$$H_z^s = \sum_{n=-\infty}^{\infty} S_n^m H_n(\tilde{k}_e r) F_n, \quad (2.82)$$

where  $a_n^e$ ,  $S_n^e$ ,  $a_n^m$ , and  $S_n^m$  are the field coefficients inside and outside the cylinder for both the TE and TM polarizations, respectively. The  $\phi$ -components of the fields are obtained from Maxwells equations and are given as:

$$E_r = \frac{1}{i\omega\varepsilon} \left( \frac{1}{r} \frac{\partial H_z}{\partial \phi} - \frac{\partial H_\phi}{\partial z} \right), \quad H_\phi = -\frac{1}{i\omega\mu} \left( \frac{\partial E_r}{\partial z} - \frac{\partial E_z}{\partial r} \right), \quad (2.83)$$

From the incident wave we know  $\partial/\partial z = -ih = -ik_e \cos \theta$  and substituting  $E_r$  in to  $H_\phi$  in the above equation we obtain

$$H_\phi = \frac{h}{ir\tilde{k}} \left( \frac{\partial H_z}{\partial \phi} + \frac{k^2}{i\omega\mu\tilde{k}^2} \frac{\partial E_z}{\partial r} \right), \quad (2.84)$$

the  $\phi$ -components of the magnetic field assume the following form

$$H_\phi^i = \sum_{n=-\infty}^{\infty} \frac{-ik_e^2 E_0 \sin \theta}{\omega\mu_e \tilde{k}_e} i^n J'_n(\tilde{k}_e r) F_n, \quad (2.85)$$

$$H_\phi^s = \sum_{n=-\infty}^{\infty} \left( -\frac{n S_n^m h}{r \tilde{k}_e^2} H_n^{(1)}(\tilde{k}_e r) - \frac{i S_n^e k_0^2}{\omega\mu_e \tilde{k}_e} H_n^{(1)\prime}(\tilde{k}_e r) \right) F_n, \quad (2.86)$$

$$H_\phi^0 = \sum_{n=-\infty}^{\infty} \left( -\frac{ni^n a_n^m h}{(r \tilde{k}_0^2)} J_n(\tilde{k}_e r) - \frac{ia_n^e k_0^2}{\omega \mu_0 k_0} J'_n(\tilde{k}_0 r) \right) F_n, \quad (2.87)$$

similarly the  $\phi$ -components of the electric field are given by

$$E_\phi^i = \sum_{n=-\infty}^{\infty} -\frac{nh E_0 \sin \theta}{r \tilde{k}_e^2} i^n J_n(\tilde{k}_e r) F_n, \quad (2.88)$$

$$E_\phi^s = \sum_{n=-\infty}^{\infty} \left( -\frac{n S_n^e h}{r \tilde{k}_e^2} H_n^{(1)}(\tilde{k}_e r) + \frac{i \omega \mu_1 S_n^m}{\tilde{k}_e} H_n^{(1)'}(\tilde{k}_e r) \right) F_n, \quad (2.89)$$

$$E_\phi^0 = \sum_{n=-\infty}^{\infty} \left( -\frac{n a_n^e h}{r \tilde{k}_0^2} J_n(\tilde{k}_0 r) + \frac{i \omega \mu_0 S_n^m}{\tilde{k}_0} J'_n(\tilde{k}_0 r) \right) F_n. \quad (2.90)$$

Considering  $\mu_0 = \mu_1 = 1$  the scattering coefficients obtained by matching the boundary

conditions  $E_\phi^s + E_\phi = E_\phi^0$ ,  $H_\phi^s + H_\phi = H_\phi^0$ ,  $E_z^s + E_z = E_z^0$ , and  $H_z^s + H_z = H_z^0$  at  $r = r_0$

are given by

$$S_n^e = \frac{i^n E_0 \sin \theta ((r_0 \tilde{k}_0 \tilde{k}_e)^2 (J_n(\tilde{k}_0 r_0) J'_n(\tilde{k}_e r_0) \tilde{k}_0 - m_0^2 J_n(\tilde{k}_e r_0) J'_n(\tilde{k}_0 r_0) \tilde{k}_e) + J_n(\tilde{k}_e r_0) \Lambda)}{(r_0 \tilde{k}_0 \tilde{k}_e)^2 (J_n(\tilde{k}_0 r_0) H_n^{(1)'}(\tilde{k}_e r_0) \tilde{k}_0 - m_0^2 H_n^{(1)}(\tilde{k}_e r_0) J'_n(\tilde{k}_0 r_0) \tilde{k}_e) + H_n^{(1)}(\tilde{k}_e r_0) \Lambda}, \quad (2.91)$$

$$S_n^m = \frac{i^n E_0 \sin \theta h^2 n k_e^2 \tilde{k}_0^2 \tilde{k}_e (\tilde{k}_0^2 - \tilde{k}_e^2) J_n(\tilde{k}_0 r_0)^2 \Delta}{(r_0 \tilde{k}_0 \tilde{k}_e)^2 (J_n(\tilde{k}_0 r_0) H_n^{(1)'}(\tilde{k}_e r_0) \tilde{k}_0 - m_0^2 H_n^{(1)}(\tilde{k}_e r_0) J'_n(\tilde{k}_0 r_0) \tilde{k}_e) + H_n^{(1)}(\tilde{k}_e r_0) \Lambda} \quad (2.92)$$

where  $m_0 = k_0/k_e$  and

$$\Lambda = \frac{(nh)^2 H_n^{(1)}(\tilde{k}_e r_1) J_n^2(\tilde{k}_0 r_1) (\tilde{k}_0^2 - \tilde{k}_e^2)}{J_n(\tilde{k}_0 r_0) H_n^{(1)'}(\tilde{k}_e r_0) \tilde{k}_0 - H_n^{(1)}(\tilde{k}_e r_0) J'_n(\tilde{k}_0 r_0) \tilde{k}_e}, \quad (2.93)$$

$$\Delta = \frac{H_n^{(1)'}(\tilde{k}_e r_0) J_n(\tilde{k}_e r_0) - H_n^{(1)}(\tilde{k}_e r_0) J'_n(\tilde{k}_e r_0)}{J_n(\tilde{k}_0 r_0) H_n^{(1)'}(\tilde{k}_e r_0) \tilde{k}_0 - H_n^{(1)}(\tilde{k}_e r_0) J'_n(\tilde{k}_0 r_0) \tilde{k}_e} \quad (2.94)$$

For perpendicular incidence (i.e.  $\theta = 90^\circ$ ),  $\tilde{k}_0 \rightarrow k_0$ ,  $\tilde{k}_e \rightarrow k_e$ ,  $h \rightarrow 0$ ,  $\Lambda \rightarrow 0$  and

$S_n^m \rightarrow 0$  and Eq. (2.85) reduces to Eq. (2.69). Similarly we can also obtain the scattering coefficients for the incident magnetic field by replacing  $E$  by  $H$ ,  $H$  by  $-E$  and  $\varepsilon$  by  $\mu$ , and  $\mu$  by  $\varepsilon$  in the above equations.

# CHAPTER 3

## MANY PARTICULATE SYSTEMS

Mathematical analysis of scattering of electromagnetic radiation by a homogeneous sphere and an infinite cylinder are presented in the previous chapter. One can extended those mathematical techniques to analyze the scattering and extinction properties of complex inhomogeneous, anisotropic or irregular particles.

In this chapter we study the optical properties of inhomogeneous particles such as layered cylinders and spheres. Moreover, we also present a discussion on the scattering by randomly distributed inhomogeneous particles whose properties can be studied using a homogeneous effective permittivity or permeability.

### 3.1 Coated Cylinder

Coated/layered cylinder is an example of an inhomogeneous structure for which exact solution of the scattering coefficient can be obtained. These systems are of particular important to astronomers as they occupy a great volumes of interstellar atmosphere.

The geometry of the problem is depicted in Fig. 3.1. The system is a concentric cylindrical structure with shell radii  $r_0, r_1$  ( $r_0 < r_1$ ) and permittivities  $\varepsilon_0, \varepsilon_1$ , respectively. The system is embedded in an environment with permittivity  $\varepsilon_e$ . The scattering coefficients of the system were obtained by solving the Maxwell's curl

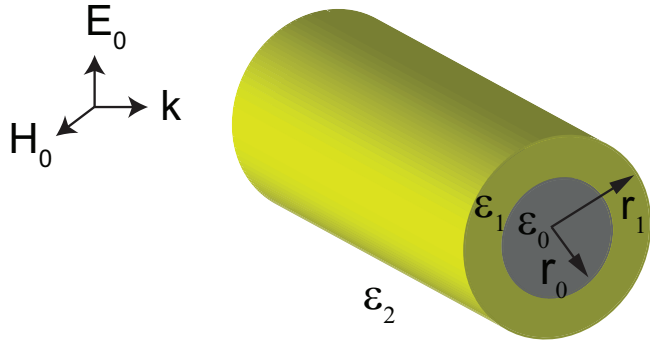


**Figure 3.1:** Coated cylinder with core permittivity  $\epsilon_0$  and coating permittivity  $\epsilon_1$  illuminated by a plane wave. Magnetic field  $\mathbf{H}$  is parallel to the axes of the cylinder.

equations in cylindrical coordinates. For an incident plane TM wave the components of the incident field will be

$$H_z^i = H_0 \sum_{i=-\infty}^{\infty} i^n J_n(k_e r) e^{in\varphi}, \quad (3.1)$$

the magnetic field inside the core  $0 \leq r \leq r_0$  and coating  $r_0 \leq r \leq r_1$ ,

$$H_z^0 = H_0 \sum_{i=-\infty}^{\infty} i^n A_n J_n(k_0 r) e^{in\varphi}, \quad (3.2)$$

$$H_z^1 = H_0 \sum_{i=-\infty}^{\infty} i^n [B_n J_n(k_1 r) + C_n H_n^1(k_1 r)] e^{in\varphi}, \quad (3.3)$$

and the scattered field is

$$H_z^s = H_0 \sum_{i=-\infty}^{\infty} i^n S_n H_n^1(k_e r) e^{in\varphi}, \quad (3.4)$$

where  $J_n, H_n^1$  are the Bessel and Henkel functions of the first kind, respectively.  $k_0, k_1, k_e$  are the wave numbers in the core, coating and the background medium, respectively. By applying the boundary conditions at  $r = r_0$  and  $r = r_1$ , yield a set of four linear equations in the arbitrary constants  $A_n, B_n, C_n, S_n$

$$A_n J_n(k_0 r_0) - B_n J_n(k_1 r_0) - C_n H_n^1(k_1 r_0) = 0, \quad (3.5)$$

$$k_1 A_n J'_n(k_0 r_0) - k_0 B_n J'_n(k_1 r_0) - k_0 C_n H_n^{1\prime}(k_1 r_0) = 0, \quad (3.6)$$

$$B_n J_n(k_1 r_1) + C_n H_n^1(k_1 r_1) + J_n(k_e r_1) + S_n H_n^1(k_e r_1) = 0, \quad (3.7)$$

$$k_e B_n J'_n(k_1 r_1) + k_2 C_n H_n^{1\prime}(k_1 r_1) + k_1 J'_n(k_e r_1) + k_1 S_n H_n^{1\prime}(k_e r_1) = 0, \quad (3.8)$$

the above equations can be solved for the scattering coefficient ( $S_n$ ):

$$S_n = \frac{k_e J_n(k_e r_1) [H_n^{1\prime}(k_1 r_1) \Lambda_n + J'_n(k_1 r_1)] - k_1 J'_n(k_e r_1) [J_n(k_1 r_1) - H_n^1(k_e r_1) \Lambda_n]}{k_1 H_n^{1\prime}(k_e r_1) [J_n(k_1 r_1) + H_n^1(k_1 r_1) \Lambda_n] - k_e H_n^1(k_e r_1) [H_n^{1\prime}(k_1 r_1) \Lambda_n + J'_n(k_1 r_1)]}, \quad (3.9)$$

$$\Lambda_n = \frac{k_1 J_n(k_1 r_0) J'_n(k_0 r_0) - k_0 J_n(k_0 r_0) J'_n(k_1 r_0)}{k_0 H_n^{1\prime}(k_1 r_0) J_n(k_0 r_0) - k_1 J'_n(k_0 r_0) H_n^1(k_1 r_0)}. \quad (3.10)$$

if  $\varepsilon_0 = \varepsilon_1$  then  $\Lambda_n = 0$  and the scattering coefficient in Eq. (3.9) reduces to that of a homogeneous infinite cylinder (see Eq. (2.72)). Moreover, in the limit  $r_0 \rightarrow 0$ ,  $\Lambda_n \rightarrow 0$  then the scattering coefficient in Eq. (3.9) reduces to that of a homogeneous infinite cylinder of radius  $r_1$  and permittivity  $\varepsilon_1$ . If we assume  $\varepsilon_1 = 1$ , then Eq. (3.9) reduces to the scattering coefficient of homogeneous cylinder of radius  $r_1$  and permittivity  $\varepsilon_0$ .

Note that similar expressions can be obtained in case of coated spheres by replacing Bessel functions with Riccati-Bessel functions.

### 3.1.1 Small Particle Limit

If  $k_e r_1 \ll 1$  i.e., for small particles the scattering coefficient in Eq. (3.9) is approximately given by

$$S_0 \simeq \frac{i\pi(k_e r_1)^4}{32} \frac{(\varepsilon_1(1-p^2) + \varepsilon_0 p^2 - \varepsilon_e)}{\varepsilon_e}, \quad (3.11)$$

$$S_1 \simeq \frac{i\pi(k_e r_1)^4}{4} \frac{(\varepsilon_0 + \varepsilon_1)(\varepsilon_1 - \varepsilon_e) + (\varepsilon_0 - \varepsilon_1)(\varepsilon_1 + \varepsilon_e)p}{(\varepsilon_0 + \varepsilon_1)(\varepsilon_1 + \varepsilon_e) + (\varepsilon_0 - \varepsilon_1)(\varepsilon_1 - \varepsilon_e)p}. \quad (3.12)$$

where  $p = (r_0/r_1)^2$  is the radii ratio.

### 3.2 Inhomogeneous Particles

Nano-composite optical materials or metamaterials are a mixture of two or more homogeneous materials, with effective properties strikingly different from their constituent bulk forms. The effective optical properties of these materials are determined using complex mixing rules, which rely on concentration, orientation, shape and size of their ingredients [15]. Thus, by controlling the individual component parameters one can engineer novel materials with desired optical properties.

In recent years, metal-dielectric composites i.e., metal particles suspended in a dielectric matrix are shown to possess incredible optical properties in the visible and near infrared spectrum that they are responsible for latest advances in metamaterial cloaking [16, 17, 18, 19, 20], surface-enhanced spectroscopy [21], hyperlens systems [22, 23], and nano-structure Fano resonances [24].

Numerous effective medium theories have been proposed to account for the effective permittivity/permeability of these structures. Most popular effective medium theories are the Maxwell-Garnett theory (MGT) and Bruggeman effective medium theory (EMT). The necessary condition for the application of MGT/EMT is that the system size must be smaller than the impinging wavelength. Thus, MGT/EMT are confined only to the quasi-static regime.

#### 3.2.1 Effective Medium Models

If the concentration, optical, and geometrical properties of all the constituents which make up the composite are known, then the effective permittivity is defined by

[25]

$$\langle \mathbf{D} \rangle = \varepsilon_{eff} \langle \mathbf{E} \rangle \quad (3.13)$$

and

$$\langle \mathbf{D} \rangle = \frac{1}{V} \int \mathbf{D}(\mathbf{r}) d\mathbf{r} = \frac{1}{V} \int \varepsilon(\mathbf{r}) \mathbf{E}(\mathbf{r}) d\mathbf{r} \quad (3.14)$$

where  $\langle \mathbf{D} \rangle$  is the average electric induction (over the volume  $V$ ),  $\mathbf{E}$  is the external electric field,  $\mathbf{E}(\mathbf{r})$  and  $\varepsilon(\mathbf{r})$  are the local electric field and permittivity, respectively. The most popular effective medium models are the Maxwell-Garnett theory (MGT) and Bruggeman effective medium theory (EMT).

### 3.2.2 Maxwell-Garnett Theory

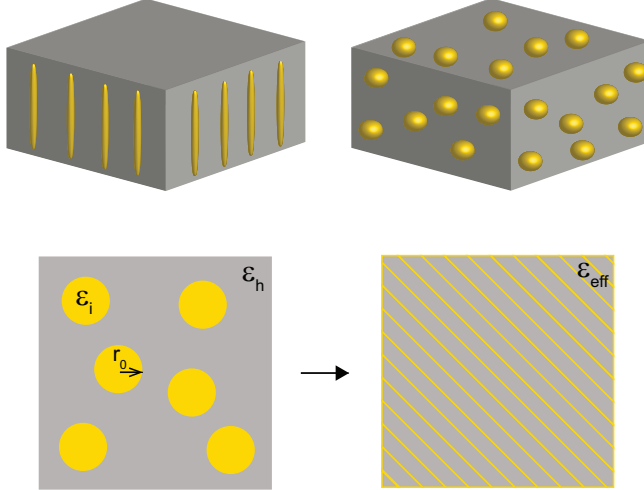


**Figure 3.2:** Geometry of the composite with inclusions of permittivity  $\varepsilon_i$  embedded in matrix  $\varepsilon_h$ .

The geometry is as shown in the Fig. 3.2. The spherical inclusions (or particles) of permittivity  $\varepsilon_i$  and radius  $r_0$  are embedded in a host (or matrix) with permittivity  $\varepsilon_h$ . Provided that, the distance between the particles is greater and the particle size

are smaller than the impinging wavelength  $r_0 \ll \lambda$ , then the polarizability is given by

[15]

$$\alpha = V(\varepsilon_i - \varepsilon_h) \frac{3\varepsilon_h}{\varepsilon_i + 2\varepsilon_h} \quad (3.15)$$

where  $V$  is the volume of the inclusions. From the *Clausius-Mossotti* formula [26] the effective permittivity can be written as

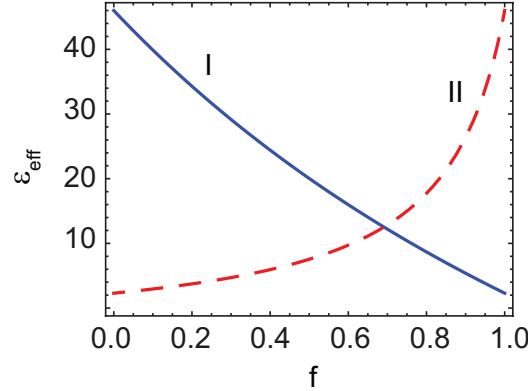
$$\frac{\varepsilon_{eff} - \varepsilon_h}{\varepsilon_{eff} + 2\varepsilon_h} = \frac{n\alpha}{3\varepsilon_h} \quad (3.16)$$

substituting Eq. (3.15) in to Eq. (3.16), one arrives at the Maxwell-Garnett formula [27]:

$$\frac{\varepsilon_{eff} - \varepsilon_h}{\varepsilon_{eff} + 2\varepsilon_h} = f \frac{\varepsilon_i - \varepsilon_h}{\varepsilon_i + 2\varepsilon_h} \quad (3.17)$$

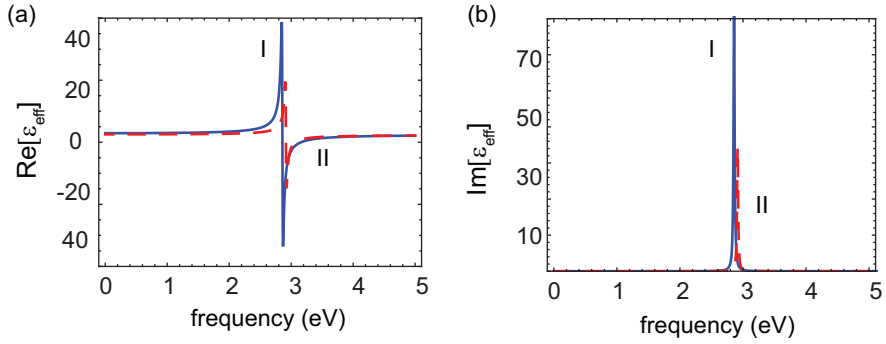
where  $f = nV$  is the volume fraction of the inclusions and is a dimension less quantity. We should note that applicability of MGT is valid for small volume fractions, usually less than 10%. Usage of higher volume fractions may not provide accurate results. In the limit  $f \rightarrow 0$ , Eq. (3.5) has a vanishing inclusion phase *i.e.*  $\varepsilon_{eff} \rightarrow \varepsilon_h$  and as  $f \rightarrow 1$ ,  $\varepsilon_{eff} \rightarrow \varepsilon_i$  which resembles vanishing host environment [15].

Figure 3.3 shows a comparison between effective permittivities vs. the inclusion volume fraction for complementary mixtures. A strong asymmetry in the effective permittivity can be observed when the permittivities of the host and inclusion phases are interchanged. Moreover, one can also see that there is no equal contributions from the constituents as the curves intersect at 70% volume fraction. However, equal contribution is not the necessary condition for the applicability of MGT.



**Figure 3.3:** A comparison of the effective permittivity in case of complementary mixtures as a function of inclusion volume fraction. In the plot we consider spherical inclusions with (I) permittivity  $\varepsilon_{eff} = 20\varepsilon_h$  and a glass host with  $\varepsilon_h = 2.2$  (blue solid line) and (II)  $\varepsilon_{eff} = 20\varepsilon_i$  and  $\varepsilon_i = 2.2$  (red dashed line).

Figure 3.4 shows the real and imaginary parts of the effective permittivity vs. frequency at different volume fractions. The host a glass with  $\varepsilon_h = 2.2$  and the metal permittivity is described by the Drude model (see Appendix),  $\varepsilon_i = \varepsilon'_i(\omega) + i\varepsilon''_i(\omega) = \varepsilon_b - \omega_p^2/\omega(\omega + i\omega_\tau)$ , where  $\omega_p$  is plasma frequency,  $\omega_\tau$  is relaxation rate and  $\varepsilon_b$  is contribution due to interband transitions. A resonance can be observed at the frequency  $\omega_{res} = \omega_p^2/\varepsilon_b + 2\varepsilon_h$  which is close to the surface plasmon resonance of the metal particles. The resonance shifts towards the lower frequencies as the volume fraction of the particles increases. This shift may be due to interaction of resonant fields in the adjacent particles. Moreover, one can also see that the behavior of the composite is different far from the plasmon frequency,  $\Re\{\varepsilon_{eff}\} > 0$  at lower frequencies a dielectric behavior and at higher frequencies it behaves as metal permittivity with  $\Re\{\varepsilon_{eff}\} < 0$  [17, 27].



**Figure 3.4:** Real and imaginary parts of the effective permittivity as a function of frequency for different volume fractions. The host is glass with  $\varepsilon_h = 2.2$  and the inclusions are Drude metal particles. Two separate designs are being investigated (I)  $f = 0.1$  (blue solid line) (II)  $f = 0.05$  (red dashed line).

### 3.2.3 Generalized Maxwell-Garnett

The MGT theory can be furthered to include particle (or inclusion) shape anisotropy, thus one can obtain the effective permittivity of composites with non-spherical inclusions. If the inclusions are randomly oriented ellipsoids with small volume fraction  $f$ , the effective permittivity of the composite is given by the Maxwell-Garnett formula [15, 28]

$$\varepsilon_{eff} = \varepsilon_h + \varepsilon_h \frac{\frac{f}{3} \sum_{j=x,y,z} \frac{\varepsilon_m - \varepsilon_h}{\varepsilon_m + \eta_j \varepsilon_h}}{1 - \frac{f}{3} \sum_{j=x,y,z} \frac{\eta_j (\varepsilon_m - \varepsilon_h)}{\varepsilon_m + \eta_j \varepsilon_h}} \quad (3.18)$$

where  $\eta_j$  are the depolarization factors of the ellipsoids satisfying the condition  $\sum_{j=x,y,z} \eta_j = 1$ . For prolate spheroids (needle shaped) i.e., ellipsoids with semi-axes  $a > b = c$ , the depolarization factor is given as

$$\eta_x = \eta = \frac{1 - e^2}{e^2} \left( \frac{1}{2e} \ln \left( \frac{1 + e}{1 - e} \right) - 1 \right), \quad (3.19)$$

where  $e^2 = 1 - (b/a)^2$  is the eccentricity. The other two depolarization factors are equal and given by  $\eta_y = \eta_z = (1 - \eta)/2$ . For oblate spheroids (pancake shaped) i.e.,

ellipsoids with semi-axes  $a = b$ , the depolarization factor is given as

$$\eta_x = \eta = \frac{g(e)}{2e^2} \left( \frac{\pi}{2} - \arctan g(e) \right) - \frac{g(e)^2}{2}, \quad (3.20)$$

where  $g(e)$  is function calculated from the relation  $g(e)^2 = (e^{-2} - 1)$ . For  $\eta_x = \eta_y = \eta_z = 1/3$ , Eq. (3.18) reduces to the Maxwell-Garnett formula in Eq. (3.17).

### 3.2.4 Tuning of the Composite

From the discussions in the previous subsection it is clear that Maxwell-Garnett effective permittivity resonance can be tuned (see Fig. 3.4). However, the tunability in case of spherical inclusion composites is constrained due to the restrictions placed on the filling fraction of the inclusions. However, composite can also be tuned by changing the constituents i.e. host or inclusions materials, shape and orientation of the inclusions. In Fig. 3.5 we show the tunability of composite with respect to the

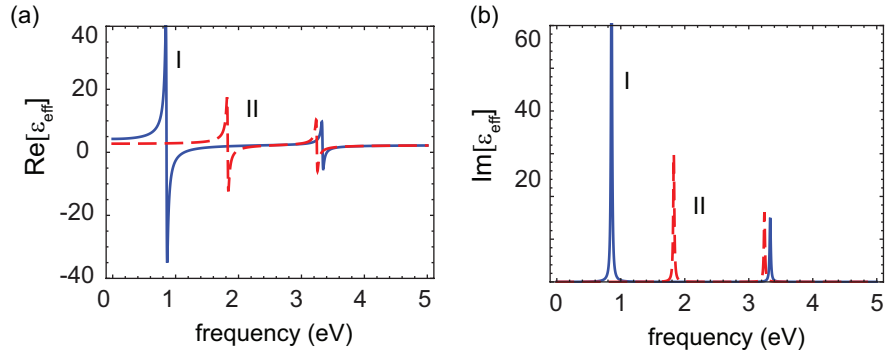


**Figure 3.5:** Real and imaginary parts of the effective permittivity as a function of frequency for different aspect ratios (a/b) at  $f = 0.05$ . The host is glass with  $\varepsilon_h = 2.2$  and the inclusions are Drude metal particles. Two separate designs are being investigated (I)  $a/b = 10$  (blue solid line) (II)  $a/b = 100$  (red dashed line).

changes in the aspect ratio of the inclusions. We consider randomly oriented metallic spheroids embedded in a host with permittivity  $\varepsilon_h = 2.2$ . As can be seen, there exist two resonances corresponding to transverse and longitudinal polarizations in case of

spheroidal particles. One can also see a red shift in the resonance as the aspect ratio of the inclusions changes from  $a/b = 10$  to  $a/b = 100$ . Thus, it is obvious that tunability of the composite enables one to design desired effective permittivities to operate in the desired spectral range.

### 3.2.5 Bruggeman Theory

Bruggeman theory or simply effective medium theory (EMT) is often used to obtain the effective properties of the composites which cannot be considered as matrix with inclusions (or host-guest). We consider an effective medium with permittivity  $\varepsilon_{eff}$  in which  $N$ -istropic spherical particles with, permittivity  $\varepsilon_j$  are present each occupying a volume fraction  $f_j$  and  $\sum_{i=1}^N f_j = 1$ , then according EMT the effective permittivity is obtained from [29]

$$\sum_{j=1}^N f_j \frac{\varepsilon_j - \varepsilon_{eff}}{\varepsilon_j + 2\varepsilon_{eff}} = 0 \quad (3.21)$$

For a two phase mixture Eq. (3.21) can be written as

$$f_1 \frac{\varepsilon_1 - \varepsilon_{eff}}{\varepsilon_1 + 2\varepsilon_{eff}} + f_2 \frac{\varepsilon_2 - \varepsilon_{eff}}{\varepsilon_2 + 2\varepsilon_{eff}} = 0 \quad (3.22)$$

where  $f_1 + f_2 = 1$ . The host-guest hierarchy is no longer valid in case of EMT, the mixture can be treated symmetrically. This implies that in case of complementary mixtures, there is no dissimilarity between the phases i.e., they possess same effective permittivity. The Bruggeman formula in case of randomly ellipsoidal inclusions is given by [30]

$$\varepsilon_{eff} = \varepsilon_h + \frac{f}{3}(\varepsilon_i - \varepsilon_h) \sum_{j=x,y,z} \frac{\varepsilon_{eff}}{\varepsilon_{eff} + \eta_j(\varepsilon_1 - \varepsilon_{eff})}, \quad (3.23)$$

where  $\eta_j$  are the depolarization factors. EMT is often claimed to provide accurate results at higher volume fractions notably between  $1/3 < f < 2/3$ . Analogous arguments regarding tunability can be applied here as in case of the MGT [31].

Stroud [36] has shown that depending upon the approximation made, Maxwell-Garnett theory and Bruggeman or effective medium theory are solutions of a same integral equation. In case of a binary mixture, one can observe that MGT explicitly distinguishes between the host and embedded inclusions in the heterogeneous medium. However, EMA treats host and the inclusions symmetrically (without any distinction). A comparison of experimental data shows that neither of both the theories is truly better than the other. Both have their successes. For instance, Abeles *et. al.* [37] points out that the optical properties of the composite systems Ag–SiO<sub>2</sub>, Si–SiC, and Ge–Al<sub>2</sub>O<sub>3</sub> predicted by the MGT are compatible with their experimental observations. On the other hand, in this case, EMT completely failed to predict the optical response. An excellent agreement between experimental data and the prediction of EMT is reported in case of effective electrical resistance of binary mixtures [38].

### 3.2.6 Extended Effective Medium Theories

Equation (3.17) does not show any dependence of sphere radius ( $r$ ) on the effective permittivity. Thus, MGT can only be applied to the systems with inclusion size parameter satisfies  $k_e r \rightarrow 0$ . Doyle *et al.* [32] highlights some of the properties of the Mie theory based extended MG theory that posses an explicit dependence of particle size on the effective permittivity of the composite.

## Mie Theory Based Extension

The effective permittivity  $\varepsilon_{eff}$  of a composite with small spherical particles embedded in dielectric host  $\varepsilon_h$  is given by the Clausius-Mossotti equation

$$\frac{\varepsilon_{eff} - \varepsilon_h}{\varepsilon_{eff} + 2\varepsilon_h} = \frac{f}{r^3}\alpha \quad (3.24)$$

where  $\alpha$  is the dipolar polarizability of the inclusions and  $f = 4\pi/3na^3$  is the volume fraction and  $n$  is the particle number density. The polarizability in the Eq. (3.24) is given by

$$\alpha = i\frac{3a^3}{2(k_e r)^3}a_1 \quad (3.25)$$

where  $a_1$  is the scattering co-efficient obtained from the Mie theory (see Eq. 2.66).

Substituting Eq. (2.66) in (3.25) yields the following extended MG formula

$$\varepsilon_{eff} = \varepsilon_m \left( 1 - \frac{3}{1 - i2(k_e r)^3/3a_1 f} \right). \quad (3.26)$$

Several other approaches such as, integral formalism to obtain the size dependent polarizability of a small spherical particle by [33], dynamical Maxwell-Garnett model [34], and Dungey and Bohren's [35] effective polarizability with coupled-dipole correction were also proposed. However, most of these theories consider first order correction due to the finite system size. The effects such as higher order multipoles, field coupling between the particles, and volume fraction dependence on the composite are not explicitly discussed.

### 3.3 Multilayer Composites

#### 3.3.1 Maxwell-Garnett Theory: Multilayer Cylinder

The problem of coated cylinder discussed in section 3.1 can be modeled in the form an equivalent homogeneous cylinder whose effective permittivity. Provided that the structure is much smaller than the impinging wavelength MGT can successfully predict the effective permittivity as a function of individual layer/shell permittivities.

In section 2.3, we derived an expression for the polarizability of a homogeneous sphere (see Eq. 2.16). Using similar mathematics, the polarizability of a homogeneous cylinder of permittivity  $\varepsilon_0$  in an environment with permittivity  $\varepsilon_e$  is given by

$$\alpha = 2V\varepsilon_e \frac{\varepsilon_0 - \varepsilon_e}{\varepsilon_0 + \varepsilon_e}, \quad (3.27)$$

where  $V$  is the volume of the cylinder. Provided that the structure in Fig. 3.1 is smaller than the wavelength, the polarizability is given by [5]

$$\alpha = 2V\varepsilon_e \frac{(\varepsilon_1 - \varepsilon_e)(\varepsilon_0 + \varepsilon_1) + (r_0/r_1)^2(\varepsilon_0 - \varepsilon_1)(\varepsilon_e + \varepsilon_1)}{(\varepsilon_1 + \varepsilon_e)(\varepsilon_0 + \varepsilon_1) + (r_0/r_1)^2(\varepsilon_1 - \varepsilon_e)(\varepsilon_0 - \varepsilon_1)} \quad (3.28)$$

if  $\varepsilon_1 = \varepsilon_0$  the polarizability in Eq. (3.28) reduces to that of a homogeneous infinite cylinder  $\varepsilon_0$  and radius  $r_1$ . Moreover, in the limit  $r_0 \rightarrow 0$ , then Eq. (3.28) reduces to the polarizability of a homogeneous infinite cylinder with permittivity  $\varepsilon_1$ . If we assume  $\varepsilon_1 = 1$ , then Eq. (3.28) reduces to the polarizability of homogeneous cylinder of radius  $r_0$  and permittivity  $\varepsilon_0$ .

We can conveniently restate the famous Claisius-Mossotti equation in Eq. (3.16) to the present scenario:

$$\frac{\varepsilon_{eff} - \varepsilon_e}{\varepsilon_{eff} + \varepsilon_e} = \frac{n\alpha}{2\varepsilon_e}. \quad (3.29)$$

Then substituting Eq. (3.28) in Eq. (3.29), the effective permittivity is

$$\frac{\varepsilon_{eff} - \varepsilon_e}{\varepsilon_{eff} + \varepsilon_e} = f \frac{(\varepsilon_1 - \varepsilon_e)(\varepsilon_0 + \varepsilon_1) + (r_0/r_1)^2(\varepsilon_0 - \varepsilon_1)(\varepsilon_e + \varepsilon_1)}{(\varepsilon_1 + \varepsilon_e)(\varepsilon_0 + \varepsilon_1) + (r_0/r_1)^2(\varepsilon_1 - \varepsilon_e)(\varepsilon_0 - \varepsilon_1)} \quad (3.30)$$

where  $f = nV$  is the volume fraction. We can readily generalize the solution in Eq.

(3.30) to include mulitshell structures.

$$\frac{\varepsilon_{eff} - \varepsilon_e}{\varepsilon_{eff} + \varepsilon_e} = f \frac{(\varepsilon_2 - \varepsilon_e) + (\varepsilon_2 + \varepsilon_e) \frac{(\varepsilon_1 - \varepsilon_2)(r_1/r_2)^2 + (\varepsilon_1 + \varepsilon_2) \frac{(\varepsilon_0 - \varepsilon_1)(r_0/r_2)^2 + \dots}{(\varepsilon_0 + \varepsilon_1) + \dots}}{(\varepsilon_1 + \varepsilon_2) + (\varepsilon_1 - \varepsilon_2) \frac{(\varepsilon_0 - \varepsilon_1)(r_0/r_2)^2 + \dots}{(\varepsilon_0 + \varepsilon_1) + \dots}} \\ \frac{(\varepsilon_2 + \varepsilon_e) + (\varepsilon_2 - \varepsilon_e) \frac{(\varepsilon_1 - \varepsilon_2)(r_0/r_1)^2 + (\varepsilon_1 + \varepsilon_2) \frac{(\varepsilon_0 - \varepsilon_1)(r_0/r_2)^2 + \dots}{(\varepsilon_0 + \varepsilon_1) + \dots}}{(\varepsilon_1 + \varepsilon_2) + (\varepsilon_1 - \varepsilon_2) \frac{(\varepsilon_0 - \varepsilon_1)(r_0/r_2)^2 + \dots}{(\varepsilon_0 + \varepsilon_1) + \dots}}} \quad (3.31)$$

It is apparent from the previous discussion that the Maxwell-Garnett theory can predict the effective properties of a these multilayer inhomogeneous media in the limit of quasi-static approximation i.e., with the size of the system substantially smaller than the wavelength of the incident electromagnetic radiation. Thus, MGT places a serious restriction on the physical dimensions of the composite constituents. It should be noted that there is no exact theory to predict the effective optical response of multi-layered systems whose sizes are comparable or greater than the wavelength of the incident radiation.

Recently, the study of optical properties of multi-layer/shells of all sizes have received greater attention due to applications in electromagnetic cloaking [16, 17, 18, 19, 20, 39, 40, 41, 42]. Here, we consider the problem of obtaining the effective properties of a layered cylinder without imposing any restrictions on the sizes of the shells.

Before solving for the complex cylindrical structure, let us first study in to already established rigorous theory of multilayered slabs. We must note that introduction of effective (input) impedances have played an important role in determining the transmission and reflection coefficient of multi-layer planar composites [43, 44].

### 3.3.2 Multilayer Planar Composites

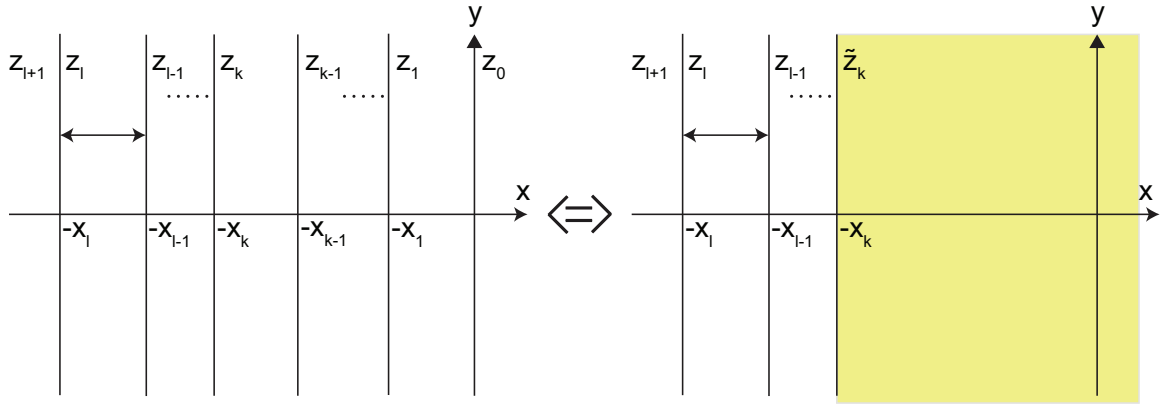


**Figure 3.6:** Perpendicular incidence of a plane wave on a multilayered structure with  $l$ -layers.

Figure 3.6 illustrates the geometry of the problem. Consider a TM-polarized electromagnetic wave propagating in the  $x$ -direction is normally incident on the interface at  $x = 0$  from the right. The electric and the corresponding magnetic fields are given by

$$\mathbf{H}_0 = A_0 e^{ik_0 x} \hat{\mathbf{z}}, \quad (3.32)$$

$$\mathbf{E}_0 = z_0 A_0 e^{ik_0 x} \hat{\mathbf{y}}, \quad (3.33)$$

$$\mathbf{H}_1 = (A_1 e^{ik_1 x} + B_1 e^{-ik_1 x}) \hat{\mathbf{z}}, \quad (3.34)$$

$$\mathbf{E}_1 = z_1 (A_1 e^{ik_1 x} - B_1 e^{-ik_1 x}) \hat{\mathbf{y}}, \quad (3.35)$$

$$\mathbf{H}_2 = (A_2 e^{ik_2 x} + B_2 e^{-ik_2 x}) \hat{\mathbf{z}}, \quad (3.36)$$

$$\mathbf{E}_2 = z_2(A_2 e^{ik_2 x} - B_2 e^{-ik_2 x})\hat{\mathbf{y}}, \quad (3.37)$$

Now, in media 1 we define the position dependent impedance as

$$\tilde{z}_1(x) = \frac{E_1(x)}{H_1(x)} = z_1 \left( \frac{A_1 e^{ik_1 x} - B_1 e^{-ik_1 x}}{A_1 e^{ik_1 x} + B_1 e^{-ik_1 x}} \right) = z_1 \left( \frac{1 - r_{10} e^{-2ik_1 x}}{1 + r_{10} e^{-2ik_1 x}} \right) \quad (3.38)$$

where  $r_{10} = B_1/A_1 = -(z_0 - z_1/z_0 + z_1)e^{-2ikx_0}$  is the reflection coefficient at the (1-0) interface. Clearly if  $x = -x_0$  we have

$$\tilde{z}_1(-x_0) = z_1 \left( \frac{1 - r_{10} e^{2ik_1 x_0}}{1 + r_{10} e^{2ik_1 x_0}} \right) = z_0 \quad (3.39)$$

Now we consider the (1,2) interface

$$\mathbf{E}_2(-x_1) = z_2 A_2 e^{-ik_2 x_1} \left( 1 - r_{21} e^{2ik_2 x_1} \right) \hat{\mathbf{z}} = \mathbf{E}_1(-x_1), \quad (3.40)$$

$$\mathbf{H}_2(-x_1) = A_2 e^{-ik_2 x_1} \left( 1 + r_{21} e^{2ik_2 x_1} \right) \hat{\mathbf{y}} = \mathbf{H}_1(-x_1), \quad (3.41)$$

where we have introduced the reflection coefficient at the (2-1) interface  $r_{21} = B_2/A_2$ .

Taking the ratio of Eqs. (3.40) and (3.41), we obtain

$$\frac{E_2(-x_1)}{H_2(-x_1)} = z_2 \left( \frac{1 - r_{21} e^{2ik_2 x_1}}{1 + r_{21} e^{2ik_2 x_1}} \right) = \tilde{z}_1(-x_1) \quad (3.42)$$

Solving for the reflection coefficient we obtain

$$r_{21} = -\frac{\tilde{z}_1(-x_1) - z_2}{\tilde{z}_1(-x_1) + z_2} e^{-2k_2 x_1} \quad (3.43)$$

So the reflection coefficient is equivalent to the case of reflection from a single interface with effective impedance  $\tilde{z}_1$  which plays the role of input impedance. For  $l$  interfaces the reflection coefficient is

$$r_{l+1,l} = -\frac{\tilde{z}_l(-x_l) - z_{l+1}}{\tilde{z}_l(-x_l) + z_{l+1}} e^{-2k_{l+1} x_l} \quad (3.44)$$

where the effective impedance is obtain through the recursion procedure

$$\tilde{z}_k = z_k \frac{1 + \frac{\tilde{z}_{k-1} - z_k}{\tilde{z}_{k-1} + z_k} e^{2ik_k \Delta_k}}{1 - \frac{\tilde{z}_{k-1} - z_k}{\tilde{z}_{k-1} + z_k} e^{2ik_k \Delta_k}}, \quad (3.45)$$

$$\tilde{z}_0 = z_0 \quad (3.46)$$

where  $\Delta_k = x_k - x_{k-1}$ . Clearly the TE case can be obtained from the TM case by replacing  $\varepsilon_l \rightarrow \mu_l$  or  $z_l \rightarrow 1/z_l$  in Eqs. (3.44) and (3.45).

Now we can extended this idea to complex geometries like concentric cylinders and spheres. For simplicity, we consider here a concentric cylinder.

### 3.3.3 Quasi-Effective Medium Theory: Multilayer Cylindrical Composites

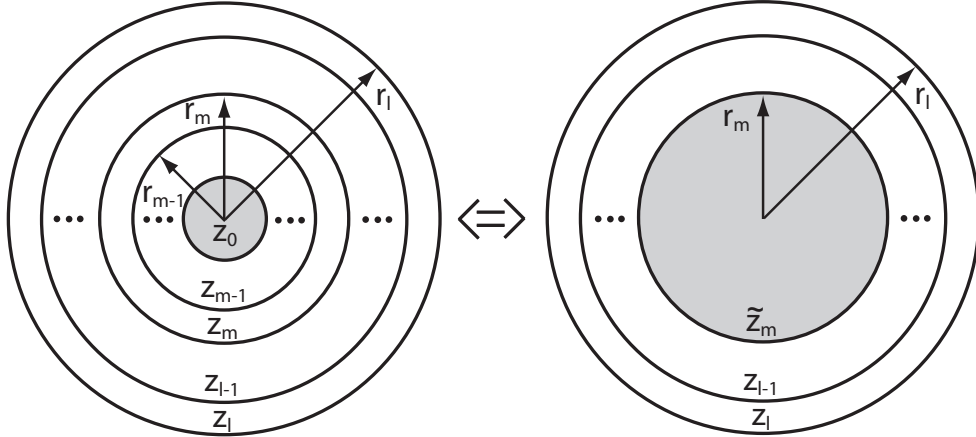


**Figure 3.7:** A schematic representing the quasi-effective medium approach for concentric multi-shell objects. (a) The concentric  $l$ -shell system with shell radii  $r_m$  and impedance  $z_m$  is (b) equivalent to a system consisting of  $l - m$  shells and a core with effective impedance  $\tilde{z}_m$  and radius  $r_m$  immersed in a homogeneous background with impedance  $z_{l+1}$ .

The geometry of the problem is depicted in Fig. 1. The system consists of  $l$  concentric cylindrical shells with arbitrary shell radii  $r_m (m = 0, 1, \dots, l)$ , and impedances  $z_m$ , respectively. The multi-shell structure is embedded in a host medium with impedance  $z_{l+1}$ . Considering a transfer magnetic (TM) polarization of the incident

radiation ( $\mathbf{H}_0 = \mathbf{z}H_0$ ) the magnetic field inside the  $m$ -th shell assume the general solution of the Maxwell's curl equations for cylindrical symmetry

$$\mathbf{H}^{(m)} = \mathbf{z}H_0 \sum_{n=-\infty}^{\infty} [A_n^{(m)} J_n(k_m r) + B_n^{(m)} H_n^1(k_m r)] e^{in\phi}, \quad (3.47)$$

where  $\mathbf{z}$  is unit vector along the magnetic field,  $J_n$ , and  $H_n^1$  are the Bessel and Henkel functions of the first kind, respectively,  $k_m$  are the wave vectors, and  $A_n^{(m)}$  and  $B_n^{(m)}$  are the field coefficients.

we define the mode dependent quasi-effective impedance at the core boundary ( $r = r_0$ ) as

$$\tilde{z}_n^{(0)}(r_0) = i \left( \frac{E_\phi^{(0)}(r_0)}{H_z^{(0)}(r_0)} \right) = z_0 \left( \frac{J'_n(k_0 r_0)}{J_n(k_0 r_0)} \right) \quad (3.48)$$

applying the boundary conditions for the magnetic and electric fields at the first interface leading to the following system of equations for the field amplitudes

$$A_n^{(1)} J_n(k_1 r_0) + B_n^{(1)} H_n^1(k_1 r_0) = A_n^{(0)} J_n(k_0 r_0), \quad (3.49)$$

$$z_1 [A_n^{(1)} J'_n(k_1 r_0) + B_n^{(1)} H_n'^1(k_1 r_0)] = z_0 A_n^{(0)} J'_n(k_0 r_0)$$

where the derivative is taken with respect to the entire argument and  $B_n^{(0)} = 0$  at the origin. Taking the ratio in Eq. 3.49 and introducing the scattering amplitude in the first shell  $S_n^{(1)} = B_n^{(1)}/A_n^{(1)}$  we obtain

$$z_1 \frac{J'_n(k_1 r_0) + S_n^{(1)} H_n'^1(k_1 r_0)}{J_n(k_1 r_0) + S_n^{(1)} H_n^1(k_1 r_0)} = z_0 \frac{J'_n(k_0 r_0)}{J_n(k_0 r_0)} = \tilde{z}_n^{(0)}(r_0) \quad (3.50)$$

Using Eq. (3.50) the unknown scattering amplitude can be expressed in terms of the quasi-effective impedance of the core

$$S_n^{(1)} = - \frac{z_1 J'_n(k_1 r_0) - \tilde{z}_n^{(0)} J_n(k_1 r_0)}{z_1 H_n'^1(k_1 r_0) - \tilde{z}_n^{(0)} H_n^1(k_1 r_0)} \quad (3.51)$$

We proceed by considering the boundary conditions at the next interface ( $r = r_1$ ),

where we have

$$H_z^{(2)} = A_n^{(2)} \left[ J_n(k_2 r_1) + S_n^{(2) H_n^1(k_2 r_1)} \right] e^{in\phi} = H_z^{(1)}(r_1) \quad (3.52)$$

$$E_\phi^{(2)} = -iz_2 A_n^{(2)} \left[ J'_n(k_2 r_1) + S_n^{(2) H_n'^1(k_2 r_1)} \right] e^{in\phi} = E_\phi^{(1)}(r_1) \quad (3.53)$$

Now, taking the ratio of Eqs. (3.52) and (3.53), we obtain

$$i \left( \frac{E_\phi^{(2)}}{H_z^{(2)}} \right) = z_2 \frac{J'_n(k_2 r_1) + S_n^{(2) H_n'^1(k_2 r_1)}}{J_n(k_2 r_1) + S_n^{(2) H_n^1(k_2 r_1)}} = i \left( \frac{E_\phi^{(1)}}{H_z^{(1)}} \right) = \tilde{z}_n^{(1)}(r_1) = \tilde{z}_n^{(1)} \quad (3.54)$$

which gives for the scattering amplitude

$$S_n^{(2)} = - \frac{z_2 J'_n(k_2 r_1) - \tilde{z}_n^{(1)} J_n(k_2 r_1)}{z_2 H_n'^1(k_2 r_1) - \tilde{z}_n^{(1)} H_n^1(k_2 r_1)} \quad (3.55)$$

We note that Eq. (3.55) is similar to Eq. (3.51) but now with  $\tilde{z}_n^{(0)} \rightarrow \tilde{z}_n^{(1)}$  and  $z_1 \rightarrow z_2$ .

By proceeding in similar fashion we obtain the scattering coefficients within each shell

$$S_n^{(m+1)} = - \frac{z_{m+1} J'_n(k_{m+1} r_m) - \tilde{z}_n^{(m)} J_n(k_{m+1} r_m)}{z_{m+1} H_n'^1(k_{m+1} r_m) - \tilde{z}_n^{(m)} H_n^1(k_{m+1} r_m)} \quad (3.56)$$

where the effective quasi-impedance is given as

$$\tilde{z}_n^{(m)} = \tilde{z}_n^{(m)}(r_m) = i \left( \frac{E_\phi^{(m)}}{H_z^{(m)}} \right) = z_m \frac{J'_n(k_m r_m) + S_n^{(m) H_n^1(k_m r_m)}}{J_n(k_m r_m) + S_n^{(m) H_n^1(k_m r_m)}} \quad (3.57)$$

Finally, substituting the scattering amplitude Eq. (3.56) in Eq. (3.57) and simplifying

we obtain the recurrence sequence

$$\tilde{z}_n^{(m)} = z_m \Lambda_n^{(m)} \frac{z_m - \tilde{z}_n^{(m-1)} \Delta_n^{(m)}}{z_m - \tilde{z}_n^{(m-1)} \Omega_n^{(m)}}, \quad (3.58)$$

where

$$\Lambda_n^{(m)} = \frac{H_n'^1(k_m r_{m-1}) J'_n(k_m r_m) - J'_n(k_m r_{m-1}) H_n'^1(k_m r_m)}{H_n'^1(k_m r_{m-1}) J_n(k_m r_m) - J'_n(k_m r_{m-1}) H_n^1(k_m r_m)} \quad (3.59)$$

$$\Delta_n^{(m)} = \frac{H_n^1(k_m r_{m-1}) J'_n(k_m r_m) - J_n(k_m r_{m-1}) H_n'^1(k_m r_m)}{H_n'^1(k_m r_{m-1}) J'_n(k_m r_m) - J'_n(k_m r_{m-1}) H_n^1(k_m r_m)} \quad (3.60)$$

$$\Omega_n^{(m)} = \frac{H_n^1(k_m r_{m-1}) J_n(k_m r_m) - J_n(k_m r_{m-1}) H_n^1(k_m r_m)}{H_n'^1(k_m r_{m-1}) J_n(k_m r_m) - J_n'(k_m r_{m-1}) H_n^1(k_m r_m)} \quad (3.61)$$

The recurrence process starts with the quasi-effective impedance of the core  $\tilde{z}_n^{(0)} = z_0 J'_n(k_0 r_0) / J_n(k_0 r_0)$ . The scattering and extinction cross sections of the entire system then follow

$$\begin{aligned} \sigma_{sca}^{(l)} &= \frac{4}{k_{l+1}} \sum_{n=-\infty}^{\infty} |S_n^{(l+1)}|^2, \\ \sigma_{ext}^{(l)} &= -\frac{4}{k_{l+1}} \sum_{n=-\infty}^{\infty} \Re[S_n^{(l+1)}]. \end{aligned} \quad (3.62)$$

Under this approach the far-field scattering from a multi-shell structure is equivalent to that of a single particle with radius  $r_l$  and an effective mode dependent impedance  $\tilde{z}_n^{(l)}$ . This is evident by considering the large wavelength limit  $k_l r_l \ll 1$  where Eqs. (3.56) and (3.58) reduces to

$$S_n^{(l+1)} = \frac{i\pi}{\Gamma(n)\Gamma(n+1)} \left( \frac{k_{l+1} r_l}{2} \right)^{2n} \left( \frac{\tilde{\varepsilon}_n^{(l)} - \varepsilon_{l+1}}{\tilde{\varepsilon}_n^{(l)} + \varepsilon_{l+1}} \right) \quad (3.63)$$

and

$$\tilde{\varepsilon}_n^{(l)} \rightarrow \varepsilon_l \frac{\varepsilon_l (1 - p_l^n) + \tilde{\varepsilon}_n^{(l-1)} (1 + p_l^n)}{\varepsilon_l (1 + p_l^n) + \tilde{\varepsilon}_n^{(l-1)} (1 - p_l^n)} \quad (3.64)$$

where  $p_l = (r_{l-1}/r_l)^2$  are the shells geometrical factors. Indeed Eq. (3.63) coincides with the large wavelength asymptotic of the scattering amplitude for a single cylindrical particle with permittivity  $\tilde{\varepsilon}_n^{(l)}$  immersed in a host material with permittivity  $\tilde{\varepsilon}_n^{l+1}$ . Furthermore, in the dipolar case the effective permittivity Eq. (3.64) coincides with the classical Maxwells Garnet theory. More importantly, under the current approach we can also estimate the effective impedance/permittivity of an arbitrary monopole which has important practical ramification as will be shown below. Finally, we note

that the extension of the developed quasi-effective theory for transfer electric (TE) waves is straightforward and is achieved by exchanging the shell permittivities with the corresponding permeabilities and vice versa ( $\varepsilon_l \leftrightarrow \mu_l$ ). We must note that similar expressions for effective impedance can be obtained for coated spheres by replacing Bessel functions with Riccati-Bessel functions.

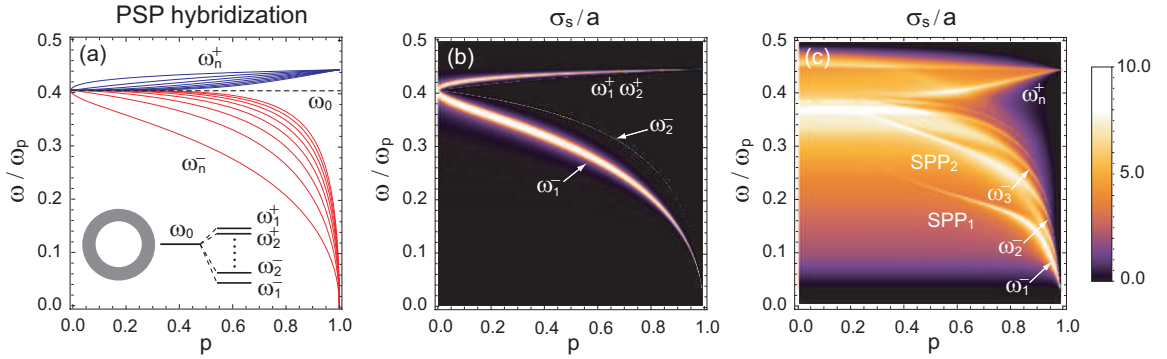


**Figure 3.8:** Particle surface plasmon (PSP) hybridization. (a) The effect of the shell geometrical factor  $p$  on the resonance frequencies are calculated using Eq. 8 for a system comprising of a metal (silver) shell and a core with permittivity equal to that of the host  $\varepsilon_0 = \varepsilon_3 = 1$ . (b) The core-shell particle scattering cross section normalized by the particle radius is calculated using the quasi-effective medium theory Eq. 2. Due to the small particle size  $a = r_0 = 10\text{nm}$ , the dipolar response is dominant while the quadrupole contribution to the far field scattering is only marginal. (c) For a large core-shell particle with radius  $a = 200\text{nm}$ , the scattering cross-section revels both the quasi-static resonances for large  $p$  and the branches due to the surface plasmon polariton (SPP) resonances of the shell.

### 3.3.4 Application: Surface Plasmon (PSP) Hybridization

To demonstrate the simplicity and physical insight that is to be gained through the use of the proposed quasi-effective theory we consider two practical examples. We consider the PSP hybridization in a particle consisting of a dielectric core and single metal shell with of permittivities  $\varepsilon_0$  and  $\varepsilon_1$ , respectively. If the size of the particle is small compared to the incident wavelength its extinction cross section will

manifest resonance behavior for a set of frequencies  $\omega_n$ , determined by the resonance condition  $\Re[\tilde{\varepsilon}_n^{(1)}(\omega_n)] = -\varepsilon_2$  (see equation (3.63)), where  $\varepsilon_2$  is the permittivity of the host. Using the Drude model to describe the metal permittivity of the shell i.e.  $\varepsilon_1(\omega) = \varepsilon_b - \omega_p^2/(\omega^2 + i\omega\omega_\tau)$ , where  $\varepsilon_b$  is the contribution due to the bound electrons,  $\omega_p$  is the plasma frequency and  $\omega_\tau$  is the relaxation rate, a straightforward calculation based on equation (3.63) gives two discrete resonance bands

$$\omega_n^\pm = \omega_p \left( \varepsilon_b + \varepsilon_0 q_n^\pm \right)^{-1/2}, \quad n = 1, 2, 3 \dots \quad (3.65)$$

where  $q_n^+ = 1/q_n^- = (1 - \sqrt{p^n})/(1 + \sqrt{p^n})$  are the geometrical or depolarization factors with  $p = (r_0/r_1)^2$  being the surface fraction of the core. For simplicity, in obtaining Eq. (3.65) we have assumed the core and host materials to have the same permittivity  $\varepsilon_2 = \varepsilon_0$  and neglected terms of the order of  $\omega_\tau/\omega_p \ll 1$ . The resonance frequencies as function of the surface fraction  $p$  are depicted in Fig. 3.5(a). In the case of purely metallic particle ( $p = 0$ ), the response is degenerate with a single resonance frequency  $\omega_0 = \omega_p/\sqrt{\varepsilon_b + \varepsilon_0}$ , referred to as surface plasmon frequency. The introduction of a dielectric core ( $p > 0$ ), result in lifting of the degeneracy or hybridization (see insert in Fig. 3.5(a)) with each monopole manifesting two resonance frequencies  $\omega_n^+ > \omega_0 > \omega_n^-$ , corresponding to anti-symmetric and symmetric mode configurations, respectively. This type of hybridization is not new and has been already studied using coupled RC(Resistor-Capacitor) models in core-shell spherical particles [45, 46]. However, what makes the introduced quasi-effective medium theory unique is its inherent simplicity. Complex calculations of the exact field profiles in the system are not required. The quasi-effective theory provides the exact scattering/extinction

properties of the system, and can be applied for particles with arbitrary sizes. This is demonstrated in Figs. 3.8(b) and 3.8(c), where the scattering cross sections of small and large core-shell particles are calculated. For small particles with radius  $a \ll \lambda$ , the far field scattering manifests resonance behavior at the monopole static resonance frequencies (Eq. (3.65)), with the dipolar term dominating the response. For large particles, apart from the monopole static resonances that are still present at low frequencies one observes the appearance of surface plasmon polariton (SPP) resonances. The SPPs are surface waves that propagate at the core-shell and host-shell interfaces and have the typical resonance conditions  $\lambda_{SPP} = 2\pi a/n (n = 0, 1, \dots)$ , with  $\lambda_{SPP}$  being the SPP wavelength.

## CHAPTER 4

### INVISIBILITY

In the preceding chapters 2–3, we have discussed scattering and extinction properties of homogeneous and inhomogeneous cylindrical and spherically symmetric particles. In section 3.3 we showed that the problem of scattering by a coated cylindrical assemblage can be treated as a homogeneous cylinder/composite media with an effective dielectric function. In this chapter we apply these mathematical methods and physical insights to explore the possibility of achieving *invisibility* or *cloaking* of an arbitrary object.

#### 4.1 Theory

The geometry of the cloak is illustrated in figure 1. An object of arbitrary shape and permittivity  $\varepsilon_0$  is placed inside a cylindrical or spherical domain of radius  $r_0$  (core) surrounded by a system of  $l$  shells of radii  $r_1, r_2, \dots, r_l$  ( $r_0 < r_1 < r_2 \dots < r_l$ ) and permittivities  $\varepsilon_1, \varepsilon_2, \varepsilon_3, \dots, \varepsilon_l$  respectively. The cloak is embedded in a medium with permittivity  $\varepsilon_e$  and illuminated by a uniform electric field  $E_0$  polarized along  $+x$  axis (or transfer magnetic (TM) wave). In section 3.3, we obtained a recurrence formula for estimating the scattering coefficient of multilayered dielectric particles with effective permittivity  $\varepsilon_{eff}^l$  immersed in a host environment with permittivity  $\varepsilon_e$  (see Eq. 3.58).

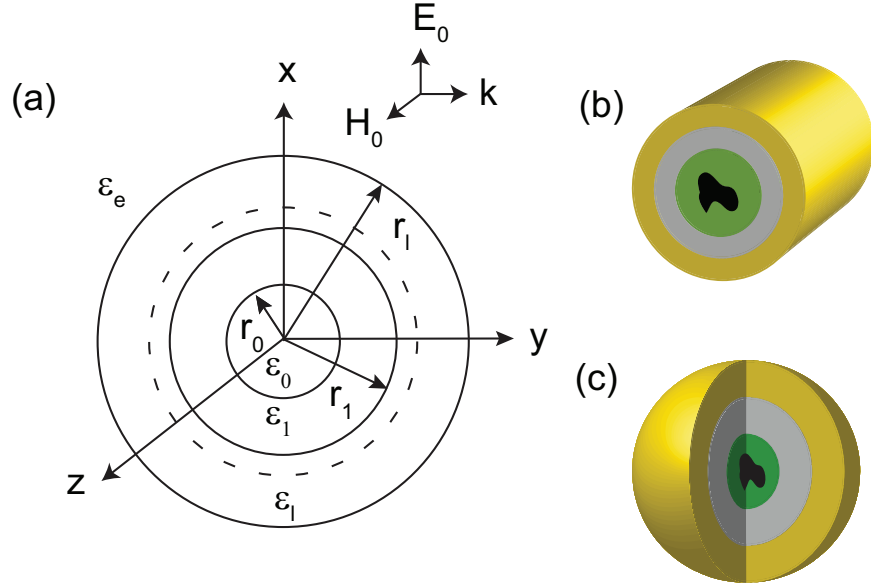


**Figure 4.1:** (a) Generic multi-shell cloaking system with shell radii  $r_i$  and permittivity  $\epsilon_i$ , a two shell (b) cylindrically symmetric cloaking system and (c) spherically symmetric cloaking system.

In the long wavelength limit, Eqs. (3.56)and (3.58) can be written as:

$$S_1^d = r_l^d \frac{\epsilon_{eff}^l - \epsilon_e}{\epsilon_{eff}^l + (d-1)\epsilon_e} \quad (4.1)$$

where

$$\epsilon_{eff}^l = \epsilon_l + \frac{d\epsilon_l p_l (\epsilon_{eff}^{l-1} - \epsilon_l)}{d\epsilon_l + (1-p_l)(\epsilon_{eff}^{l-1} - \epsilon_l)} \quad (4.2)$$

is effective permittivity of the  $l$ -shell system, and  $p_l = (r_{l-1}/r_l)^d$  are the shells surface/volume ratios, and  $d$  is the dimensionality ( $d = 2$  or  $d = 3$ ). We must note that one can obtain the same expressions for scattering amplitude and effective permittivity by explicitly solving the boundary value problem in the quasi-static limit.

Alú et al.[18] and Zhou et al.[19] have shown that, in the quasi-static limit, complete elimination of dipolar scattering can be achieved by a proper choice of the shell(s) radii. Following their hypothesis, in the limit  $S_1^d \rightarrow 0$  ( $\epsilon_{eff}^l = \epsilon_e$ ) we obtain

a general transparency condition for  $l$ -shell cloaking system which depends on the object permittivity and size:

$$p_l = \left( \frac{\varepsilon_l - \varepsilon_e}{\varepsilon_l - \varepsilon_{eff}^{l-1}} \right) \left( \frac{\varepsilon_{eff}^{l-1} + (d-1)\varepsilon_l}{\varepsilon_e + (d-1)\varepsilon_l} \right), (l \geq 1), \quad (4.3)$$

The condition in Eq. (4.3) is consistent with the transparency conditions reported in Refs. 18 and 19 for single-shell and two-shell geometries. As evident from Eq. (4.3), this design does not require high refractive indices or optical magnetism as in the case of transformational optics (TO)[47]. However, realization of such cloaking systems presents a serious disadvantage; redesign of the entire cloak is necessitated for any change in the objects properties ( $\varepsilon_0$  and  $r_0$  are the permittivity and radius of the object), and it is applicable only for spherically/cylindrically symmetric objects. Alternatively, here we propose a different condition to achieve complete elimination of dipolar scattering for a cloak with  $l \geq 2$  shells. By inspection (see Eqs. (4.1) and (4.2)) this is achieved ( $\varepsilon_{eff}^l = \varepsilon_e$ ), if the two outermost cloaking shells have permittivities that satisfy the following conditions

$$\varepsilon_{l-1} = 0, \quad \varepsilon_l = \varepsilon_e \frac{1 + p_l/(d-1)}{1 - p_l}. \quad (4.4)$$

Provided a zero index material can be designed the permittivity of the outermost shell is dependent only on the radii of the  $l^{th}$ , and  $(l-1)^{th}$  shells which is in sharp contrast with the transparency condition given by Eq. (4.3). Thus, in the quasi-static limit, a cloaking system parameterized by the transparency condition Eq. (4.4) has the potential to cloak objects with arbitrary optical properties. Interestingly, a striking similarity exists between the cloak designs based on our approach and those on conventional transformation optics. In case of transformation optics, perfect cloaking

can be achieved provided the permittivity or/and permeability of the anisotropic shell is zero at the boundary between the shell and the object [42]. Zero-index materials correspond to a situation where the local electromagnetic field does not experience phase shift as it travels through the material. In the case of cloaking this also implies a singular value of the local wavelength ( $\lambda \rightarrow \infty$ ) or an effective size of the object equal to zero. This explains why in the case of transformation optics and under the here-proposed transparency condition Eq. (4.4), the invisibility devices operate independently of the object geometrical or/and material properties. An object with effective size equal to zero does not interact with the impinging light. For the here-proposed cloak, the simplest realization is the two-shell design.

## 4.2 Cloak Design and Tunability

### 4.2.1 Metallic Inner shell

We consider two-shell cylindrical and spherical cloaking systems [see Figures 1(b) and 1(c)] with air ( $\varepsilon_e = 1$ ) as environment. To satisfy the transparency condition in Eq. (4.4), we use a metallic inner shell whose permittivity is given by the Drude model,

$$\varepsilon_m(\omega) = \varepsilon'_m(\omega) + i\varepsilon''_m(\omega) = \varepsilon_b - \frac{\omega_p^2}{\omega(\omega + i\omega_\tau)}, \quad (4.5)$$

where  $\omega_p$  is plasma frequency,  $\omega_\tau$  is relaxation rate, and  $\varepsilon_b$  is contribution due to interband transitions. At the modified plasma frequency  $\tilde{\omega}_p = \omega_p/\sqrt{\varepsilon_b}$ , the metal permittivity  $\varepsilon'_m(\tilde{\omega}_p) = 0$  ( for  $\omega_\tau/\tilde{\omega}_p \ll 1$  ) and a metal shell can be used to implement the cloak. To characterize the cloak performance we define the relative scattering length (RSL), for the cylindrical case  $d = 2$ , and relative scattering cross section

(RSCS) for spherically symmetric case  $d = 3$  as

$$\sigma_R^d = \frac{\sigma_{cloak}^d}{\sigma_{object}^d} = \frac{|S_{1,cloak}^d|^2}{|S_{1,object}^d|^2}. \quad (4.6)$$

where  $\sigma_{cloak}^d$  and  $\sigma_{object}^d$  are the scattering length (scattering-cross section) of the cloak and object, respectively. Substituting the transparency condition Eq. (4.4) in Eq. (4.1) and using  $\varepsilon_2 = \varepsilon_m(\tilde{\omega}_p) = i\varepsilon''_m(\tilde{\omega}_p)$  (here  $\varepsilon''_m$  is the imaginary part of the metal permittivity), in the second order of the small parameter  $\varepsilon''_m \approx \varepsilon_b \omega_\tau / \tilde{\omega}_p \ll 1$  we obtain

$$\sigma_R^d(\tilde{\omega}_p) \approx \left( \frac{d\varepsilon''_m(\tilde{\omega}_p)}{p_1} \right)^2 \left( \frac{(\varepsilon_0 + d - 1)(1 + (d - 1)p_1)}{(\varepsilon_0 - 1)(1 - p_1)(p_2 + d - 1)^2} \right)^2 \quad (4.7)$$

The most important conclusion one can infer from Eq. (4.7) is that the presence of material dissipation affects the cloak performance with  $\sigma_R^d(\tilde{\omega}_p) \approx (\omega_\tau / \omega_p)$  increasing quadratically with the realxation rate  $\omega_\tau$ . Moreover, an assesment of Eq. (4.7) also indicates that a geometrical optimization could be achived with the scattering minimum at  $p_1 = 1/(1 + \sqrt{d})$ . The optimal RSL/RSCS can be written as a function of outer shell permittivity

$$\sigma_{R,min}^d \approx \varepsilon_b^3 \left( \frac{\omega_\tau}{\omega_p} \right)^2 \left( \frac{(\varepsilon_0 + d - 1)(d - 1 + 1/\varepsilon_2)^2}{d(\varepsilon_0 - 1)(1 - \sqrt{d})^2} \right)^2, \quad (4.8)$$

Figures 4.2(a) and 4.2(b) demonstrates the cloak performance as a function of the outer shell permittivity  $\varepsilon_2$  for both cylindrical and spherical geometries, respectively. We chose bulk silver with  $\hbar\omega_p = 9.1\text{eV}$ ,  $\hbar\omega_\tau = 0.02\text{eV}$  and  $\varepsilon_b = 5$  [48] for the inner shell due to its lower dissipative losses. In Fig. 2, we also included the RSL/RSCS of the ideal systems (without dissipative losses) along with a silver inner shell for the sake of comparison. As can be seen from the figure RSL/RSCS of the ideal systems approaches zero, implying perfect invisibility at the outer shell permittivity

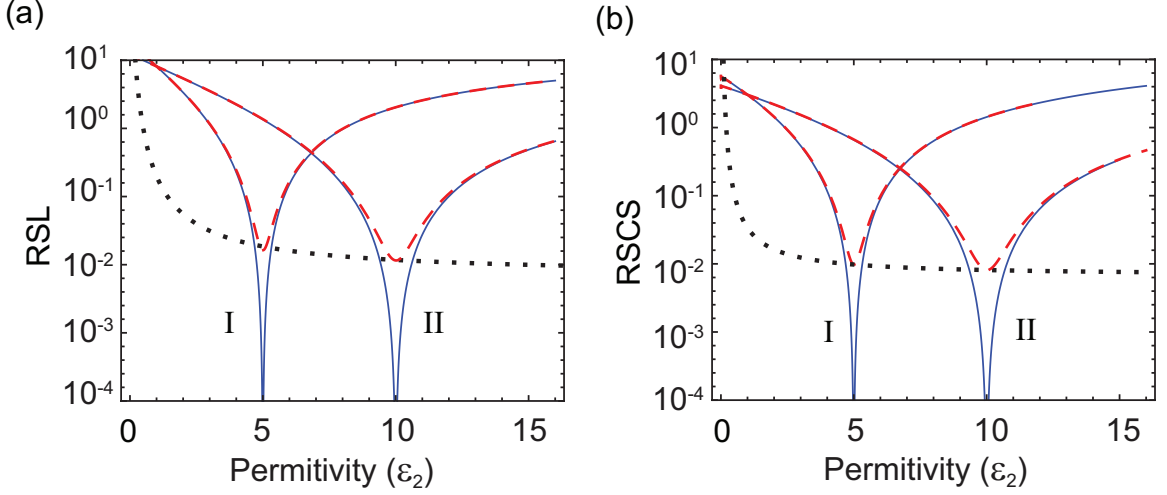


**Figure 4.2:** (a) Relative scattering length (RSL) and cross-section (RSCS) versus outer shell permittivity for two-shell (a) cylindrically symmetric cloak and (b) spherically symmetric cloak with inner shell made of bulk silver. Two separate designs are being investigated in case of cylindrical system: (I)  $p_2 = 0.67$  and (II)  $p_2 = 0.82$ , and spherical system (I)  $p_2 = 0.73$  and (II)  $p_2 = 0.86$ . The object permittivity is  $\varepsilon_0 = 10$  and for all cases we use the optimal radii ratio  $p_1 = 1/(1 + \sqrt{d})$ . The limiting case as per Eq. (4.8) is presented with dotted (black) lines.

values  $\varepsilon_2 = 5$  and  $\varepsilon_2 = 10$  in cases I and II (see Fig. 2), for cylindrical and spherical geometries. These results are in excellent agreement with the values predicted by the transparency condition Eq. (4.4). A significant reduction in scattering for the metal shell systems are also observed at the predicted outer shell dielectric permitivities  $\varepsilon_2$  (see Fig. 2, dashed lines). In the figures we have also included the minimal RSL and RSCS as given by Eq. (4.8), providing a guideline of the maximal affects that can be achieved with proposed design. At the optimal outer shell permittivity the exact result correlates well with the predicted values, and for strongly scattering objects ( $\varepsilon_0 \rightarrow \infty$ ) asymptotically approaches the limit  $\sigma_{RSCS}^{min} \rightarrow \varepsilon_b^3(\omega_\tau/\omega_p)^2(1 + 1/\sqrt{d})^4 \ll 1$ .

Finally, we must note that the cloak based on the metal shell design has inherently a rather narrow frequency range of operation.

#### 4.2.2 Cloaking system with Composite Inner shell

In the previous section we demonstrated and discussed the ability of the bulk metal shells to provide substantial reduction in scattering at the respective modified plasma frequencies. However, their response cannot be tuned to operate across a broader spectral range. In order to tune the response to an arbitrary frequency, we use nano-composite materials realized by embedding metal inclusions of permittivity  $\varepsilon_m$  in a dielectric host with permittivity  $\varepsilon_h$  (see section 3.2). If the inclusions are randomly oriented ellipsoids with small volume fraction  $f$ , the effective permittivity of the composite is given by the Maxwell-Garnett formula (see Eq. 3.18). As we have already discussed that the effective permittivity of the composite depends on the physical and geometrical properties of the spheroids. This allows for substantial flexibility in satisfying the transparency condition in Eq. (4.4). Since Eq. (3.18) is valid for small volume fractions, usually less than 5%, we study the effects due to change in the depolarization factor, i.e. the shape of the inclusions or the host material of the composite, or both. Figures 4.3(a) and (b) illustrate the real and imaginary parts of the composite effective permittivity for different depolarization factors:  $\eta = 0.1$  (prolate spheroids) (solid line) and  $\eta = 1/3$  (spherical metal inclusions) (dotted line) at  $f = 0.05$ . To operate at reduced losses and simplify the design we consider only the ellipsoids low frequency resonance set by the condition  $\varepsilon'_m(\omega) = -\varepsilon_h(1 - \eta)/\eta$ .

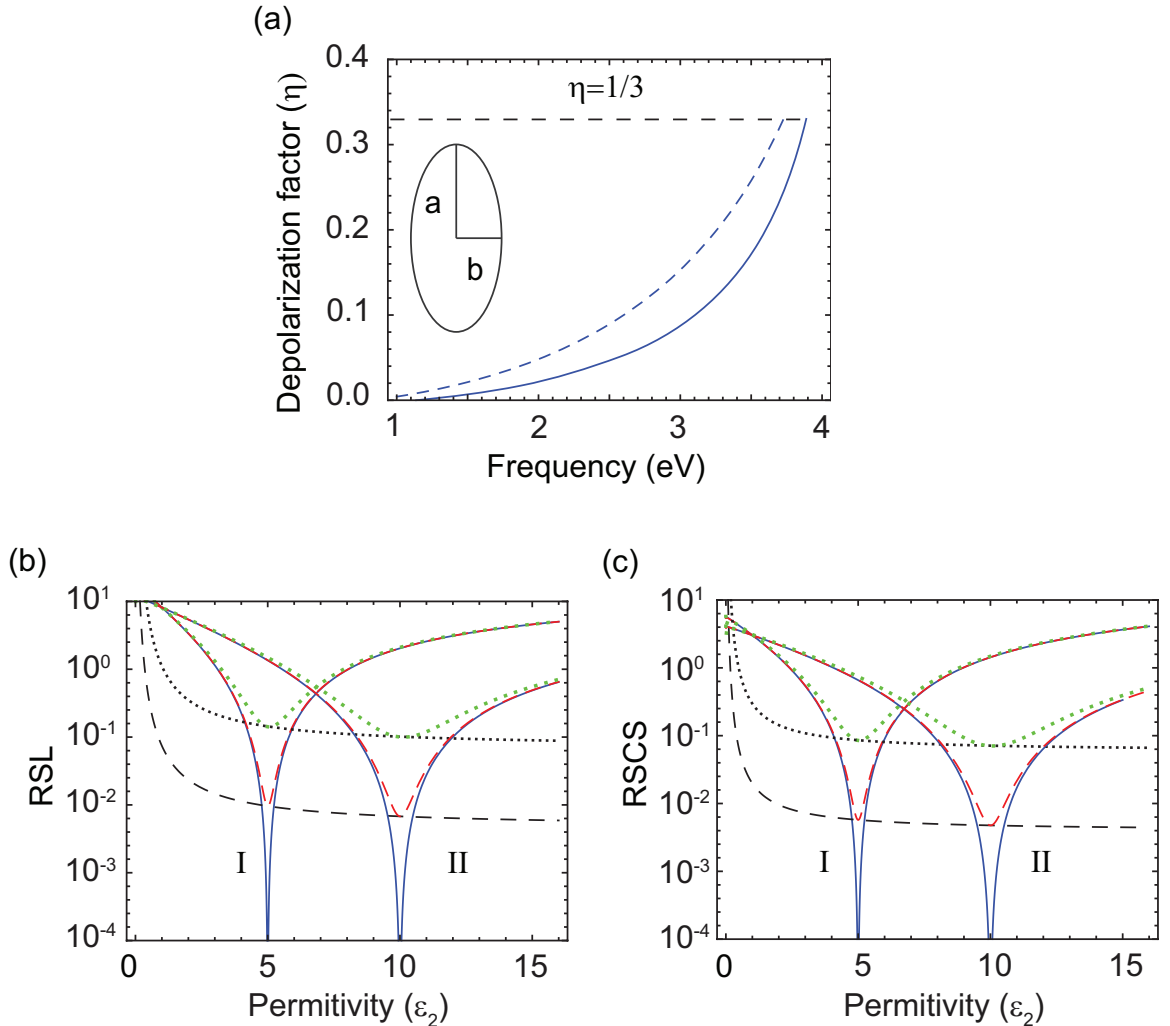


**Figure 4.3:** (a) Depolarization factor for composite host materials  $\varepsilon_h = 1$ (solid line) and  $\varepsilon_h = 2$ (solid line)(dashed line) at different frequencies and  $f=0.05$ . Relative scattering length (RSL) and cross-section (RSCS) versus outer shell permittivity of two-shell (b) cylindrically symmetric cloaking system and (c) spherically symmetric cloaking system, respectively. The composite inner shell is designed with two different hosts  $\varepsilon_h = 1$ (dashed red line) and  $\varepsilon_h = 2$  (dotted green line) at  $\omega = 1.14\text{eV}$ . In the plots we also consider two separate shell designs; cylindrical system (I)  $p_2 = 0.67$  and (II)  $p_2 = 0.82$ , and spherical system (I)  $p_2 = 0.73$  and (II)  $p_2 = 0.86$ . The embedded object has permittivity  $\varepsilon_0 = 10$  and for all cases we use the optimal shell radii ratio  $p_1 = 1/(1 + \sqrt{d})$ . The ideal lossless cases are represented with solid (blue) lines. The limiting case (as per Eqs. (4.7) and (4.9)) is presented with horizontal (dotted and dashed) black lines for both the host media.

From  $\varepsilon'_{eff}(\omega_{op})=0$ , and for small metal losses ( $\varepsilon''_m/\varepsilon'_m \ll 1$ ), the depolarization factor that satisfies the transparency condition in Eq. (6) can be written as

$$\eta = \frac{1}{1 - \varepsilon'_m(\omega_{op})/\varepsilon_h} - \frac{f}{3}, \quad (4.9)$$

where  $\omega_{op}$  is the operation frequency, and the depolarization factor must vary from  $\eta=0$  (needles) to  $1/3$  (spheres). Concurrently, the operation frequency for a given depolarization factor is obtained as  $\omega_{op} = \omega_p / \sqrt{\varepsilon_b - \varepsilon_h + 3\varepsilon_h/(3\eta + f)}$ . We must note that Eq. (4.9) is only valid for  $f > 6\varepsilon_h\varepsilon''_m/[(\varepsilon''_m)_2 + (\varepsilon_h - \varepsilon'_m)^2]$ , and for lower concentrations the transparency condition cannot be satisfied ( $\varepsilon'_{eff} > 0$ ).

Figure 4.3(a) depicts the operational frequency range of the composite cloak. As can be seen, with air as the host medium and tuning the depolarization factor of the ellipsoidal inclusions the operation frequency range is  $\hbar\omega_{op} \in (1.14 - 3.89)\text{eV}$ . As similar situation can also be observed in case of ellipsoidal particles in glass host (see figure 4.3(a) dashed line). However, in latter case a red shift is noticeable with operational frequency in the range  $\hbar\omega_{op} \in (0.83 - 3.74)\text{eV}$ . Thus, it is apparent from the above discussion that by varying the ellipsoidal aspect ratio and the composite host material, one can tune the operational frequency over a wide range of the visible and near-infrared spectra. Nevertheless, one should enforce the restriction  $1/3 \geq \eta > 1/10$  i.e. ellipsoid aspect ratios with in the range  $1 \leq a/b < 3$ , because the lower depolarization factors become prohibitive pertaining to the design of the cloak (the physical size of the system should be smaller than the incident wavelength). This restriction is sufficiently weak enough to allow effective cloaking throughout the entire optical spectral range.

To estimate the RSL /RSCS of the composite cloak we rely on Eq. (4.7) with the substitution  $\varepsilon'_m \rightarrow \varepsilon''_{eff}(\omega_{op})$  and we obtain the composite effective permittivity using Eqs. (3.18) and (4.9),

$$\varepsilon_1 = i\varepsilon''_{eff}(\omega_{op}) = \frac{3\varepsilon_h^2}{f} \frac{i\varepsilon''_m}{(\varepsilon_h - \varepsilon'_m)^2}, \quad (4.10)$$

we note that for geometrically optimized design ( $p_1 = 1/(1 + \sqrt{d})$ ), low frequency of operation and strongly scattering objects( $\varepsilon_0 \rightarrow \infty$ ) the RSL/RSCS asymptotically approaches the limit

$$\sigma_{R,min}^d(\omega_{op}) = \left( \frac{3\omega_\tau \omega_{op} \varepsilon_h^2}{f \omega_p^2} \right)^2 \left( \frac{1 + \sqrt{d}}{\sqrt{d}} \right)^4, \quad (4.11)$$

Figures 4.3(b) and 4.3(c) present the RSL/RSCS of two-shell cylindrical and spherical cloaking systems with inner-shells made of different metal-dielectric composites for different outer-shell permittivities ( $\varepsilon_2$ ) at the operational frequency  $h\omega = 1.14$  eV. For comparison purposes, we also depict the RSL/RSCS ideal cloaking system (non-dispersive media), and include air (dotted line) and glass (dashed line) as the composite host materials. As can be seen, the composite designed with air as the host media shows a drastic reduction in the scattering/extinction (see Eq. (4.11)). Again the minimal RSCS and RSL are obtained at outer-shell permittivity ( $\varepsilon_2$ ) corresponding to the transparency condition Eq. (4.4). As can be seen from the figures, we also included the geometrically optimized results (See Eqs. (4.7) and (4.10)), that closely match the minimal values due to exact calculations.

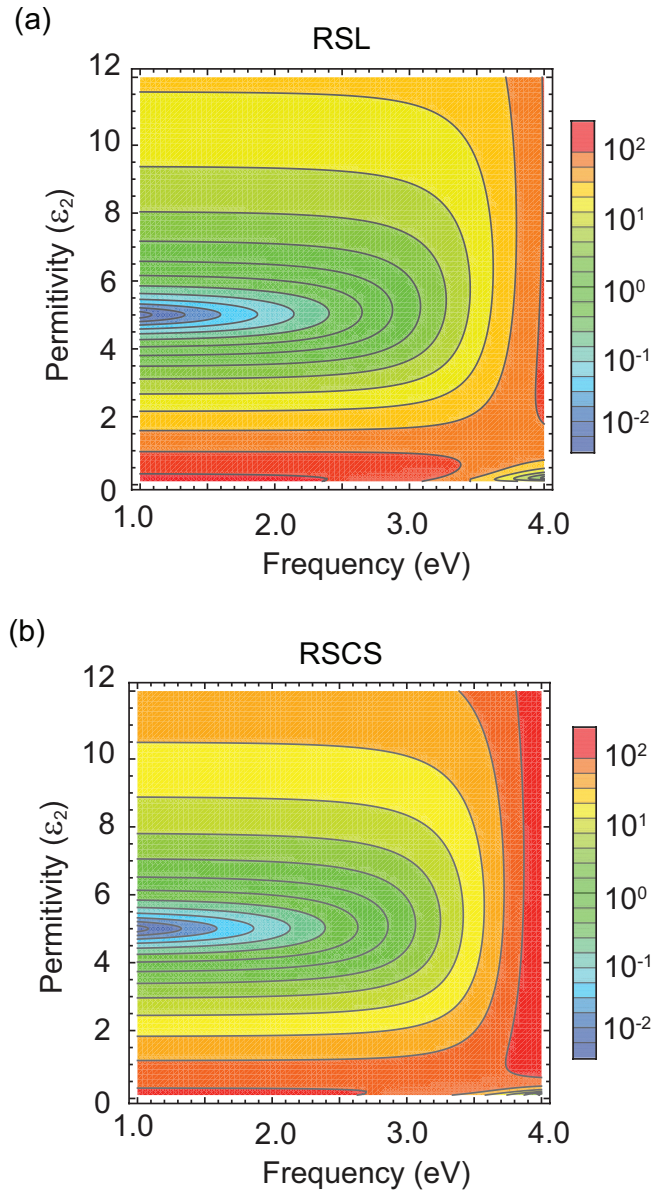


**Figure 4.4:** (a) Relative scattering length (RSL) and (b) relative scattering cross-section (RSCS) calculated as function of outer-shell permittivity ( $\varepsilon_2$ ) and incident light frequency for a dielectric particle( $\varepsilon_0 = 12$ ) with  $\varepsilon_h = 1$  and spheroids volume/surface fraction  $f = 0.05$ . The shells radii ratios are (a) cylindrical system  $(p_1, p_2) = (0.41, 0.67)$ , and (b) spherical system  $(p_1, p_2) = (0.37, 0.73)$ .

Finally, to provide a complete picture of the cloaks performance, in Figs. 4.4(a) and 4.4(b) we vary the outer shell permittivity  $\varepsilon_2$  and operational frequency  $\omega_{op}$ ,

respectively. A substantial decrease in the RSL and RSCS are observed across the entire optical and near infrared spectral range. As predicted by Eq. (4.11), the scattering increases with increasing frequency to the point where the effect of the shell on the scattering cross-section is no longer beneficial (for  $\sigma_{R,min} > 1$  and  $\hbar\omega_{op} > 3.2\text{eV}$ ). We should note that further decrease in scattering may be achieved by increasing the volume fraction of the spheroids provided the applicability of Eq. (3.18) is not violated

### 4.3 Full Wave Analysis of the Generic Cylindrical Cloak

The transparency condition Eq. (4.4) proposed in this work is valid for small objects, i.e. those whose physical size is much smaller than the wavelength of the impinging light. If the object size is comparable to the incident wavelength, the quasi-static analysis is no longer valid and the transparency condition is expected to fail. To study this transition and better understand the limiting system sizes of the design we perform a full wave analyzes of a cylindrical two shell cloak at optical and near infrared frequencies.

We consider scattering of a plane TM wave along  $z$ -direction by a cylindrically symmetric design shown in Fig. 1(a). The scattered magnetic fields assume the general form given in Eq. (3.56) with host medium  $\varepsilon_e = \varepsilon_{l+1}$ . In case of the far-field, the scattering length is then given as a sum over all multipoles:

$$\sigma = \frac{4}{k_e} \sum_{n=-\infty}^{\infty} |S_n|^2 \quad (4.12)$$

In the calculations, the geometrical parameters of the cloak are set at the optimal value  $p_1 = 1/(1 + \sqrt{d})$ ,  $p_2 = 0.67$ , and the shell permittivities are matched to the transparency condition in Eqs. (4.4) and (4.9).

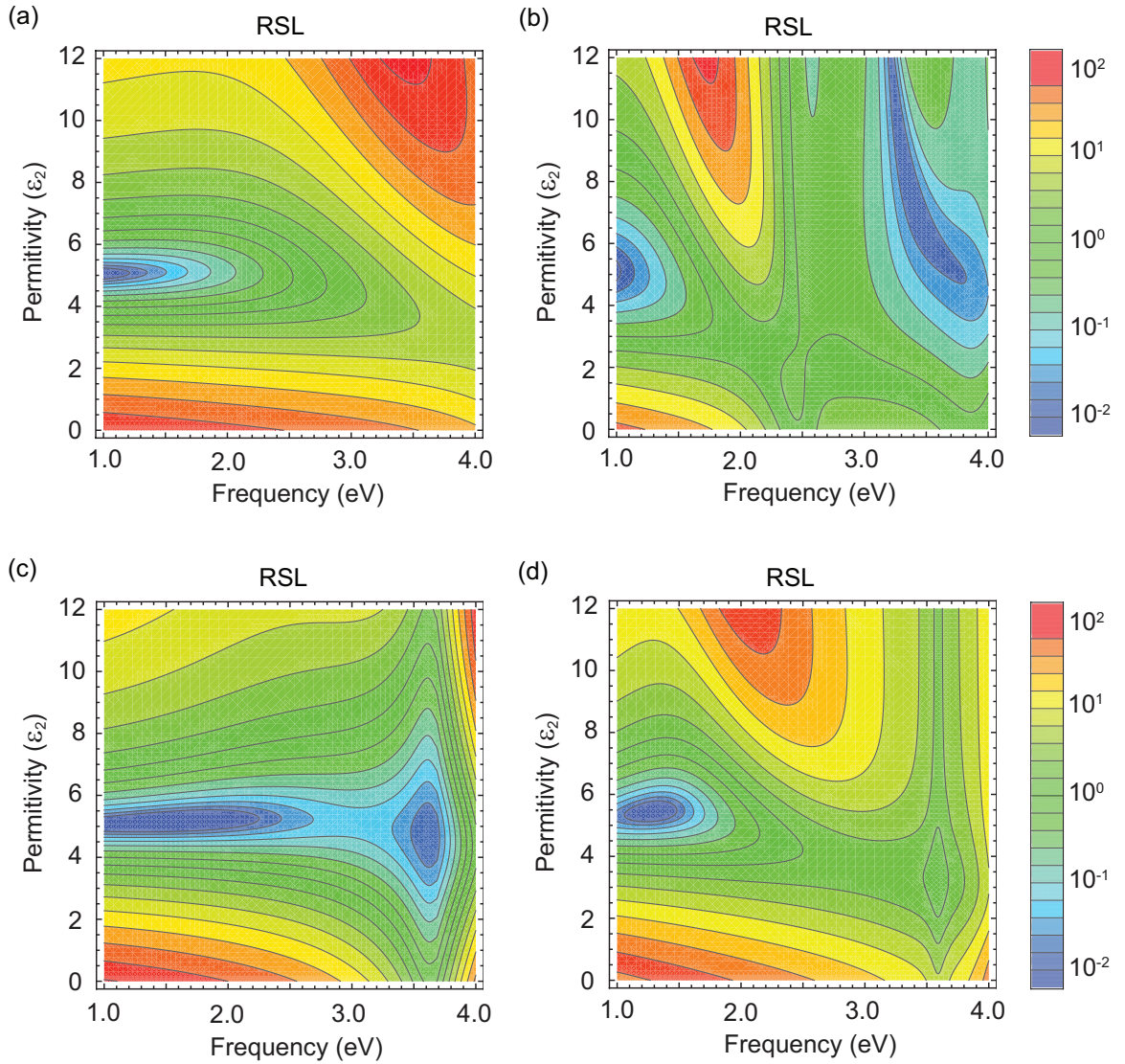


**Figure 4.5:** (a) Relative scattering length (RSL) and (b) relative scattering cross-section (RSCS) calculated as function of composite host permittivity ( $\epsilon_h$ ) and operational frequency  $\omega_{op}$  for a dielectric particle  $\epsilon_0 = 10$  and spheroids volume/surface fraction  $f = 0.05$ . The shells radii ratios are (a) cylindrical system  $(p_1, p_2) = (0.41, 0.67)$ , and (b) spherical system  $(p_1, p_2) = (0.37, 0.73)$ .

Figure. (4.5), illustrates the RSL of the composite cloak, for cylindrical dielectric and metal particles serving as an object. As expected, for systems with small overall sizes (see Fig. 4.5(a) and 4.5(c)) a drastic reduction in scattering over the entire optical

spectrum is achieved for  $\varepsilon_2 = (1+p_2)/(1-p_2)$ , thus reproducing the quasi-static result. Compared to a dielectric particle, a RSL across a broader frequency range is observed in the case of a metallic object. This is due to the dramatic enhancement of the metal particle scattering at the surface plasmon frequency  $\hbar\omega_{sp} = \hbar\omega_p/\sqrt{\varepsilon_b + \varepsilon_e} = 3.71\text{eV}$ . However, as the system size increases (see Fig 4.5(b) and 4.5(d)) the transparency condition in Eq. (4.4) is no longer sufficient to arrest the scattering process. This is an expected behavior since the contribution of the higher order multipoles in the scattering cross-length for  $k_e r_2 \leq 1$  increases with the physical size as

$$S_n = \frac{i\pi}{\Gamma(n)\Gamma(n+1)} \left( \frac{k_e r_2}{2} \right)^{2n} \frac{\varepsilon_2(1-p_2^n) - \varepsilon_e(1+p_2^n)}{\varepsilon_2(1-p_2^n) + \varepsilon_e(1+p_2^n)} \quad (4.13)$$

It is straightforward to show that the quadrupole scattering term of the cloak will overcome the dipolar term of the object for  $k_e r_2 > \sqrt{8p_1(1+p_2+p_2^2)}$  (assuming  $\varepsilon_0 \gg 1$ ). Overall, for particle diameters larger than 400 nm a substantial reduction in scattering/extinction cannot be expected in the optical spectral range.

Finally, we would like to address generic property of our cloak design, namely its object independence. The condition  $\varepsilon_{l-1} = 0$ , leads to  $\varepsilon_{eff}^{l-1} = 0$  (see Eq. (4.2)) regardless of the effective permittivity  $\varepsilon_{eff}^{l-2}$  of the underlying shell/object substructure. This allows the design to cloak virtually arbitrary in shape and composition objects provided the objects are encapsulated by  $l \leq 2$  shells.

### 4.3.1 Full Wave Simulation

To verify the generic properties of the cloak, full wave simulations using a finite-difference frequency domain (FDFD) software package (COMSOL Multiphysics) are performed. A metallic rounded star shaped object is placed inside the cloak. The

permittivities of the shells are set at  $\varepsilon_2 = 5$  and  $\varepsilon_1 = 0$  with radii ratio  $p_1 = 0.67$  ( $r_2 = 106$  nm and  $r_1 = 87$  nm). The system is illuminated by a TM polarized from a point source positioned at 130 nm from the center of the object.

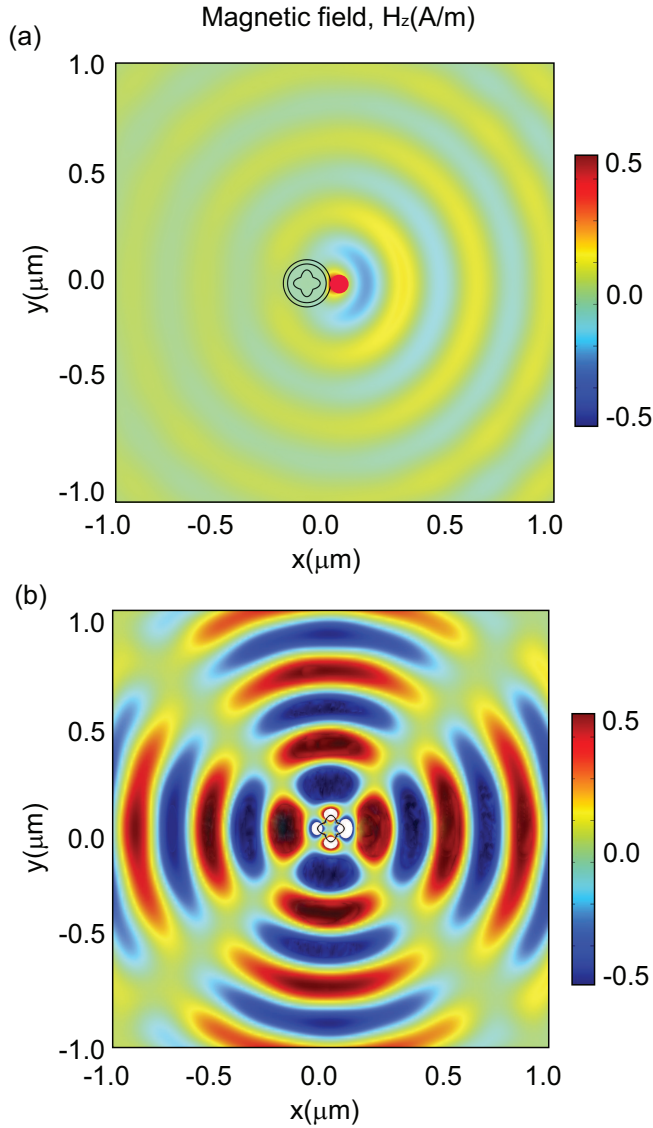


**Figure 4.6:** Full wave calculations of the relative scattering length (RSL) as function of outer shell permittivity ( $\varepsilon_2$ ) and incident light frequency for dielectric particle  $\varepsilon_0 = 10$  enclosed in a cloaking system with radii (a)  $r_2 = 50$  nm and (b)  $r_2 = 100$  nm.

The magnetic field distribution is shown in Fig. 4.6. The cylindrical wave generated by the source smoothly bends around the cloaked region indicating reduced scattering (see Fig. 4.6(a)). The phase fronts remain undisturbed as they exit the cloak and no shadow formation is noted. Figure 4.6(b) illustrates the magnetic field distribution when the cloak is removed. In this case the incident wave is strongly scattered and the phase fronts appear severely disturbed after traversing the object. The formation of shadows and presence of resonances within the object are clearly observed. The difference between the systems response shows that the cloak design based on the transparency condition Eq. (4.4) can considerably reduce scattering from objects with diverse optical and geometrical properties

#### 4.4 Invisibility by Eliminating Two Arbitrary Monopoles

In the previous sections, we showed that an object independent elimination of the scattering due to an arbitrary monopole can be achieved in a two shell systems, provided the bottom shell have a near zero permittivity ( $\varepsilon_1 \rightarrow 0$ ), while the top shell has a permittivity given by Eq. (4.4). Use of  $l$ -shell designs can provide simultaneously removal of  $l - 1$  multipoles from the far field. As a particular example we propose a three shell system with shell radius given by the geometric means  $r_m = \sqrt{r_{m-1}r_{m+1}}$  (or equivalently fixed shells surface fractions  $p_m = p$ ). Short inspection of Eq. (3.64) with  $\varepsilon_1 = 0$  shows that the transparency condition can be satisfied for two arbitrary monopoles (say  $n$  and  $m$ ) provided

$$\varepsilon_2 = \varepsilon_4 \frac{q_n + q_m}{q_n q_m (1 + q_n q_m)}, \quad \varepsilon_3 = q_n q_m \varepsilon_2 \quad (4.14)$$

where  $q_k = (1 - p^k)/(1 + p^k)$  are the shells mode dependent geometrical factors. We must emphasize that the same conditions Eq. (4.4) and Eq. (4.14) will hold for TE polarization under the exchange  $\varepsilon_l \leftrightarrow \mu_l$ .

To demonstrate the concept we consider a three shell design that simultaneously eliminates the dipolar and quadrupole radiation. In the calculations, we use an inner shell made of silver and operate at a frequency equal to the renormalized plasmon frequency  $\tilde{\omega}_p = \omega_p/\sqrt{\varepsilon_b} = 4.06\text{eV}$ . Under these conditions the metal permittivity of the  $l = 1$  shell is small and due to the resistive losses is purely imaginary  $\varepsilon_1 = i\omega_\tau\varepsilon_b/\tilde{\omega}_p \ll 1$ , thus it satisfies well the near zero permittivity condition for object independent cloaking. The far field scattering amplitudes are depicted in Figs 4.7(a) and 4.7(b), where the object is a dielectric cylinder with permittivity  $\varepsilon_0 = 10$  and we have fixed the shells geometrical parameter at  $p = 0.7$ . In the figures, we have also included the scattering amplitudes due to the two shell design (Eq. (4.4)) applied to the dipolar case. As expected in both cases and for objects with diameter  $d = 2r_0 < 100\text{nm}$  the dipolar scattering is dramatically reduced up to a factor of  $10^4$ . However, only in the three shells design the quadrupole terms are eliminated. For large particles both designs will fail to conceal the object due to the increased importance of the higher order multipoles and the appearance of SPP resonances. The reduction of the total scattering corrections as a function of the geometrical factor  $p$  of the shells and the second shell permittivity are shown in Figs 4.7(c)-4.7(f). Provided the permittivity  $\varepsilon_2$  coincides with the transparency conditions Eqs. (4.4) and (4.14) the total scattering cross sections are substantially reduced. Again, the effect is persistent for particle sizes up to half the wavelength of the incident radiation.

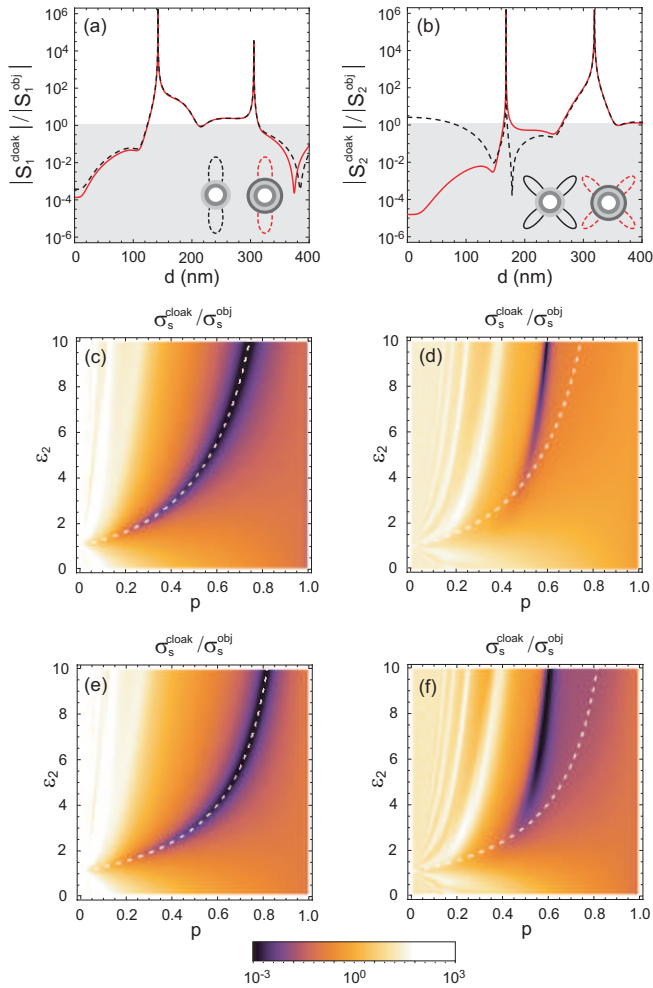


**Figure 4.7:** Quasi-static cloaks. The dipole (a) and quadrupole (b) scattering amplitudes vs. the corresponding scattering amplitudes of the object (core) calculated as function of the core diameter. Dramatic reduction in dipolar scattering is observed in the three shells (red solid line) and two shells designs (dashed black lines). The quadrupole scattering is only reduced in the three shell design as expected. Schematics of the scattering far field profiles are also included as inserts with dashed lines corresponding to elimination of a particular multipole while a solid line correspond to uninterrupted mode radiation. The effects of the second shell permittivity and geometrical factor  $p$  on the total scattering cross section in the case of two shells (c, d) and three shell (e,f) cloaks are calculated for object (core) sizes equal to (c,e)  $d = 20\text{nm}$  and (d, f)  $d = 100\text{nm}$ . The cloak's transparency conditions Eq. 4.4 and Eq. 4.4 are represented with dashed lines. Provided the transparency conditions are satisfied the total cross sections for small particles are reduced by a factor up to  $10^3$ . The effect is persistent for particle's sizes comparable to the wavelength of the incoming radiation  $\lambda = 2c/\tilde{\omega}_p = 306\text{nm}$ . In the calculations, we have used silver to form the internal near-zero permittivity shell.

In contrast to previous works [18, 19] the proposed cloak designs are object independent. This important characteristic is due to the fact that the  $l = 1$  shell has a near zero permittivity which results in an effective permittivity of the system consisting of the object and the bottom shell being effectively zero. A wave incident on a zero refractive index material will not experience a phase shift which also implies a singular value of the local wavelength or an effective size of the object equal to zero. This fact alone explains why in the case of transformation optics and under the here-proposed transparency conditions, the invisibility devices operate independently of the object geometrical or/and material properties.

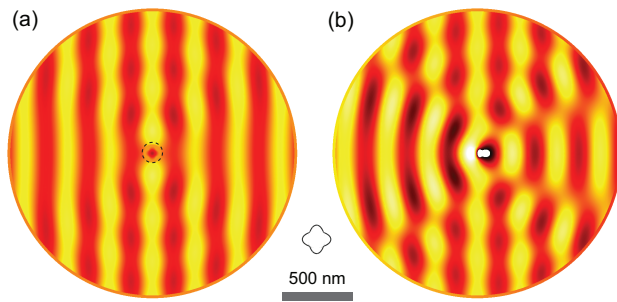


**Figure 4.8:** Object independent cloaking. The scattering effects due to the object are tested for a cross shape inclusion (see the schematics on the top of the scale bar) positioned at the core. The size of the inclusion is  $100\text{nm}$  and has permittivity  $\varepsilon = 10$ . (a) The magnetic field profiles under a plain wave illumination with (a) and without (b) the cloak are calculated using finite difference commercial software (COMSOL Multiphysics). The bare object strongly disturbs the incoming wave while the introduction of the three shell cloak (Eq. 4.14) around the object substantially eliminates scattering.

To demonstrate the object independent operation of the cloak in Fig. 4.8 we consider the interaction of a plain wave with a relatively large cross shaped object.

The introduction of the cloak dramatically reduces the near- and far-field scattering which is consistent with the already studied cases of cylindrical objects. Finally, we must recognize that the use of metals to provide near zero permittivity of the inner shell inherently restricts the cloaks frequency of operation. This problem arises in invisibility devices based on the transformation optics approach and is one of the main obstacles in creating such devices. Possible approach toward a tunable operation may be achieved using metal-dielectric composite materials. The permittivity of the composite depends on the shapes and concentrations of the metal inclusions and thus the operation frequency where near zero permittivity is achieved can be carefully tuned.

# CHAPTER 5

## QUANTUM INVISIBILITY

The previous chapter outlined the design of a cloaking device that can render an arbitrary object invisible to the external observer elimination of electromagnetic scattering. In this chapter, we will study the quantum analogue of a classical generic cloak design. The idea is straight forward: The classical wave equation and the Schrodinger's equation that represents the state of a quantum system are analogous to each other.

### 5.1 Analogy to Optical Index of Refraction

The time-independent Schrödinger's equation can be written as [55, 56]:

$$H\psi = -\frac{\hbar^2}{2m(r)}\nabla^2\psi + V(r)\psi = E\psi \quad (5.1)$$

where  $m$  and  $V$  are spatially dependent mass and potential, respectively.  $E$  is the energy of the particles. We may also write Eq. (5.1) in the following form

$$\nabla^2\psi + k^2\psi = 0, \quad (5.2)$$

provided

$$k = \frac{\sqrt{2m(E - V(x))}}{\hbar}, \quad (5.3)$$

where  $k$  is the magnitude of the wave vector. In optics, for a definite angular frequency  $\omega$ , the wave equation is given by

$$\nabla^2 F + \frac{\omega^2}{c^2} n^2 F = 0, \quad (5.4)$$

where  $n$  is the refractive index,  $c$  is the velocity of light in vacuum. The Schrödinger's wave equation now resembles the wave equation of light in a medium with the refractive index:

$$n^2 = \frac{2m}{\hbar^2} [E - V(x)] \frac{c^2}{\omega^2} \quad (5.5)$$

From this analogy, it is apparent that plane wave is a solution of the Schrodinger's wave equation for a free particle and so is each partial wave.

## 5.2 Partial Wave Analysis: Faxen–Holtsmark's Theory

Classical (see section 2.2) [57] analogue of the quantum scattering theory was proposed by Faxén *et. al* [58]. A plane wave traveling in the  $z-$  direction is incident on a spherically symmetric potential. Since each partial wave is also a solution of the Schrödinger's wave equation, we can expand the incident wave as

$$\psi_i = e^{ikz} = e^{ikr \cos \theta} = \sum_{n=0}^{\infty} (2n+1) i^n j_n(kr) P_n(\cos \theta) \quad (5.6)$$

where  $j_n(kr)$  are the spherical Bessel functions, and  $P_n(\cos \theta)$  are the Legendre polynomials of order  $n$ . The scattered wave at a point  $(r, \theta, \phi)$  far away from the potential has the following form:

$$\psi_s = f(\theta, \phi) \frac{e^{ikr}}{r} \quad (5.7)$$

where  $f(\theta, \phi)$  is the scattering amplitude. In most of the cases potential is spherical or approximately spherically symmetric, thus scattering amplitude is independent of  $\phi$ ; mathematically,  $f(\theta, \phi) = f(\theta)$ .  $f(\theta)$ , being a function of  $\theta$ , can be expressed in term of partial waves as follows:

$$f(\theta, \phi) = f(\theta) = \sum_{n=0}^{\infty} A_n \frac{1}{2k} i P_n(\cos \theta) \quad (5.8)$$

where  $A_n$  are unknown coefficients, usually complex. Now, we can readily express the outgoing wave far beyond the potential as

$$\psi(r, \theta, \phi) = \psi_i + \psi_s \rightarrow e^{ikr \cos \theta} + f(\theta, \phi) \frac{e^{ikr}}{r} \quad (r \rightarrow \infty), \quad (5.9)$$

Substituting Eqs. (5.6), (5.8) in to Eq. (5.9), we have

$$\psi \rightarrow \sum_{n=0}^{\infty} (2n+1) \left\{ i^n j_n(kr) P_n(\cos \theta) + A_n \frac{1}{2k} i P_n(\cos \theta) \frac{e^{ikr}}{r} \right\} \quad (5.10)$$

For large distance i.e.,  $r \rightarrow \infty$ , we need to consider the asymptotic expansion of the spherical Bessel function

$$j_n(kr) \rightarrow \frac{\sin \left( kr - \frac{l\pi}{2} \right)}{kr} \quad (5.11)$$

Substituting Eq. (5.11) in (5.10) and simplifying, we obtain

$$\psi \rightarrow \frac{1}{2ikr} \sum_{n=0}^{\infty} i^n (2n+1) \left\{ (1 - A_n) \exp \left[ i \left( kr - \frac{n\pi}{2} \right) \right] \right. \quad (5.12)$$

$$\begin{aligned} & \left. - \exp \left[ i \left( kr - \frac{n\pi}{2} \right) \right] \right\} P_n(\cos \theta) \\ &= \frac{1}{2ikr} \sum_{n=0}^{\infty} (2n+1) [(1 - A_n) e^{ikr} - (-1)^n e^{-ikr}] P_n(\cos \theta) \end{aligned} \quad (5.13)$$

The general solution for the time-independent, Schrödinger's equation with spherically symmetric potential is given by [56]

$$\psi(r, \theta) = \sum_{i=0}^{\infty} \frac{(2l+1)}{k} i^n \frac{1}{r} f_n(r) P_n(\cos \theta) \quad (5.14)$$

where  $f_n(r)$  can be obtained from the equation

$$\frac{d^2 f_n}{dr^2} + \left[ k^2 - U(r) - \frac{n(n+1)}{r^2} \right] f_n = 0 \quad (5.15)$$

where  $k = 2mE/\hbar^2$  and  $U(r) = 2mV(r)/\hbar^2$ . For  $r \rightarrow \infty$ , the general form of  $f_n(r)$  and

its asymptotic behavior is given by [56]

$$f_n(r) \rightarrow a_n j_n(kr) - b_n n_n(kr) = \frac{c_n}{kr} \sin \left( kr - \frac{n\pi}{2} + \delta_n \right), \quad (5.16)$$

where  $a_n, b_n$  are constants and related to  $c_n$  and  $\delta_n$  as

$$\tan \delta_n = \frac{b_l}{a_l}, \quad c_n^2 = a_n^2 + b_n^2. \quad (5.17)$$

On equating, Eq.(5.13) and (5.16) and solving for  $A_n$  and  $c_n$ , we obtain

$$A_n = [1 - \exp(2i\delta_n)], \quad (5.18)$$

$$c_n = \exp(i\delta_n). \quad (5.19)$$

Substituting Eq. (5.18) in to Eq. (5.8), yields the scattering amplitude

$$f(\theta) = \frac{1}{2ik} \sum_{n=0}^{\infty} (2n+1)[1 - \exp(2i\delta_n)] P_n(\cos \theta) \quad (5.20)$$

The differential scattering cross-section is

$$\sigma(\theta) = |f(\theta)|^2 = \frac{1}{k^2} \left| \sum_{n=0}^{\infty} (2n+1) e^{i\delta_n} \sin \delta_n P_n(\cos \theta) \right|^2 \quad (5.21)$$

taking the integral of Eq. (5.20) over the sphere, we obtain the total scattering cross-section [56]

$$\sigma = 2\pi \int_0^\pi \sigma(\theta) \sin \theta d\theta = \frac{4\pi}{k^2} \sum_{n=0}^{\infty} (2n+1) \sin^2 \delta_n \quad (5.22)$$

One can also express  $\sigma$  in terms of  $f(0)$ . Eq. (5.19) for  $\theta = 0$  becomes

$$f(0) = \frac{1}{2ik} \sum_{n=0}^{\infty} (2n+1) [1 - \exp(2i\delta_n)] \quad (5.23)$$

By comparing this with (5.22) we get

$$\sigma = \frac{4\pi}{k} \Im\{f(0)\} \quad (5.24)$$

Eq. (5.24) is known as the *optical theorem* (see Eq. 2.23). This implies that scattering of a beam of particles by an obstacle removes an amount of the incident particles proportional to  $\sigma$  behind the scattering region  $\theta = 0$ .

### 5.2.1 Phase shifts

The  $\delta_n$  represents the phase shift between the asymptotic forms radial function of the solution of Eq. (5.15) and the radial function in the absence of scattering potential. It is apparent from Eq. (5.22) that scattering cross-section is determined  $\delta_n$ . Provided that  $\delta_n = 0$  or  $\pi$ ,  $\sigma \rightarrow 0$  i.e., matter waves traverse a region in space with out any perturbation.

## 5.3 2-Dimensional scatterer

The wave equation is given in Eq. (5.1). For a 2D scatterer with cylindrically symmetric potential  $V(r)$ , the time-independent Schrödinger's equation for an incident beam of particles can be written as

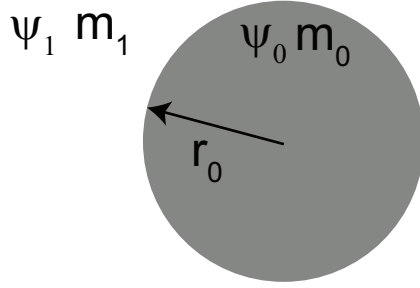


**Figure 5.1:** 2D scatterer with radius  $r_0$  and effective mass  $m_0$  located in an environment with effective mass  $m_e$ .

$$\nabla^2 \psi_e + k_e^2 \psi_e = 0 \quad (5.25)$$

where  $k_e = \sqrt{2m_e E/\hbar}$ . Since  $\psi(r)$  must vanish at the origin, the most admissible general solution inside the scatterer is

$$\psi_0 = A_n J_n(k_0 r), \quad (5.26)$$

where  $A_n$  is an arbitrary constant,  $n$  is angular momentum quantum number,  $k_0 = \sqrt{2m_0 E/\hbar}$ . Outside the scatterer the most general solution is

$$\psi_1 = B_n J_n(k_1 r) + S_n Y_n(k_1 r) \quad (5.27)$$

where  $J_n$ ,  $Y_n$  are Bessel functions of first and second kind, respectively. Matching the logarithmic derivative  $\gamma = \psi'/\psi$  at  $r = r_0$ ,

$$k_0 \frac{J'_n(k_0 r_0)}{J_n(k_0 r_0)} = k_1 \frac{B_n J'_n(k_1 r_0) + S_n Y'_n(k_1 r_0)}{B_n J_n(k_1 r_0) + S_n Y_n(k_1 r_0)} \quad (5.28)$$

Far away from the potential i.e.,  $r \rightarrow \infty$ ,

$$J_n(k_e r_0) \rightarrow \sqrt{\frac{2}{\pi k_e r_0}} \sin(k_e r_0 - \frac{1}{2} n \pi - \frac{1}{4} \pi), \quad (5.29)$$

$$Y_n(k_e r_0) \rightarrow \sqrt{\frac{2}{\pi k_e r_0}} \cos(k_e r_0 - \frac{1}{2}n\pi - \frac{1}{4}\pi), \quad (5.30)$$

Eq. (5.29) with the phase shift becomes

$$\psi_r \propto \sqrt{\frac{2}{\pi k_e r_0}} \sin(k_e r_0 - \frac{1}{2}n\pi - \frac{1}{4}\pi + \delta_n(k_e)), \quad (5.31)$$

$$= \cos \delta_n Y_n(k_e r) - \sin \delta_n J_n(k_e r) \quad (5.32)$$

comparing Eqs. (5.28) and (5.32), it is apparent that

$$\tan \delta_n = -\frac{S_n}{B_n} \quad (5.33)$$

substituting Eq. (5.33) in to Eq. (5.28), we get

$$\tan \delta_n = \frac{k_e J_n(k_e r_0) - \gamma_n J'_n(k_e r_0)}{k_e Y'_n(k_e r_1) - \gamma_n Y_n(k_e r_0)} \quad (5.34)$$

where

$$\gamma_n = k_0 \frac{J'_n(k_0 r_0)}{J_n(k_0 r_0)} \quad (5.35)$$

Analogous to classical scattering theory, one can obtain the phase shifts as follows:

The boundary conditions in the following case are due to continuity of wave function, and the probability current

$$\psi_0 = \psi_1, \quad (5.36)$$

$$\frac{1}{m_0} \partial_r \psi_0 = \frac{1}{m_1} \partial_r \psi_1 \quad (5.37)$$

By applying these boundary conditions:

$$A_n J_n(k_0 r) = J_n(k_1 r) + S_n Y_n(k_1 r) \Big|_{(r=r_0)}, \quad (5.38)$$

$$\frac{k_0}{m_0} A_n J'_n(k_0 r) = \frac{k_1}{m_1} \left( J'_n(k_1 r) + S_n Y'_n(k_1 r) \right) \Big|_{(r=r_0)} \quad (5.39)$$

Solving Eqs. (5.30) and (5.31) for the scattering coefficient  $S_n$ , we get

$$S_n = \frac{k_1 J_n(k_1 r_1) J'_n(k_1 r_0) - k_0 J'_n(k_1 r_1) J_n(k_1 r_0)}{k_1 J_n(k_1 r_1) Y'_n(k_1 r_0) - k_0 J'_n(k_1 r_0) Y_n(k_1 r_0)} \quad (5.40)$$

provided  $B_n \rightarrow 1$  in Eq. (5.33),

$$\tan \delta_n = -S_n \quad (5.41)$$

Considering particles with long wavelength and a scatterer with small size i.e., in the limit  $k_e r_0 \ll 1$   $S_n$  in Eq. (5.40) reduces to

For  $s(l=0)$  partial waves

$$S_0 = -\frac{\pi}{32} \left( \frac{m_0}{m_1} - 1 \right) (k_e r_0)^4 \quad (5.42)$$

For  $p(l=1)$  partial waves

$$S_1 = -\frac{\pi}{4} \left( \frac{m_0 - m_1}{m_0 + m_1} \right) (k_e r_0)^2 \quad (5.43)$$

Eqs. (5.42) and (5.43) are analogous to Eqs. (2.75) and (2.76), the long wave length approximations of the scattering coefficient due to scattering of TM waves by a 2D scatterer.

## 5.4 Generic quantum cloak

### 5.4.1 single shell cloak

The geometry of the problem is depicted in Fig. 5.2. The system consists of a cylindrical shell of radius  $r_1$  with an effective mass  $m_1$ , and potential  $V_1$  around a core with radius  $r_0$ , effective mass  $m_0$ , and potentials  $V_0$  in an isotropic homogeneous environment with mass  $m_e$ . The structure is illuminated by spineless quantum particles of energy  $E$  and definite momentum. These particles satisfy the time-independent

Schrodinger equation given by Eq. (1). Since  $\psi(r)$  must vanish at the origin, the general solution

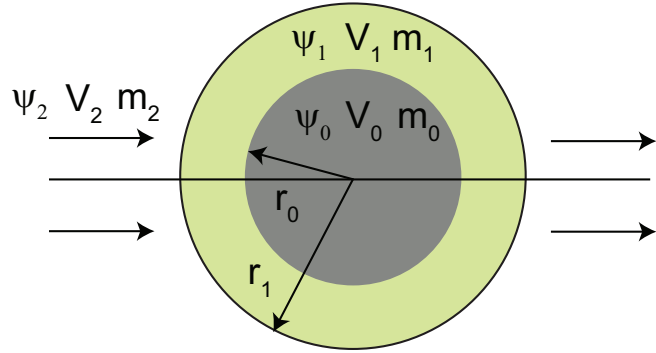


**Figure 5.2:** Matter wave incident on a 2D multilayer scatterer with layer radii  $r_0$ ,  $r_1$  and effective mass  $m_0$ ,  $m_1$ , respectively. Located in an environment with effective mass  $m_e$ .

inside the scatter is

$$\psi_0 = A_n J_n(k_0 r), \quad (5.44)$$

where  $A_n$  is an arbitrary constant. Inside the shell, the most general solution is

$$\psi_1 = B_n J_n(k_1 r) + C_n Y_n(k_1 r) \quad (5.45)$$

Outside the core-shell structure, the most general solution is

$$\psi_2 = J_n(k_2 r) + S_n Y_n(k_2 r) \quad (5.46)$$

Applying the boundary conditions in Eqs. (5.38) and (5.39), we get

$$A_n J_n(k_0 r) = B_n J_n(k_1 r) + C_n Y_n(k_1 r) \Big|_{r=r_0}, \quad (5.47)$$

$$\zeta_0 \frac{k_0}{m_0} \left( A_n J'_n(k_0 r) \right) = \frac{k_1}{m_1} \left( B_n J'_n(k_1 r) + C_n Y'_n(k_1 r) \right) \Big|_{r=r_0}, \quad (5.48)$$

$$B_n J_n(k_1 r) + C_n Y_n(k_1 r) = J_n(k_2 r) + S_n Y_n(k_2 r) \Big|_{r=r_1}, \quad (5.49)$$

$$\zeta_1 \frac{k_1}{m_1} (B_n J'_n(k_1 r) + C_n Y'_n(k_1 r)) = \frac{k_2}{m_2} (J'_n(k_2 r) + S_n Y'_n(k_2 r)) \Big|_{r=r_1} \quad (5.50)$$

where

$$\zeta(\cdot) = \begin{cases} 1 & \text{if } V < E \\ i & \text{if } V > E \end{cases} \quad (5.51)$$

where  $(\cdot) = 0$  or  $1$ . Solving Eqs. (5.47)–(5.50) for the scattering coefficient, we get,

$$S_n = \frac{k_e J_n(k_e r_1) [H_n^{1'}(k_1 r_1) \Lambda_n + J'_n(k_1 r_1)] - \zeta_1 k_1 J'_n(k_e r_1) [J_n(k_1 r_1) - H_n^1(k_e r_1) \Lambda_n]}{\zeta_1 k_1 H_n^{1'}(k_e r_1) [J_n(k_1 r_1) + H_n^1(k_1 r_1) \Lambda_n] - k_e H_n^1(k_e r_1) [H_n^{1'}(k_1 r_1) \Lambda_n + J'_n(k_1 r_1)]}, \quad (5.52)$$

$$\Lambda_n = \frac{\zeta_1 k_1 J_n(k_1 r_0) J'_n(k_0 r_0) - \zeta_0 k_0 J_n(k_0 r_0) J'_n(k_1 r_0)}{\zeta_0 k_0 H_n^{1'}(k_1 r_0) J_n(k_0 r_0) - \zeta_1 k_1 J'_n(k_0 r_0) H_n^1(k_1 r_0)}. \quad (5.53)$$

For very small slow particles (usually ultra cold particles) with incident De Broglie wavelength much greater than the size of the scatterer i.e.,  $k_e r \ll 1$ , one can write Eq. (5.52) as

$$S_1 = i \frac{(k_e r_1)^2}{4} \left( \frac{(m_0 + m_1)(m_1 - m_e) + (m_0 - m_1)(m_1 + m_e)p_0}{(m_0 + m_1)(m_1 + m_e) + (m_0 - m_1)(m_1 - m_e)p_0} \right) \quad (5.54)$$

where  $p_0 = (r_0/r_1)^2$ . In the limit  $S_n \rightarrow 0$  we obtain a transparency condition for single shell cloaking system which depends on the core, shell potentials and medium masses:

$$p_0 = \left( \frac{r_0}{r_1} \right)^2 = \frac{(m_1 - m_e)(m_1 + m_0)}{(m_1 - m_0)(m_1 + m_e)} \quad (5.55)$$

However, for  $s$  waves, the approximate form of Eq. (5.52) for small particles is

$$S_0 = -\frac{i\pi}{4} \left( 1 - \frac{k_0^2 m_1 m_e p_0 \zeta_0^2 - k_1^2 m_0 m_e (1 - p_0) \zeta_1^2}{k_e^2 m_0 m_1} \right) (k_e r_1)^2 \quad (5.56)$$

In the limit  $S_0 \rightarrow 0$ , the transparency condition for  $s$  waves is given by

$$p_0 = \frac{E - E\zeta_1^2 + V_1\zeta_1^2}{(E - V_0)\zeta_0^2 - (E - V_1)\zeta_1^2} \quad (5.57)$$

Note that the transparency condition for  $s$  waves i.e., Eq. (5.57) is a function of energy  $E$ , and the potentials  $V_0, V_1$  of the core and the layer, respectively. However, the transparency condition for  $p$  waves i.e., Eq. (5.55) depends only on the radii ratio  $p_0$ , and the effective masses  $m_0$  and  $m_1$  of the core and the layer, respectively. Moreover, realizations of such cloaking systems present a serious disadvantage; redesign of the entire cloak is necessitated for any change in the objects properties ( $m_0, r_0$  and  $V_0$  are the effective mass, radius and potential of the object/core), and it is applicable only for spherically/cylindrically symmetric potentials.

#### 5.4.2 Multi-shell cloaking system

The system consists of  $l$  concentric cylindrical shells with arbitrary shell radii  $r_m (m = 0, 1, \dots, l)$ , and impedances  $m_m$ , respectively. The multi-shell structure is embedded in a host medium with impedance  $m_{l+1}$ . Considering the incident matter wave  $\psi$  the wave equation inside the  $m$ -th shell assume the general solution for cylindrical symmetry

$$\psi_n^{(m)} = \sum_{n=-\infty}^{\infty} [A_n^{(m)} J_n(k_m r) + B_n^{(m)} H_n^1(k_m r)] e^{in\phi}, \quad (5.58)$$

By proceeding in similar fashion as in sections 3.3 and 5.4, for  $n \geq 2$ , the scattering coefficient for cold particles incident on a very small obstacle i.e.,  $k_e r_l \ll 1$  can be written as

$$S_n^l = r_l^2 \frac{m_{eff}^l - m_e}{m_{eff}^l + m_e} \quad (5.59)$$

where

$$m_{eff}^l = m_l + \frac{2m_l p_l (m_{eff}^{l-1} - m_l)}{2m_l + (1 - p_l)(m_{eff}^{l-1} - m_l)} \quad (5.60)$$

is effective mass of the  $l$ -shell system, and  $p_l = (r_{l-1}/r_l)^d$  are the shells surface/volume ratios. We must note that using the natural condition  $m_{eff}^0 = m_e$ , Eqs. (5.59) and (5.60) provide a straightforward recurrence formula for estimating the scattering coefficient of multilayered particles in the quasi-static approximation without explicitly solving the boundary value problem. This rendering of the problem also gives an intuitive understanding of the scattering process as that of an equivalent spherical/cylindrical particle with effective mass  $m_{eff}^l$  immersed in a host environment with mass  $m_e$ .

Alternatively, one can propose a different condition to achieve complete elimination of scattering for a cloak with  $l \geq 2$  shells. By inspection (see Eqs. (5.59) and (5.60)) this is achieved ( $m_{eff}^l = m_e$ ), if the two outermost cloaking shells have effective masses that satisfy the following conditions:

$$m_{l-1} = 0, \quad (5.61)$$

$$m_l = m_e \frac{(1 + p_l)/(d - 1)}{1 - p_l}, \quad (5.62)$$

Provided a material with zero effective mass for the  $l - 1$ -th shell, the effective mass of the outermost shell is dependent only on the radii of the  $l^th$ , and  $(l - 1)^th$  shells which is in sharp contrast with the transparency condition given by Eqs. (5.55). Thus, in the quasi-static limit, a cloaking system parameterized by the transparency condition Eqs. (5.61) and (5.62) has the potential to cloak objects with arbitrary electronic properties. Furthermore, the conditions  $m_{l-1} \rightarrow 0$ , allows cloaking of objects with

arbitrary potential shapes provided it is immersed within shells of order lower than  $l - 1$ .

### two-shell system

We consider a two shell cylindrical and spherical cloaking systems with GaAs ( $m_e = 0.067$ ) as substrate. To satisfy the transparency condition Eq. (5.61) we utilize a InSb inner shell with effective mass 0.013.

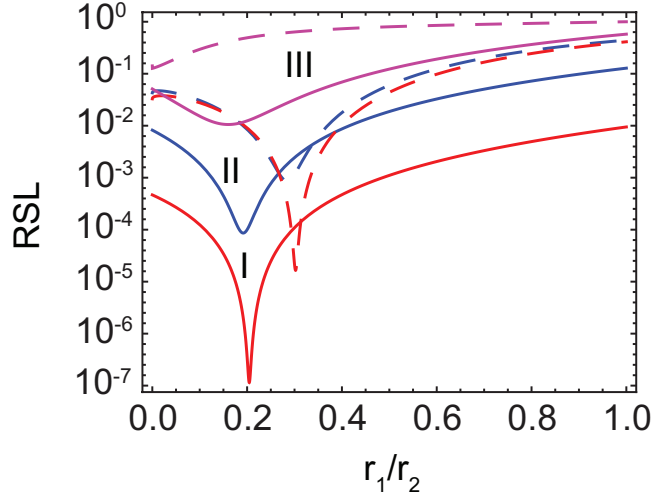


**Figure 5.3:** Relative scattering length (RSL) versus the radii ratio cylindrically symmetric cloak. The ideal case as per Eq. (5.61) is presented in solid lines. The dotted lines represent RSL with respect to physical materials. The inner and outer shell made of InSb ( $m_3 = 0.013$ ) and AlSb ( $m_2 = 0.102$ ) respectively. The host is GaAs with electron effective mass  $m_e = 0.067$ . Three separate designs are being investigated in case of cylindrical system: (I)  $r_2 = 2$  nm (Red), (II)  $r_2 = 5$  nm (Blue) and  $r_2 = 10$  nm (pink). The object electron effective mass is  $m_0 = 0.083$ .

To characterize the clock performance we define the relative scattering length (RSL), for the cylindrical case  $d = 2$ , and relative scattering cross-section (RSCS) for spherically symmetric case  $d = 3$  as

$$\sigma_R^d = \frac{\sigma_{cloak}^d}{\sigma_{object}^d} = \left| \frac{S_{1,cloak}^d}{S_{1,object}^d} \right|^2, \quad (5.63)$$

where  $\sigma_{cloak}^d$  and  $\sigma_{object}^d$  are the scattering length (scattering-cross section) of the cloak and object, respectively. Figure 5.4 illustrates relative scattering length as a function of the radii ratio. For comparison, we include the RSL of the ideal systems (with effective mass of the inner shell exactly zero) and with a InSb inner shell for different outer shell radii (I)  $r_2 = 2$  nm (Red), (II)  $r_2 = 5$  nm (Blue) and  $r_2 = 10$  nm (pink). The RSL of the ideal systems approaches zero, implying perfect invisibility at the outer shell effective mass values  $m_2 = 0.14$ . These results are in excellent agreement with the values predicted by the transparency condition Eq. (5.61). A significant reduction in scattering for the InSb shell systems are also observed at the predicted outer shell effective mass  $m_2$  (dashed lines).

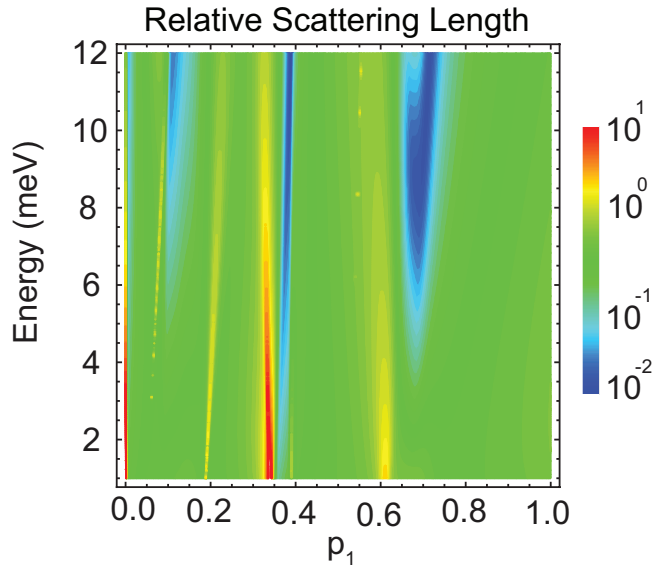


**Figure 5.4:** Relative scattering length/width (RSL) versus the radii ratio cylindrically symmetric cloak. The ideal case as per Eq. (5.61) is presented. The inner and outer shell made of  $m_1 = 0.0$  and  $m_2 = 0.102$  respectively. The potentials or the band offsets are  $V_0 = 0.48$ ,  $V_1 = 0.60$  and  $V_2 = -0.28$  respectively. The host electron effective mass  $m_e = 0.067$ . The object electron effective mass is  $m_0 = 0.083$ .

Figure. 5.6, illustrates the RSL of the cylindrically symmetric cloak, for an arbitrary object. As expected, for systems with small overall sizes a drastic reduction in scattering over the entire optical spectrum is achieved for  $m_2 = (1 + p_2)/(1 - p_2)$ , thus reproducing the quasi-static result.

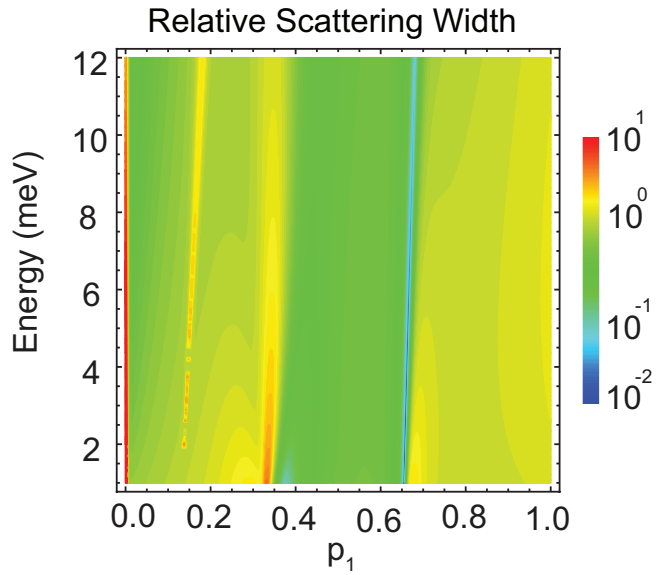


**Figure 5.5:** Relative scattering length/width (RSL) versus the radii ratio cylindrically symmetric cloak. The ideal case as per Eq. (5.61) is presented. The inner and outer shell made of  $m_1 = 0.013$  and  $m_2 = 0.102$  respectively. The potentials or the band offsets are  $V_0 = 0.48$ ,  $V_1 = 0.60$  and  $V_2 = -0.28$  respectively. The host electron effective mass  $m_e = 0.067$ . The object electron effective mass is  $m_0 = 0.083$ .

However, as the system size increases (see Fig 5.6) the transparency condition in Eq. (5.61) is no longer sufficient to arrest the scattering process. This is an expected behavior since the contribution of the higher order multipoles in the scattering cross-length.

## CHAPTER 6

### CONCLUSIONS

In conclusion, we have proposed a quasi-effective medium theory for multi-layer concentric cylindrical systems. Our approach allows for exact calculations of the scattering and extinction properties of such composite objects. In the large wavelength limit the quasi-effective medium theory reproduces the MGT in the case of the dipolar response but also provides the effective properties for higher multipoles. The proposed methodology is easy to implement, do not require tedious calculations of the field amplitudes, and provides important insights in the optical properties of complex systems. Applying the theory we have determined the complete set of hybridization resonances of multi-shell metal-dielectric particles.

In this thesis we propose a generic cloaking system based on zero-permittivity composite materials. The proposed analytical model and full wave calculations show that a dramatic suppression of dipolar scattering can be achieved for an arbitrary object enclosed within a multi-shell cloaking system. A reduction of scattering across the entire optical spectrum for dielectric objects using realistic shell materials is demonstrated. This study provides a new direction for achieving optical invisibility without the use of metamaterials and also underlines the role of zero-index materials in the general phenomenon of optical transparency. Moreover, we have developed new

type of electromagnetic cloak that are object independent and eliminate two successive monopoles from the scattering cross-section.

An optical analogue of a quantum mechanical cloaking system is proposed. A reduction of scattering across for an arbitrary object using realistic shell materials is demonstrated for different particle energies and radii of the cloak.

## **APPENDIX A**

### **APPENDICES (IF DESIRED)**

**Put your appendices here. All codes stay the same, except that the first page of an appendix should only have the headings, so follow \chapter with a \clearpage. Codes in phd\_thesis.tex take care of naming a \chapter an “APPENDIX.”**

From Louisiana Tech’s “GUIDELINES FOR THE PREPARATION AND SUBMISSION OF YOUR THESIS OR DISSERTATION” (see [?])

- Appendices are optional. They must contain extra, relevant material such as questionnaires, surveys, tables, figures, computer data, and letters of permission to reprint copyrighted material. These optional appendices must be listed in the Table of Contents, conforming to the format used there. They must also be formatted in the document in such a way that they are consistent with the other main divisions.
- Appendices must be cited in the Body of the document.
- All material in appendixes must be numbered consecutively, within the required margins, and on the same paper used throughout the document.
- All appendices must have a title page. The title page of each Appendix must have the Arabic page number centered between the left and right margins between 1/2 inch and 1 inch from the bottom edge of the page. Place the Arabic page number at the top right of subsequent pages of each Appendix.
- The Title page must have the word APPENDIX typed in all capital letters 2 inches from the top of the page followed by an informative title in all capital letters. If there is more than one appendix, then label the first title page as

APPENDIX A, the second APPENDIX B, and so on, providing an informative title for each appendix.

## BIBLIOGRAPHY

- [1] Van de Hulst, H.C., 1957. *Light Scattering by Small Particles*, Wiley, New York.
- [2] Bohren, C. F., and D. R. Huffman, 1998. *Absorption and Scattering of Light by Small Particles*, Wiley, New York.
- [3] Ishimaru, A., 1978. *Wave Propagation and Scattering in Random Media*, Academic, San Diego.
- [4] Tsang, L., J. Kong, and K-H. Ding, 2000. *Scattering of Electromagnetic Waves: Theories and Applications*, Wiley, New York.
- [5] Stratton, A. J., 1941. *Electromagnetic Theory*, McGraw-Hill, New York.
- [6] Kerker, M., 1969. *The scattering of light and other electromagnetic radiation*, Academic, San Diego.
- [7] Born. M., and E. Wolf, 1965. *Principles of Optics: Electromagnetic Theory of Propagation, Interference and Diffraction of Light*, Pergamon, Oxford.
- [8] Mie, G., 1908. Beiträge zur Optik trüber Medien, speziell kolloidaler Metallösungen, *Ann Phys.*, **330**, 377–445.
- [9] Brillouin, L., 1949. The Scattering Cross Section of Spheres for Electromagnetic Waves, *J. Appl. Phys.* **20**, 1110–1125.
- [10] Stokes, G. G., 1852. On the composition and resolution of streams of polarized light from different sources, *Trans. Camb. Philos. Soc.*, **9**, 399–416.
- [11] Wait, J. R., 1965. Scattering of a plane wave from a circular dielectric cylinder at oblique incidence, *Can. J. Phys.*, **33**, 189–195.
- [12] Wait, J. R., 1959. *Electromagnetic radiation from cylindrical structures*, Pergamon,

New York.

- [13] Farone, W. A., and C. W. Querfeld, 1965. *report ERDA-287*, U. S. Army Electronics Research and Development Activity, WhiteSands Missile Range, New Mexico.
- [14] Kerker, M., D. Cooke, A. W. Farone, R. A. Jacobsen, 1966. Electromagnetic scattering from an infinite circular cylinder at oblique incidence: I. radiance functions for  $m = 1.46$ , *J. Opt. Soc. Am.*, **56**, 487–489.
- [15] Sihvola, A., 1999. *Electromagnetic mixing formulas and applications*, The IET, London.
- [16] Cai, W., U. K. Chettiar, A. V. Kildishev, R. A. Jacobsen, and V. M. Shalaev, 2007. Optical cloaking with metamaterials, *Nat. Photonics*, **1**, 224–227.
- [17] Mundru, P. C., V. K. Pappakrishnan, and D. A Genov, 2012. Material- and geometry-independent multishell cloaking device, *Phys. Rev. B*, **85**, 045402.
- [18] Alú, A., and N. Engheta, 2005. Achieving transparency with plasmonic and metamaterial coatings, *Phys. Rev. E*, **72**, 016623.
- [19] Zhou, X., and G. Hu, 2006. Design for electromagnetic wave transparency with metamaterials, *Phys. Rev. E*, **74**, 026607.
- [20] Leonhardt, U., and T. Philbin, 1999. *Geometry and Light: The Science of Invisibility*, Dover, New York.
- [21] Xu, H., 2005. Multilayered metal core-shell nanostructures for inducing a large and tunable local optical field, *Phys. Rev. B*, **72**, 073405.
- [22] Jacob, Z., L. V. Alekseyev, and E. Narimanov, 2006. Optical hyperlens: Far-field imaging beyond the diffraction limit, *Opt. Express*, **14**, 8247–8256.
- [23] Liu, Z., H. Lee, Y. Xiong, C. Sun, and X. Zhang, 2007. Far-field optical hyperlens magnifying sub-diffraction-limited objects, *Science*, **315**, 1686.
- [24] Luk'Yanchuk, B., N. I. Zheludev, S. A. Maier, N. J. Halas, P. Nordlander, H. Giessen, and C. T. Chong, 2010. The Fano resonance in plasmonic nanostructures

- and metamaterials, *Nat. Materials*, **9**, 707–715.
- [25] Bergman, D.J., and D. Stroud, 1992. Physical Properties of Macroscopically Inhomogeneous Media, *Solid State Phys.*, **46**, 147–269.
  - [26] Jackson, J. D., 1999. *Classical electrodynamics*, John Wiley, Hoboken.
  - [27] Bergman, D.J., and D. Stroud, 1992. Physical Properties of Macroscopically Inhomogeneous Media, *Solid State Phys.*, **46**, 419–440.
  - [28] Genov, D. A., A. K. Sarychev, and V. M. Shalaev, 2003. Metal-dielectric composite filters with controlled spectral windows of transparency, *J. Nonlinear Opt. Phys. Mater.*, **12**, 385–420.
  - [29] Bruggeman, D. A. G., 1935. Berechnung verschiedener physikalischer Konstanten von heterogenen Substanzen. I. Dielektrizitätskonstanten und Leitfähigkeiten der Mischkörper aus isotropen Substanzen, *Ann. Phys. (Leipzig)*, **24**, 636–664.
  - [30] Polder, D., and J. H. Van Santeen, 1946. The effective permeability of mixtures of solids, *Physica*, **12**, 257–271.
  - [31] Golovan. L. A., V. Yu. Timoshenko, and P. K. Kashkarov, 2007. Optical properties of porous-system-based nanocomposites, *Phys.-Usp.*, **50**, 595–612.
  - [32] Doyle, W.T., 1989. Optical properties of a suspension of metal spheres, *Phys. Rev. B*, **39**, 9852–9858.
  - [33] Lakhtakia, A., 1992. Size-dependent MaxwellGarnett formula from an integral equation formalism, *Optik*, **91**, 134–137.
  - [34] Foss, C. A., G. L. Hornyak, J. A. Stockert, and C. R. Martin, 1994. Template-Synthesized nanoscopic gold particles: optical spectra and the effects of particle size and shape, *J. Phys. Chem.*, **98**, 2963–2971.
  - [35] Dungey, C. E., and C. F. Bohren, 1991. Light scattering by nonspherical particles: a refinement to the coupled-dipole method, *J. Opt. Soc. Am. A*, **8**, 81–87.
  - [36] Stroud, D., 1975. Generalized effective-medium approach to the conductivity of an inhomogeneous material, *Phys. Rev. B*, **12**, 3368–3373.

- [37] Abeles, B., and J. I. Gittleman, 1976. Composite material films: optical properties and applications, *Appl. Opt.*, **15**, 2328–2332.
- [38] Landauer, R., 1952. The Electrical Resistance of Binary Metallic Mixtures, *J. Appl. Phys.*, **23**, 779–784.
- [39] Cummer, S. A., B. I. Popa, D. Schurig, D. R. Smith, and J. Pendry, 2006. Full-wave simulations of electromagnetic cloaking structures, *Phys. Rev. E*, **74**, 036621.
- [40] Leonhardt, U., 2006. Optical conformal mapping, *Science*, **312**, 1777–1780.
- [41] Pendry, J. B., D. Schurig, and D. R. Smith, 2006. Controlling electromagnetic fields, *Science*, **312**, 1780–1782.
- [42] Leonhardt, U., and T. Philbin, 2006. General relativity in electrical engineering, *New J. Phys.*, **8**, 247.
- [43] Wait, J.R., 1985. *Electromagnetic wave theory*, Harper & Row, New York.
- [44] Harrington, R.F., 1961. *Time harmonic electromagnetic fields*, McGraw-HILL, New York.
- [45] Genov, D.A., R.F. Oulton, G. Bartal, and X. Zhang, 2011. Anomalous spectral scaling of light emission rates in low-dimensional metallic nanostructures, *Phys. Rev. B*, **83**, 245312.
- [46] Prodan, E., C. Radloff, N.J. Halas, and P. Nordlander, 2003. A Hybridization Model for the Plasmon Response of Complex Nanostructures, *Science*, **302**, 419–422.
- [47] Huang, Y., Y. Feng, and T. Jiang, 2007. Electromagnetic cloaking by layered structure of homogeneous isotropic materials, *Opt. Express*, **15**, 11133–11141.
- [48] Palik, E., 1997. *Handbook of Optical Constants of Solids*, Academic Press, London.
- [49] Lai, Y., N. Jack, H. Chen, D. Han, J. Xiao, Z-Q. Zhang, and C. T. Chan, 2009. Illusion Optics: The Optical Transformation of an Object into Another Object, *Phys. Rev. Lett.*, **102**, 253902.

- [50] Pendry. J. B., and S.A. Ramakrishna, 2002. Near-field lenses in two dimensions, *J. Phys.: Condens. Matter*, **14**, 8463–8479.
- [51] McCall M. W., A. Favaro, P. Kinsler and A. Boardman, 2011. A spacetime cloak, or a history editor, *J. Opt.*, **13**, 024003.
- [52] Kerker. M., 1975. Invisible bodies, *J. Opt. Soc. Am.*, **65**, 376–379.
- [53] Kerker, M., 1982. Lorenz-Mie Scattering by Spheres: Some Newly Recognized Phenomena, *Aerosol. Sci. Technol.*, **1**, 275–291.
- [54] Dentcho. D. A., P. C. Mundru, 2014. Quasi-effective medium theory for multilayered magneto-dielectric structures, *J. Opt.*, **16**, 015101.
- [55] Bohm, D., 1951. *Quantum theory*, Prentice-Hall, New York.
- [56] Schiff. L. I., 1955. *Quantum mechanics*, McGraw-Hill, New York.
- [57] Rayleigh. J. W. S., 1878. *The Theory of Sound vol.II*, Macmillan, London.
- [58] Faxén. H., J. Holtsmark, 1927. Beitrag zur Theorie des Durchganges langsamer Elektronen durch Gase, *Zeits. f. Physik*, **45**, 307–324.

## **VITA (IF REQUIRED)**

- The Vita is a one-page biographical sketch of the author written in paragraph form and in 3rd person. It is the last item of the document and must appear in the Table of Contents.
- The heading must have identical font, value, size, and position/location in the page as other major headings.